



**NTNU – Trondheim**  
Norwegian University of  
Science and Technology

# Analysis of Diffusion Models in Eclipse 300

**Gulnara Marselevna  
Shafikova**

Petroleum Engineering

Submission date: June 2013

Supervisor: Curtis Hays Whitson, IPT

Norwegian University of Science and Technology  
Department of Petroleum Engineering and Applied Geophysics



Gulnara Shafikova

---

Analysis of Diffusion Models in Eclipse 300

---

Thesis for the degree of Master of Science

Trondheim  
June , 2013

Norwegian University of Science and Technology  
Faculty of Engineering Science and Technology  
Department of Petroleum Engineering and Applied Geophysics



## **Abstract**

Molecular diffusion could be an efficient recovery mechanism in many applications in reservoir engineering. Proper modelling of diffusion in hydrocarbon mixtures at the reservoir conditions is not a simple task and requires reliable diffusion coefficients for accurate diffusion flux calculations.

The main objective of this study is to analyse diffusivity models for a wide range of experimental conditions, so that to examine diffusion performance driven by concentration and chemical potential gradients. We simulate the diffusion experiments in the porous media, considering mixing in the binary system composed of C1 and C2 components. The commercial compositional simulator Eclipse 300 with fully implicit solution method is used for simulation study. In the all run cases, the system is assumed to be isothermal. The study was restricted to diffusion in the single gas phase, unless the cross-phase diffusion was under investigation.

This work is also directed to determine diffusion coefficients from simulated diffusion experiments. The conventional approach to estimate diffusion coefficients from laboratory experiments is adopted to determine mass transfer coefficients from simulation results. It has been proved that numerical solution is a result of pure diffusion transfer and unequal bulk flows of C<sub>1</sub> and C<sub>2</sub> particles.

The effect of mixture molar density variation with composition on diffusion behaviour has been studied. It will be shown that fluctuations of mixture volumetric properties create convective bulk fluxes, which can either intensify or oppose mass transfer by pure diffusion flow.

The study of the effect of molar density variation on diffusion performance considering a simple binary mixture, however, provides a basis for a better understanding of more realistic situations in which the mixture consist of more than two components.

## **Acknowledgements**

I would like to express my deepest gratitude to my supervisor Professor Curtis H. Whitson. The thesis would not have been possible without his excellent professional guidance, valuable suggestions and comments while working on this project. He has made generous contribution of his precious knowledge and experience, but also cultivated in me love for critical engineering thinking.

I acknowledge Petrostreamz a/s for the Pipe-It license and PhazeComp PVT Software license.

I would like to thank Wynda Astutik from PERA for valuable technical discussions and advices, but also for her personal support, inspiration and friendship.

I am also grateful to Sayyed Ahmad Alavian, for his fresh and critical look on my work, and his readiness to help even being in the other country.

I thank my friends in Norway and Russia for their support and invaluable encouragement on personal level, for what I am extremely grateful.

Last, but not the least important, I owe more than thanks to my dearest parents, for their financial support and great encouragement at all times, keeping me harmonious. I will be grateful forever for your unconditional love. I dedicate this work for you.

Gulnara Shafikova

---

## Table of contents

|   |     |
|---|-----|
| <b>Abstract</b> .....   | i   |
| <b>Acknowledgements</b> .....   | ii  |
| <b>Table of contents</b> .....  | iii |
| <b>List of Tables</b> .....   | v   |
| <b>List of Figures</b> .....  | vi  |
| <b>Nomenclature</b> .....   | x   |
| <b>1 Introduction</b> .....   | 1   |
| 1.1 Background.....   | 1   |
| 1.2 Study objectives.....   | 2   |
| 1.3 Description of Employed Software .....  | 3   |
| <b>2 Diffusion: fundamentals and basic concept</b> .....  | 5   |
| 2.1 Fickian diffusion and chemical potential driven diffusion.....                                    | 5   |
| 2.2 Estimating low pressure diffusion coefficients.....   | 7   |
| 2.3 The extended Sigmund correlation .....  | 8   |
| 2.4 Diffusion coefficients determined from laboratory experiments.....                                | 12  |
| 2.5 Variation of diffusion coefficients with composition.....   | 14  |
| <b>3 Model description</b> .....  | 16  |
| 3.1 Data description .....  | 16  |
| 3.1.1 The Phase behavior of methane-ethane mixture .....  | 16  |
| 3.1.2 The effect of composition on binary diffusion coefficients<br>for methane - ethane mixture..... | 18  |

---

|          |  |           |
|----------|--|-----------|
| 3.2      | Eclipse 300 Model description.....   | 23        |
| 3.3      | Grid sensitivity analyses.....   | 27        |
| 3.4      | Automated model post-processing.....   | 30        |
| <b>4</b> | <b>Interpreting simulated diffusion experiments.....</b>                           | <b>34</b> |
| 4.1      | Low pressure simulation results.....   | 34        |
| 4.2      | High-pressure simulation results .....   | 38        |
| 4.3      | Cross-phase diffusion.....   | 44        |
| 4.4      | The effect of convection on the diffusion process.....                             | 49        |
| 4.5      | Features of mass transfer and diffusion in the near-critical regions ..            | 57        |
| 4.5.1    | Diffusion in the near critical region of pure ethane.....                          | 57        |
| 4.5.2    | Diffusion in the methane-ethane mixture critical region.....                       | 69        |
| <b>5</b> | <b>Diffusion coefficients determined from simulated diffusion experiments.....</b> | <b>75</b> |
| <b>6</b> | <b>Conclusions.....</b>  | <b>86</b> |
|          | <b>Bibliography.....</b>   | <b>88</b> |
|          | <b>Appendix A.....</b>   | <b>92</b> |



---

## List of tables

|     |   |    |
|-----|---|----|
| 3.1 | Critical points for C <sub>1</sub> -C <sub>2</sub> mixture..... | 17 |
| 3.2 | Fluid properties for the 2-component SRK characterization.....  | 26 |
| 3.3 | Computing time summary.....                                     | 28 |
| 5.1 | Results from simulated diffusion experiments .....              | 84 |

---

## List of figures

|      |   |    |
|------|---|----|
| 2.1  | The modified Sigmund diffusion coefficient correlation.....   | 10 |
| 2.2  | The Loschmidt tube set-up.....  | 12 |
| 2.3  | Experiment diffusion coefficients for the methane-ethane system at $T=104^{\circ}\text{F}$  | 15 |
| 3.1  | Phase diagram of methane-ethane system at various components concentration  | 17 |
| 3.2  | Diffusion coefficients for methane-ethane system at at $T=90^{\circ}\text{F}$ .....   | 18 |
| 3.3  | The molar density of the methane-ethane mixture for different compositions as a function of pressure. Temperature $T=90^{\circ}\text{F}$ .....  | 19 |
| 3.4  | Diffusion coefficients for methane-ethane system for different compositions as a function of pressure. Temperature $T=90^{\circ}\text{F}$ ..... | 19 |
| 3.5  | The molar density for $50\%C_1:50\%C_2$ mixture as a function of pressure. $T=90^{\circ}\text{F}$   | 22 |
| 3.6  | Diffusion coefficients for $50\%C_1:50\%C_2$ mixture. $T=90^{\circ}\text{F}$ . ....   | 23 |
| 3.7  | The model set-up with total dimensions (in cm) .....  | 24 |
| 3.8  | Oil and gas relative permeability.....  | 26 |
| 3.9  | $C_2$ distribution profile at time $T=10$ hours. Concentration diffusivity model.....   | 29 |
| 3.10 | $C_2$ distribution profile at time $T=10$ hours. Chemical potential diffusivity model   | 29 |
| 3.11 | Pipe-It project architecture comprising four parts.....   | 31 |
| 3.12 | The "Diffusion coefficients" composite structure.....   | 31 |
| 3.13 | The "Eclipse300_MODEL" composite structure.....   | 31 |
| 3.14 | Outline of Pipe-It Optimizer used to set up optimizations.....  | 32 |
| 3.15 | The «Generating tables and plots» composite structure.<br>Plotting streamz files within Pipe-It.....  | 33 |
| 4.1  | Density-diffusivity product of $C_1-C_2$ mixture at $T=90^{\circ}\text{F}$ as a function of:<br>a) pressure, b) mixture molar density.....      | 34 |
| 4.2  | Pressure-distance profile at different time steps for initialisation pressure   |    |

---

|  |    |
|--|----|
| a) $P_{init}=1\text{ atm}$ , b) $P_{init}=5\text{ atm}$ .....  | 36 |
| <b>4.3</b> $C_2$ mole fraction-distance profile at different time steps for initialisation pressure:                 |    |
| a) $P_{init}=1\text{ atm}$ , b) $P_{init}=5\text{ atm}$ .....  | 37 |
| <b>4.4</b> $C_2$ mole fraction in the grid blocks versus time for initialisation pressure:                           |    |
| a) $P_{init}=1\text{ atm}$ , b) $P_{init}=5\text{ atm}$ .....  | 37 |
| <b>4.5</b> Region pore volume as function of pressure.....   | 39 |
| <b>4.6</b> Component concentration as a function of pressure.....  | 39 |
| <b>4.7</b> Concentration-distance profile at different time steps at $P=440\text{ psia}$ : a) $C_1$ b) $C_2$ .....   | 41 |
| <b>4.8</b> $\ln(\text{fugacity})$ as a function of molar density at $P=440\text{ psia}$ : a) $C_1$ b) $C_2$ .....    | 41 |
| <b>4.9</b> Concentration-distance profile at different time steps at $P=1200\text{ psia}$ : a) $C_1$ b) $C_2$ ....   | 42 |
| <b>4.10</b> $\ln(\text{fugacity})$ as a function of molar density at $P=1200\text{ psia}$ : a) $C_1$ b) $C_2$ .....  | 42 |
| <b>4.11</b> Concentration-distance profile at different time steps at $P=2000\text{ psia}$ : a) $C_1$ b) $C_2$ ..... | 43 |
| <b>4.12</b> $\ln(\text{fugacity})$ as a function of molar density at $P=2000\text{ psia}$ : a) $C_1$ b) $C_2$ .....  | 43 |
| <b>4.13</b> Schematics of: a) intra-phase diffusion, b) phase discontinuity at interphase boundary.....              | 45 |
| <b>4.14</b> $C_2$ mole fraction profile as a function of time.....   | 47 |
| <b>4.15</b> Oil saturation profile as a function of time for grid block NY=51 .....                                  | 47 |
| <b>4.16</b> $C_2$ mole fraction and pressure profiles as a function of time.....                                     | 48 |
| <b>4.17</b> Mixture molar density variation with composition. $C_1$ - $C_2$ system at:                               |    |
| a) $P=73.48\text{ psia}$ and $T=90^0\text{ F}$ , b) $P=2000\text{ psia}$ and $T=90^0\text{ F}$ .....                 | 49 |
| <b>4.18</b> Mixture compressibility variation with composition. $C_1$ - $C_2$ system at:                             |    |
| a) $P=73.48\text{ psia}$ and $T=90^0\text{ F}$ , b) $P=2000\text{ psia}$ and $T=90^0\text{ F}$ .....                 | 49 |
| <b>4.19</b> Molar density versus distance at different time steps. $P_{init}=30\text{ atm}$ .                        |    |
| No convection.....   | 53 |
| <b>4.20</b> Pressure versus distance at different time steps. $P_{init}=30\text{ atm}$ .                             |    |
| No convection. ....  | 53 |
| <b>4.21</b> Molar density versus distance at different time steps. $P_{init}=30\text{ atm}$ .                        |    |
| With convection.....   | 54 |
| <b>4.22</b> Pressure versus distance at different time steps. $P_{init}=30\text{ atm}$                               |    |
| With convection.....   | 54 |

---

|  |    |
|--|----|
| <b>4.23</b> Molar density versus distance at different time steps. $P_{init}=136\text{atm}$ .<br>No convection.....                                    | 55 |
| <b>4.24:</b> Pressure versus distance at different time steps. $P_{init}=136\text{atm}$ .<br>No convection.....  | 55 |
| <b>4.25</b> Molar density versus distance at different time steps. $P_{init}=136\text{atm}$ .<br>With convection.....                                  | 56 |
| <b>4.26</b> Pressure versus distance at different time steps. $P_{init}=136\text{atm}$ .<br>With convection.....                                       | 56 |
| <b>4.27</b> $C_1$ - $C_2$ system volumetric properties at $P=707$ psia and $T=90^0\text{F}$ :<br>a) molar density, b) compressibility factor $Z$ ..... | 60 |
| <b>4.28</b> $C_1$ concentration-distance profile at different time steps at $P=707$ psia and $T=90^0\text{F}$  | 61 |
| <b>4.29</b> $C_2$ concentration-distance profile at different time steps at $P=707$ psia and $T=90^0\text{F}$  | 61 |
| <b>4.30</b> Pressure-distance profile at different time steps at $P=707$ psia and $T=90^0\text{F}$ .....   | 62 |
| <b>4.31</b> $\ln(\text{fugacity})$ as a function of molar density at $P=707$ psia and $T=90^0\text{F}$ : a) $C_1$ b) $C_2$ ....                        | 62 |
| <b>4.32</b> Concentration and pressure as a function of time. $NY=100$ .....   | 63 |
| <b>4.33</b> $C_2$ component inter-block flow rate. $NY=100$ .....  | 63 |
| <b>4.34</b> $P/Z$ ration as a function of time. $NY=100$ .....   | 64 |
| <b>4.35</b> Fluid compressibility as a function of pressure. $NY=100$ .....  | 64 |
| <b>4.36</b> Concentration and pressure as a function of time. $NY=80$ .....  | 65 |
| <b>4.37</b> $C_2$ component inter-block flow rate. $NY=80$ .....   | 65 |
| <b>4.38</b> $P/Z$ ration as a function of time. $NY=80$ .....  | 66 |
| <b>4.39</b> Fluid compressibility as a function of pressure. $NY=80$ .....   | 66 |
| <b>4.40</b> Concentration and pressure as a function of time. $NY=1$ .....   | 67 |
| <b>4.41</b> $C_1$ component inter-block flow rate. $NY=1$ . ....   | 67 |
| <b>4.42</b> $P/Z$ ration as a function of time. $NY=1$ .....   | 68 |
| <b>4.43</b> Fluid compressibility as a function of pressure. $NY=1$ .....  | 68 |
| <b>4.44</b> $C_1$ concentration-distance profile at different time steps at $P=800$ psia and $T=74^0\text{F}$ ...                                      | 71 |
| <b>4.45</b> $C_1$ mole fraction-distance profile at different time steps at $P=800$ psia and $T=74^0\text{F}$ ...                                      | 71 |
| <b>4.46</b> $C_2$ concentration-distance profile at different time steps at $P=800$ psia and $T=74^0\text{F}$ ...                                      | 72 |
| <b>4.47</b> $C_2$ mole fraction-distance profile at different time steps at $P=800$ psia and $T=74^0\text{F}$ ...                                      | 72 |
| <b>4.48</b> $Z$ factor as a function of a) pressure, b) composition.....   | 73 |

---

|             |   |    |
|-------------|---|----|
| <b>4.49</b> | $C_1$ mole fraction and pressure profiles as a function of time.....  | 73 |
| <b>4.50</b> | P/Z ration as a function of time.....   | 74 |
| <b>4.51</b> | $C_1$ component inter-block flow rate. NY=51,52,53.....   | 74 |
| <b>4.52</b> | $C_2$ component inter-block flow rate. NY=51,52,53.....   | 74 |
| <b>5.1</b>  | Diffusion coefficients obtained from simulated diffusion experiments.<br>Concentration driven diffusion.....  | 78 |
| <b>5.2</b>  | Diffusion coefficients obtained from simulated diffusion<br>experiments.....  | 78 |
| <b>5.3</b>  | Density-diffusivity product as a function of pressure.....  | 79 |
| <b>5.4</b>  | Diffusion coefficients from simulated experiments as a function of time<br>(P=707psia, T=90 <sup>0</sup> F) .....   | 81 |
| <b>5.5</b>  | $C_2$ component inter-block flow rate. NY=100 ( P=707psia, T=90 <sup>0</sup> F) .....   | 81 |
| <b>5.6</b>  | $C_1$ component inter-block flow rate. NY=1 ( P=707psia, T=90 <sup>0</sup> F).....  | 81 |
| <b>5.7</b>  | Dimensionless concentration changes (P=707psia, T=90 <sup>0</sup> F):<br>a) Concentration driven diffusivity model, b) Chemical potential diffusivity model... 82                 |    |
| <b>5.8</b>  | Diffusion coefficients obtained from simulated diffusion experiments ( P=707psia,<br>T=90 <sup>0</sup> F) a) Concentration- b) Chemical potential- driven diffusivity model ..... | 82 |

## Nomenclature

|                               |   |
|-------------------------------|---|
| $J_i$                         | = the molar flux of component i per unit area                                     |
| $C$                           | = the total molar concentration   |
| $X_i$                         | = mole fraction of component i  |
| $D_i$                         | = diffusion coefficient of component i  |
| $D_i^a$                       | = activity corrected diffusion coefficient of component i                         |
| $\frac{\partial}{\partial d}$ | = the gradient in the direction of flow   |
| $F_i$                         | = the component fugacity  |
| $\rho_m^0 D_{ij}^0$           | = density-diffusivity product   |
| $\rho_{p,r}$                  | = reduced molar density, dimensionless  |
| $\rho_m$                      | = molar density, gmole/cm <sup>3</sup>  |
| $\sigma_{ij}$                 | = collision diameter, dimensionless   |
| $\Omega_{ij}$                 | = collision integral, dimensionless   |
| $T_{ij}$                      | = temperature   |
| $M_i, M_j$                    | = molecular weight of i and j components, g/mole                                  |
| $z_i$                         | = mole fraction of component i  |
| $D_{im}$                      | = diffusion coefficient for each component in a multicomponent system,<br>cm/hour |
| $D_{ieff}$                    | = diffusion coefficient corrected on rock tortuosity, cm/hour                     |
| $m$                           | = cementation factor from Archie equation   |
| $\Phi$                        | = porosity, fraction, %   |
| $T_r, P_r$                    | = reduced temperature and pressure  |
| $T, P$                        | = reduced temperature and pressure  |
| $T_{pc}, P_{pc}$              | = mixture pseudocritical temperature and pressure                                 |
| $T_{ci}, P_{ci}$              | = component critical temperature and pressure                                     |
| $z_i$                         | = mixture composition (mole fraction)   |

- 
- $\Phi_A, \Phi_B$  = the dimensionless average concentration changes
- $L_A, L_B$  = length of the top and bottom cells
- $C_B, C_A$  = the average initial concentrations in the top and bottom cells
- $\overline{C_B}, \overline{C_A}$  = the average final concentrations in the top and bottom cells
- $\theta$  = time of experiment
- $Y_B, Y_A$  = the initial fluid composition in the top and bottom cells
- $\overline{Y_B}, \overline{Y_A}$  = the average final fluid composition in the top and bottom cells
- $\rho_B, \rho_A$  = the initial fluid molar density in the top and bottom cells
- $\overline{\rho_B}, \overline{\rho_A}$  = the average final fluid molar density in the top and bottom cells

## Chapter 1

# Introduction

---

### 1.1 Background

Binary and multicomponent diffusion is fundamental process in a wide range of operations in the oil and gas industry. Molecular diffusion may play a key role in a number of oil recovery processes such as heavy oil and naturally fractured reservoirs (Hussein Hoteit, 2011). In the porous media molecular diffusion is generally small. By contrast, in naturally fractured reservoirs molecular diffusion may play an important role and even override viscous displacement (da Silva, Belery 1989).

Molecular diffusion describes movement of molecules due to composition, chemical potential, pressure or temperature gradients in a mixture. The diffusive mass transfer is controlled by molecular diffusion coefficients, generally presented by  $D$ .

Proper modelling of diffusion in hydrocarbon mixtures at the reservoir conditions is not a trivial task. The challenge is computing the diffusion coefficients for the non-ideal multicomponent mixtures in gas and oil phases, and in physically accurate modelling of the diffusion driving force (Hussein Hoteit 2011).

During the mass transfer by random mixing of components consists of two associated mechanisms: molecular diffusion and convective bulk flow. A measure of the amount of mixing due to molecular diffusion is given by the diffusion coefficient  $D$ . Accurate diffusion coefficients prediction or measurement is crucial for diffusion flux calculations. In order to apply experimentally obtained data for adequate modelling of natural diffusion



processes, it is necessary to have a realistic value for actual diffusion coefficients and quantify the effect of bulk flow on total mass transfer.

In this work we focus on determination of the diffusion coefficients from simulated diffusion experiments, employing the commercial compositional simulator Eclipse 300, which support two diffusivity models. The fundamental difference is in the driving force that is based on concentration or chemical potential gradients. To the best of author knowledge, during most experiments to measure diffusion coefficients in terms of molecular motion an inherent assumption of constant mixture molar density is made (Sigmund 1976, Carmichael 1955, Berry and Koeller 1960). However, significant variation in mixture molar density with compositional variation might be the case in some hydrocarbon systems containing near-critical fluid mixtures. Therefore, simulation of diffusion experiments with strong compositional variation of mixture molar density is of special interest in this study.

This work investigates diffusion performance for binary mixture of methane-ethane, employing diffusivity model driven by concentration and chemical potential gradients. The study of the effect of molar density variation on diffusion behaviour considering a simple binary mixture, however, provides a basis for a better understanding of more realistic situations in which the mixture consist of more than two components.

## **1.2 Study objectives**

The main objective of this study is to analyse the diffusion models built in the compositional simulator Eclipse 300, where diffusive flux can be driven by concentration or chemical potential gradient. A great number of simulated diffusion experiments were conducted for wide range of reservoir pressure in order to examine the effect of diffusivity driving force on mixing performance.

The other objective of this work is to predict real diffusive behaviour, thus to understand the possible occurrence and absence of convective bulk flows and to semi-quantitatively predict bulk flow profiles and direction. The consistent comparison between theoretically found diffusion coefficients from empirical Sigmund correlation and that obtained from simulated diffusion experiments is carried out, helping to size approximately the contribution of convective flow into total mass transfer coefficients. The study was restricted to diffusion in the single gas phase, unless the cross-phase diffusion was under investigation.

### **1.3 Description of Employed Software**

#### **PhazeComp**

PhazeComp is Zick Technologies' program for compositional phase behavior computations using an equation of state (EOS). It acts as a virtual PVT (pressure-volume-temperature) laboratory and as a vehicle for tuning EOS fluid characterizations. It can simulate practically any single-cell PVT experiment one can imagine (and many multi-cell experiments as well). It will accept, as input, virtually any data that can be measured in such an experiment. It will then adjust any user-selected combination of EOS parameters to optimize the predictions of the experimental data. PhazeComp performs all of the calculations expected of a petroleum engineering PVT program, including the simulation of all standard PVT experiments, the generation of black oil PVT tables and many other capabilities. It uses any of the industry standard cubic equations of state and allows easily interface with other industry standard software, such as reservoir simulators. PhazeComp also has many other unique features. (<http://www.zicktech.com>, PhazeComp flyer).

In this study, PhazeComp used to predict mixture volumetric properties, and to generate the simulation model EOS properties of the components using Soave-Redlich-Kwong (SRK) EOS.

### **Eclipse 300**

Eclipse reservoir simulation software provides an entire spectrum of reservoir simulation, including black-oil, compositional, thermal options. It has a wide range of additional capabilities such as coal and shale gas, Enhanced oil recovery, and advanced wells modeling, CO<sub>2</sub> storage and EOR.

Eclipse 300 Compositional simulator allows to model multicomponent hydrocarbon flow. This software provides a detailed description of reservoir fluid phase behavior and compositional changes.

This numerical simulator was used to perform current simulation study dedicated to diffusivity process investigation. Eclipse 300 allows diffusion within both the oil and gas phases with specified diffusion coefficients. More importantly, it supports two diffusion models: molecular diffusion driven by concentration and chemical potential gradient, whose inter-comparison is one of the objectives of this study.

### **Petrostreamz Pipe-It**

*Petrostreamz Pipe-It* is unique software generated by Petrostreamz AS, a software company developed at PERA AS. This software allows the user to graphically and computationally integrate models and optimize petroleum assets. The main idea behind Pipe-It, is to represent a workflow in a same way it exists in reality.

In order to model any real process in oil and gas industry, has to pipe its streams computationally just as it is piped physically. User can launch any software on any operating system within Pipe-It. It chains applications together, automatically knowing the most-efficient and consistent launching sequence of all applications.

Visualization capability with an intuitive graphical layout design provides a clear vision of the project organization in a multi-level architecture, similarly as from top-level management point of view (Petrostreamz, 2013).

In this study, Pipe-It is used to simplify and summarize the Eclipse 300 runs. The basic applications inside Pipe-It were also used in extracting and post-processing data from simulation output, thus avoiding lots of manual copy and paste work that can be time consuming.

---

## Diffusion: Fundamentals and Basic Concept

---

### 2.1 Fickian diffusion and chemical potential driven diffusion

Molecular diffusion could be an efficient recovery mechanism in many applications in reservoir engineering. It plays a vital role in the oil recovery during miscible gas injection, such as CO<sub>2</sub>, in naturally fractured reservoirs. In case of low matrix permeability, thin matrix blocks, or insignificant density difference between the oil and the injected gas, viscous forces and gravity drainage become inefficient. In these cases molecular diffusion control mass-transfer rates between the matrix and fracture (Hoteit and Firoozabadi 2006). Molecular diffusion allows producing trapped oil in the matrix by creating counter current material transfer between the fracture and the matrix. In the heavy oil recovery scheme based on vapor hydrocarbon solvents, the gas solvent mixes with the heavy oil what results in viscosity reduction. The process of mixing of the solvent with the highly viscous oil in the reservoir implies a mass transfer process which is governed by a diffusion coefficient (Guerrero-Aconcha U. and Kantzas A. 2009). In rich gas flooding, injection gases containing intermediate hydrocarbon may develop miscibility with in place oil. Molecular diffusion is responsible for mixing at the pore level and has been shown to be an important rate controlling mechanism in gas flooding (Grogan and Pinczewski 1987).

Diffusion is the process by which matter is transported from one part of a system to another as a result of random molecular motions. Both experiments and theory have shown that diffusion can result from pressure gradients (pressure diffusion), temperature gradients (thermal diffusion), external force fields (forced diffusion), concentration and chemical potential gradients (Reid, R.C., Prausnitz, J.M. and Poling, B.E. 1987).

There are two widely used models to describe molecular diffusion flux for multicomponent mixtures. The first model is based on classical Fick's law. Fick presented the equation for molecular diffusion in 1885 and stated that the flux of a substance diffusing through a unit area of cross section is proportional to the concentration gradient that is measured perpendicular to the cross section:

$$J_i = -cD_i \frac{\partial x}{\partial d} \dots\dots\dots(2.1)$$

The classical Fick's law assumes that each component in the mixture transfers independently and does not interact with the other components (Hussein Hoteit 2011). The driving force for a given component is the self-concentration gradient multiplied by a diffusion coefficient.

The second approach was developed from irreversible thermodynamics of diffusion. This model assumes that diffusion occurs in order to minimize the free energy so that conditions for diffusion equilibria are that the chemical potentials be equal in each phase. The chemical potential gradient arises as the proper driving force for diffusion of each component, giving complex composition dependence of the behavior in addition to that from pressure and temperature.

Therefore, diffusion is affected by more than just intrinsic concentration gradient. It would be more appropriate to use a diffusion flux that is driven by the total potential given by chemical, gravity, and thermal forces (Bird, Stewart and Lightfoot 1960):

$$J_i = -cD_i^a x_i \frac{1}{RT} \frac{\partial}{\partial d} (\mu_i - M_i G(h - h_0) + M_i D_i^T \ln(T)) \dots\dots\dots(2.2)$$

If gravity and the thermal diffusion term in Eq. (2.2) are omitted, Eq. (2.2) can be written as:

$$J_i = -cD_i^a x_i \frac{1}{RT} \frac{\partial \mu_i}{\partial d} \dots\dots\dots(2.3)$$

where  $\mu_i = \mu_0 + RT \ln(f_i) \dots\dots\dots(2.4)$

Substituting equation for chemical potential in Eq.(2.3) gives:

$$J_i = -cD_i^a x_i \frac{\partial(\ln(f_i)_{T,P})}{\partial d} \dots\dots\dots(2.5)$$

Using the chain rule, Eq. (2.4) can be rewritten as

$$J_i = -cD_i^a \frac{\partial(\ln(f_i))}{\partial(\ln(x_i))} \frac{\partial x_i}{\partial d} \dots\dots\dots (2.6)$$

Comparing Eq. (2.1) and Eq. (2.6), the activity-corrected diffusion coefficient (Reid, Prausnitz and Poling 1998) is given by:

$$D_i^a = \frac{D_i}{\partial \ln(f_i) / \partial \ln(x_i)} \dots\dots\dots (2.7)$$

where  $D_i$  and  $D_i^a$  – classical Fickian and activity corrected diffusion coefficient respectively.

Consequently the accurate prediction or measurement of the diffusion coefficient is extremely important for diffusion flux calculation. This, however, presents a significant amount of challenges in the laboratory and in the data analysis.

## 2.2 Estimating low pressure diffusion coefficients

Binary diffusion coefficients for low pressure gases ( $D_{ij}^0$ ) can be calculated using Chapman-Enskog dilute theory resulting in the Hirschfeld et al equation (Reid, R.C., Prausnitz, J.M. and Poling, B.E. 1987):

$$D_{ij}^0 = \frac{0,001883}{P\sigma_{ij}^2\Omega_{ij}} \left( \frac{1}{M_i} + \frac{1}{M_j} \right)^{0.5} T^{1.5} \dots\dots\dots (2.8a)$$

Eq.(2.8a) based upon only a first approximation of the probability of a binary molecular interaction given by Lennard-Jones model, where:

$$\Omega_{ij} = \frac{1.06036}{T_{ij}^{0.1561}} + \frac{0.193}{\exp(0.47635T_{ij})} + \frac{1.03587}{\exp(1.52996T_{ij})} + \frac{1.76474}{\exp(3.89411T_{ij})} \dots (2.8b)$$

$$T_{ij} = \frac{T}{(\varepsilon/k)_{ij}} \dots\dots\dots (2.8c)$$

$$(\varepsilon/k)_{ij} = [(\varepsilon/k)_i(\varepsilon/k)_j]^{0.5} \dots\dots\dots (2.8d)$$

$$(\varepsilon/k)_i = 65.3T_{ci}Z_{ci}^{18/5} \dots\dots\dots (2.8e)$$

$$\sigma_{ij} = 0.5(\sigma_i + \sigma_j) \quad \dots\dots\dots(2.8f)$$

$$\sigma_i = 0.1866 \frac{V_{ci}^{1/3}}{Z_{ci}^{6/5}} \dots\dots\dots(2.8g)$$

with the diffusion coefficient,  $D_{ij}^0$  in  $\text{cm}^2/\text{s}$ ; molecular weight,  $M$ , in  $\text{g/mol}$ ; temperature,  $T$ , in  $\text{K}$ ; pressure,  $P$ , in  $\text{bar}$ ; characteristic length,  $\sigma$ , in  $\text{\AA}$ ; Lennard-Jones 12-6 potential parameter,  $\epsilon/k$ , in  $\text{K}$ ; critical volume  $V_c$  in  $\text{cm}^3/\text{gmol}$  and critical compressibility factor  $Z_c$ .

The Lennard-Jones 12-6 force potential parameter is used as the expression for the intermolecular forces between the molecules. Lennard-Jones collision diameter and the temperature are taken from correlations by Stiel and Thodos (1962) which are based on viscosity data for 16 hydrocarbon and 11 non-hydrocarbon gases.

To calculate the low-pressure density-diffusivity product one should use ideal gas law  $P^0 = \rho_m^0 RT$  inserted into Eq. 2.8a (Sigmund 1976, Whitson and Brule 2000):

$$\rho_m^0 D_{ij}^0 = \frac{0,000022648}{\sigma_{ij}^2 \Omega_{ij}} \left( \frac{1}{M_i} + \frac{1}{M_j} \right)^{0.5} T^{0.5} \dots\dots\dots(2.9)$$

### 2.3 The extended Sigmund correlation

At low to moderate pressures, binary diffusion coefficients vary inversely with pressure or density as suggested by Eq. (2.8a). At high pressures the ideal gas law does not hold anymore, because the volume of constituent molecules and their intermolecular forces strongly affect the volumetric behaviour of the gas (Whitson and Brule, 2000 ). The product  $D\rho$  is no longer constant but decreases with an increase with either  $P$  or  $\rho$ . Therefore, Eq.(2.8a) is applicable only to gases at low pressures and does not remain valid for high pressure condition in oil/gas reservoirs.

A polynomial correction for high pressure and temperature proposed by Sigmund (Sigmund 1976):

$$\frac{\rho_m D_{ij}}{\rho_m^0 D_{ij}^0} = 0.99586 + 0.096016 \rho_{pr} + 0.22035 \rho_{pr}^2 + 0.032874 \rho_{pr}^3 \dots\dots\dots (2.10)$$

The Sigmund correlation for estimating high-pressure binary diffusion coefficients requires only the component critical properties and it is based on following polynomial equation:

$$\frac{\rho_m D_{ij}}{\rho_m^0 D_{ij}^0} = A + B\rho_{pr} + C\rho_{pr}^2 + D\rho_{pr}^3 \dots\dots\dots(2.11)$$

To obtain the “universal” coefficients the large body of self- and mutual-diffusion coefficients data for a variety of systems was gathered, and a general least-squares fit of Eq. (2.11) to those data was made. The “best-fit” coefficients A, B, C, D from Eq. (2.11) was based on 344 vapor diffusion coefficients for pressures up to 690 bar, and 52 liquid diffusion coefficients of light hydrocarbons for pressures up to 275 bar. Both binary and self-diffusion data was used. There was found a good agreement between given correlation and published experiment data for many different investigations (Christoffersen 1992). Therefore Sigmund generalized correlation (Eq.2.10) is widely used in petroleum engineering.

Binary diffusion coefficients are given as a function of the mixture molar density, the low pressure density-diffusivity product and a correction factor:

$$D_{ij} = \frac{\rho_m^0 D_{ij}^0}{\rho_m} (0.99586 + 0.096016\rho_{pr} + 0.22035\rho_{pr}^2 + 0.032874\rho_{pr}^3) \dots\dots\dots(2.12)$$

The key parameter in the generalised Sigmund correlation is the mixture reduced molar density defined as :

$$\rho_{pr} = \frac{\rho_m}{\rho_{mc}} \dots\dots\dots(2.13)$$

where the mixture pseudo-critical density is obtained from :

$$\rho_{mc} = \frac{\sum_{i=1}^n Z_i V_{ci}^{2/3}}{\sum_{i=1}^n Z_i V_{ci}^{5/3}} \dots\dots\dots(2.14)$$

where  $Z_i$  and  $V_{ci}$  are the component critical molar volume and mole fraction respectively.



da Silva and Belery<sup>3</sup> noted that the Sigmund correlation does not work well for very dense gases and liquid systems and proposed the following extrapolation for  $\rho_{pr} > 3$

(Whitson and Brule 2000):

$$\frac{\rho_m D_{ij}}{\rho_m^0 D_{ij}^0} = 0.18839 \exp(1 - \rho_{pr}) \dots\dots\dots(2.15)$$

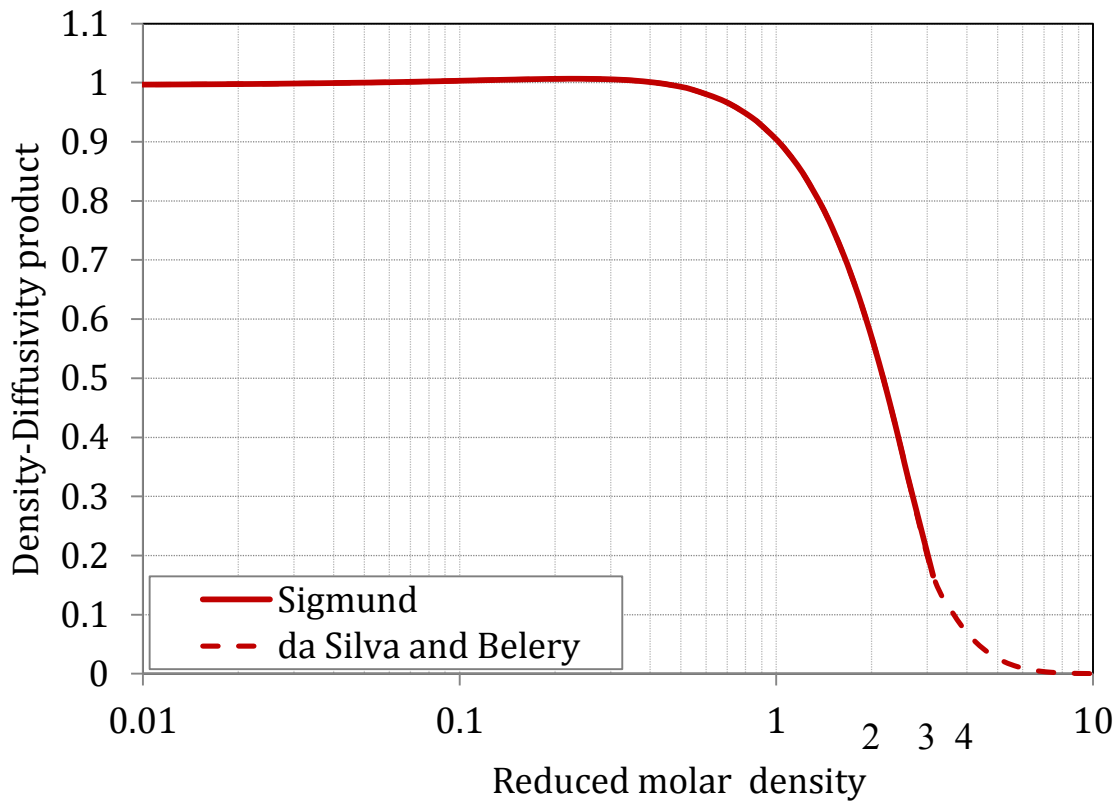


**Fig. 2.1:** The modified Sigmund diffusion coefficient correlation

Fig.2.1 shows a plot of the extended Sigmund correlation indicating the range of reduced molar densities for hydrocarbon vapour and liquid. It is clearly seen that extended Sigmund correlation is very sensitive to reduced density for liquids and dense gases ( $\rho_{mr} > 1.5$ ).

The effective diffusion coefficient for each component in a multicomponent system is given by Wilke's equation (Wilke 1950):

$$D_{im} = \frac{1 - z_i}{\sum_{\substack{j=1 \\ j \neq i}}^N z_j / D_{ij}} \dots\dots\dots(2.16)$$

where

$D_{ij}$  – binary diffusion coefficient,  $\text{cm}^2/\text{hour}$

$z_i$  - vapour or liquid mole fractions

Eq.(2.16) is based on the Stefan-Maxwell diffusion equations, and simply a weighted harmonic mean.

The diffusion coefficient from the Eqs.(2.12, 2.16) is obtained in the absence of porous media(free space). For use in porous media, the diffusion coefficient for a component should be corrected for the bulk tortuosity,  $\tau$ . Based on equation has been proposed in the literature (Brakel and Heertjes, 1974, Ulman and Aller 1982) and Archie's law the following equation is suggested for correcting the diffusion coefficient for bulk tortuosity and porosity:

$$D_{i,eff} = D_{im} \cdot \phi^{m-1} \dots\dots\dots(2.17)$$

where  $m$  is cementation factor ranging from 1 to 2.

## 2.4 Diffusion coefficients determined from laboratory experiments

This part describes the procedure of laboratory experiments, conducted by Sigmund to determine diffusion coefficients and provides a simple approximation for calculating the diffusion coefficients from experiment results. The same simplified approximation is adopted to calculate the diffusion coefficients from simulated diffusion experiments in this work, what will be discussed in Chapter 5.

A sketch of the experiment set-up is shown in Fig. 2.2.

Sigmund developed improved predictive methods for molecular diffusion coefficients in the high pressure dense gases which is commonly encountered under reservoir conditions.

To obtain diffusion coefficients from the experiments the Loschmidt diffusion apparatus was used and detailed experiment procedure has been described in the original paper (Sigmund 1976). The diffusion cell was held in vertical position and consisted of upper and lower cells. The cells had a known fixed diameter and known, approximately equal fixed lengths, designated as  $L_B$  and  $L_A$  respectively

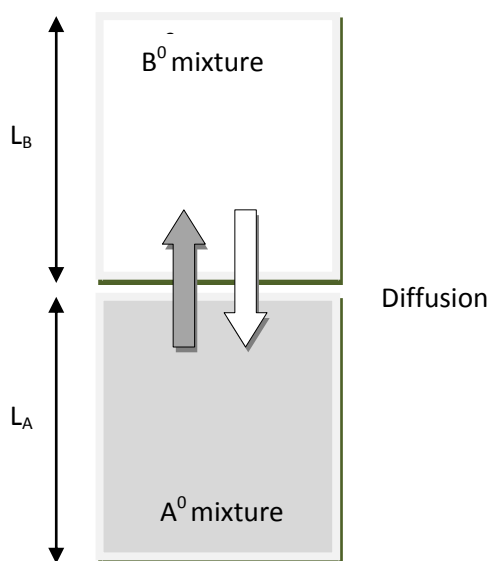


**Fig.2.2:** The Loschmidt tube set-up

for upper and lower cells. Both cells maintained at constant pressure ( $P$ )

and temperature ( $T$ ). Initially, the lower chamber was filled with gas mixture  $A^0$  to some density  $\rho_A^0$  and composition was measured and reordered  $Y_A^0$ . The gas the top chamber was filled with gas  $B^0$  to some density  $\rho_B^0$  with composition in  $Y_B^0$ .

To prevent convective mixing resulting from gravitational instability, upper mixture  $B^0$  was less dense of the pair under investigation.

The initial concentration of fluid B<sup>0</sup> in the upper cell and fluid A<sup>0</sup> in the lower cell respectively:

$$C_B^0 = \rho_B^0 \cdot Y_B^0 \text{ and } C_A^0 = \rho_A^0 \cdot Y_A^0 \dots\dots\dots(2.18)$$

At time t=0 the two chambers was connected, initiating inter-diffusion between two cells, what resulted in concentration changes between lower and upper cells. After a measured time t=θ the two chambers were again separated The final contents of each cell collected, and average final concentrations in the top and bottom cells,  $\overline{Y_B}$  and  $\overline{Y_A}$  , were then measured. Knowing volumetric properties (molar volume and density) of the fluid pairs being studied, the final concentration could be found as:

$$\overline{C_B} = \overline{\rho_B} \cdot \overline{Y_B} \dots\dots\dots(2.19)$$

and

$$\overline{C_A} = \overline{\rho_A} \cdot \overline{Y_A} \dots\dots\dots(2.20)$$

The rate of loss of diffusing substance from the semi-infinite medium is given by:

$$D \left( \frac{\partial C}{\partial x} \right)_{x=0} = \frac{DC_0}{\sqrt{\pi Dt}} \dots\dots\dots(2.22)$$

The total amount M<sub>t</sub> of diffusing substance lost from unit area in the time interval from t=0 to t=θ is given by integrating Eq. (2.22) with respect to time (J.Crank 1975):

$$M_t = \int_0^\theta \frac{DC_0}{\sqrt{\pi Dt}} dt = 2C_0 \left( \frac{D\theta}{\pi} \right)^{0.5} \left[ \frac{mole}{area} \right] \dots\dots\dots(2.23)$$

Assuming the total volumetric content of diffusing substance and applying simple rearrangements the mutual diffusion coefficients from the experiments may be determined from Eq. (2.23) by following approximations for the upper and lower cells respectively:

$$D_B = \pi \phi_B^2 L^2 \frac{1}{\theta} \dots\dots\dots(2.24)$$

$$D_A = \pi \phi_A^2 L^2 \frac{1}{\theta} \dots\dots\dots(2.25)$$

where  $\Phi_A$  and  $\Phi_B$  are the dimensionless average concentration changes in the lower and upper cells respectively. They defined as:

$$\phi_B = \frac{\overline{C_B} - C_B^0}{C_A^0 - C_B^0} \dots\dots\dots(2.26)$$

and

$$\phi_A = \frac{\overline{C_A} - C_A^0}{C_B^0 - C_A^0} \dots\dots\dots(2.27)$$

A comparison of the exact solution for diffusion in a finite cylinder with the solution given by Eq. (2.24) and (2.25) for semi-infinite cylinders has been made by McKay (McKay, 1930). His results show the difference between the two solutions to be less than 0.06% for  $\Phi$  less than 0.25. In Sigmund work the experimental times were chosen so that  $\Phi$ , in general, was between 0.15 and 0.25. The values of  $D_A$  and  $D_B$  obtained from experimental measurements for time steps (specified earlier) and the solutions to Eqs. (2.24) and (2.25) were averaged to obtain  $D_{AB}$ .

## 2.5 Variation of diffusion coefficients with composition

The Sigmund approximation and its extension (Eqs. 2.10 and 2.15) are independent of the relative proportions of the two molecular species. In such a situation it follows that for any binary system diffusion coefficients for both components are equal:  $D_{12}=D_{21}$ . As indicated earlier, at low pressures, the binary diffusion coefficients are essentially independent of composition, since molar density is proportional to pressure. However at high pressures, where the gas may deviate significantly from an ideal gas law, some effects of composition have been noted (Takahashi and Hongo 1982, Berry and Koeller 1960, Vignes 1966).

Berry and Koeller investigated diffusion in the compressed binary gaseous systems. In Fig.2.3 the experimental diffusion coefficients for methane-ethane mixture plotted as a function of gas molar densities at temperature  $T=104^0F$ . From a comparison between two trends it is seen a tendency of diffusion coefficients to decrease as molar

densities increase. The moderate effect of composition for high molar densities is apparent in the data (Fig. 2.3).

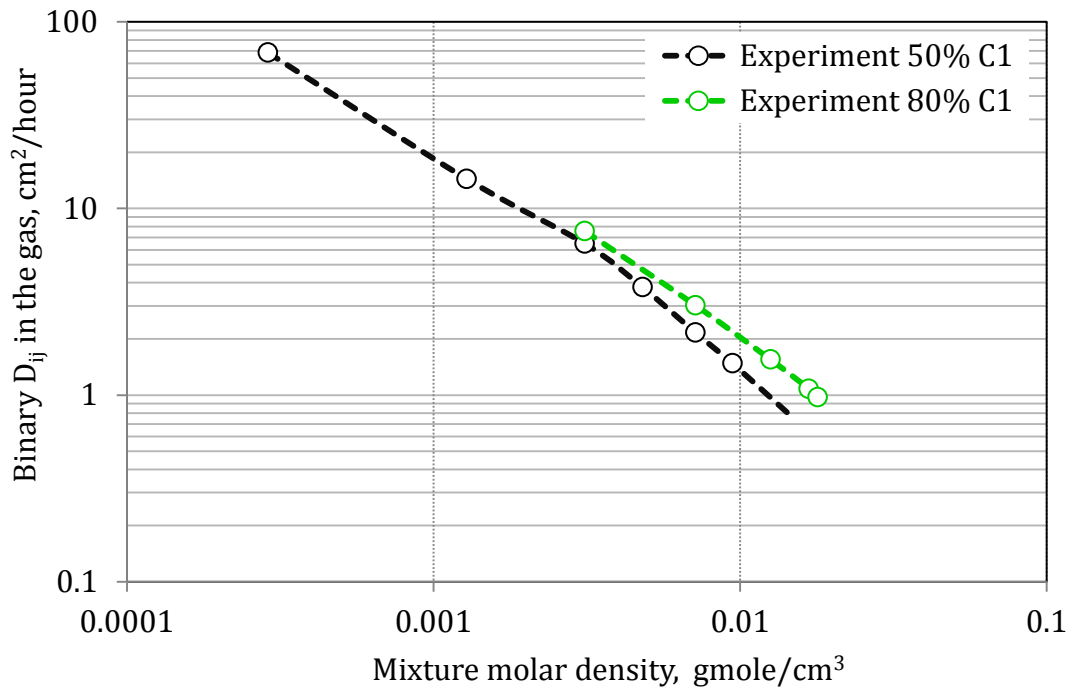


**Fig.2.3:** Experiment diffusion coefficients for the methane-ethane system at  $T=104^{\circ}\text{F}$

---

## Model description

---

### 3.1 Data description

#### 3.1.1 The Phase behavior of methane-ethane mixture

The pressure-temperature diagram (phase envelope) of the system methane-ethane is presented in Fig.3.1. The results predicted by the Soave-Redlich-Kwong (SRK) EOS using PhazeComp PVT Software. The same tool has been used to generate EOS for simulation model.

Fig. 3.1 shows the phase behavior of the binary  $C_1$ - $C_2$  mixture for several compositions and Table 3.1 summaries predicted critical points for several possible mixture compositions. On the left side of this figure, the black curve terminating at point  $C_2$ , is the vapor-pressure curve for pure ethane; the red curve on the right, terminating at point  $C_1$ , is the vapor-pressure curve for pure methane. The critical temperatures of the two pure components are connected by the other critical points of the studied mixture at different compositions, forming critical locus curve (dashed black line). With a mixture composed mainly by ethane, the critical point of the system shifts to the right toward a higher temperature, approaching that at pure ethane. The two phase region is located inside the resulting phase envelope. To the left of the phase envelope the  $C_1$ - $C_2$  mixture behaves liquid-like, and to the the right it behaves vapor-like. The region to the right from phase envelop and path along isotherm  $T=90^0F$  particularly is of our interest, since it is a minimum temperature at which  $C_1$ - $C_2$  mixture behaves vapor-like for all pressure variation at all possible composition.

| Composition, mol fraction |      | P <sub>c</sub> , psia | T <sub>c</sub> , °F |
|---------------------------|------|-----------------------|---------------------|
| C1                        | C2   |                       |                     |
| -                         | 1    | 706.6                 | 89.9                |
| 0.05                      | 0.95 | 749.9                 | 86.0                |
| 0.15                      | 0.85 | 802.84                | 73                  |
| 0.3                       | 0.7  | 884.9                 | 50.0                |
| 0.5                       | 0.5  | 968.1                 | 12.0                |
| 0.7                       | 0.3  | 968.6                 | -28.0               |
| 0.85                      | 0.15 | 876.0                 | -66.0               |
| 0.95                      | 0.05 | 748.1                 | -98.0               |
| 1                         | -    | 667.0                 | -116.7              |

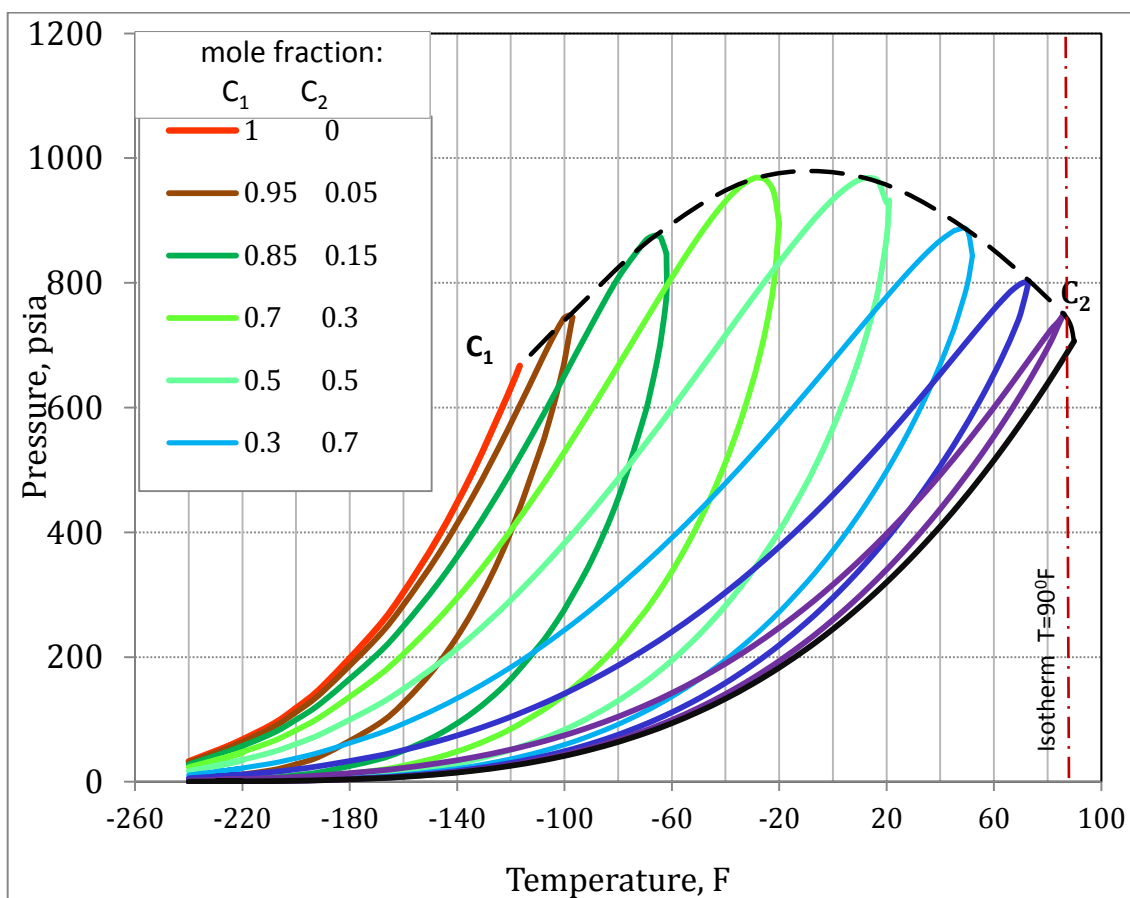


**Fig. 3.1:** Phase diagram of methane-ethane system at various components concentration



### 3.1.2 The effect of composition on binary diffusion coefficients for methane - ethane mixture

The theoretical study of diffusion coefficients has been made for the methane –ethane ( $C_1:C_2$ ) system at temperature  $T=90^0F$  and pressures up to 7000 psia (476.3 atm). To predict the variation of diffusion coefficients with composition, we considered several mixtures, consisted of : 0.9, 0.7, 0.5, 0.3 and 0.1 mole fraction of  $C_1$  in the mixture. PhazeComp PVT Software using the SRK EOS was used to determine the mixture molar densities and diffusion coefficients were calculated from extended Sigmund correlation. The Sigmund correlation for estimating high pressure binary diffusion coefficients is based on Eq. (2.12). This correlation is simple and requires only the component critical properties.

Under considering pressure-temperature combination the methane-ethane mixture exists as a single gas phase, and no phase changes occur for the whole range of mixing compositions (see chapter 3.1.1).

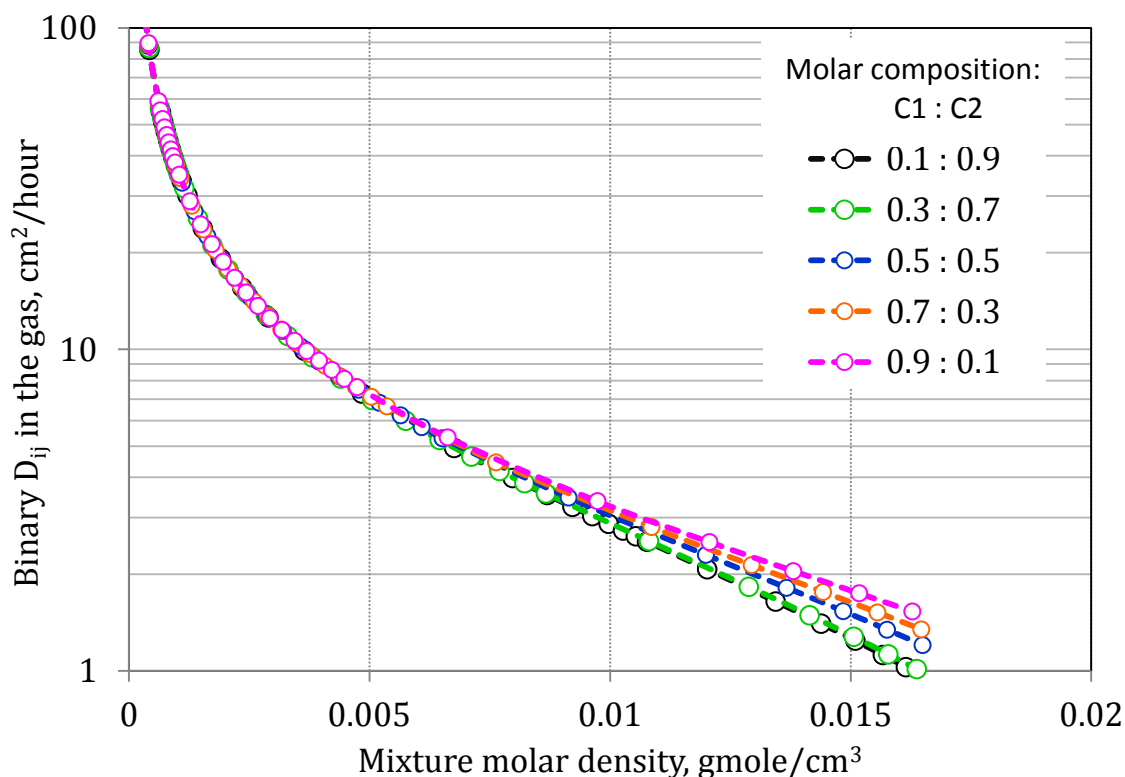


**Fig.3.2:** Diffusion coefficients for methane-ethane system at at  $T=90^0F$

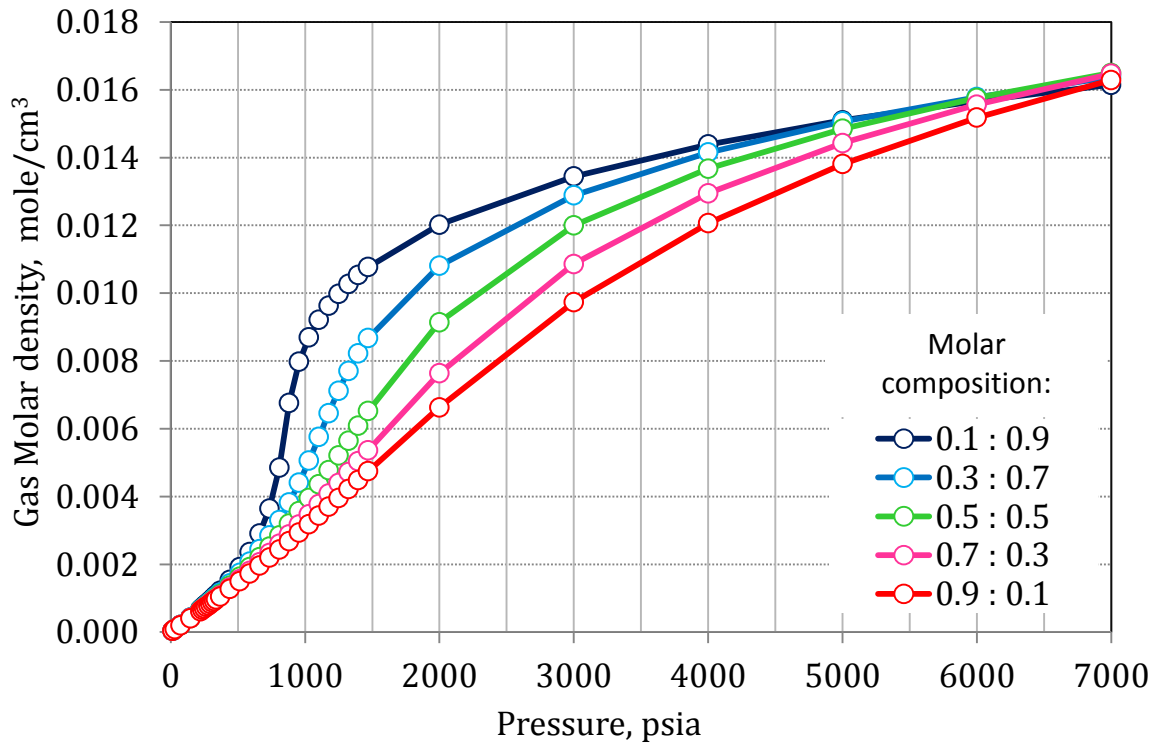


**Fig.3.3:** The molar density of the methane-ethane mixture for different compositions as a function of pressure. Temperature  $T=90^{\circ}\text{F}$

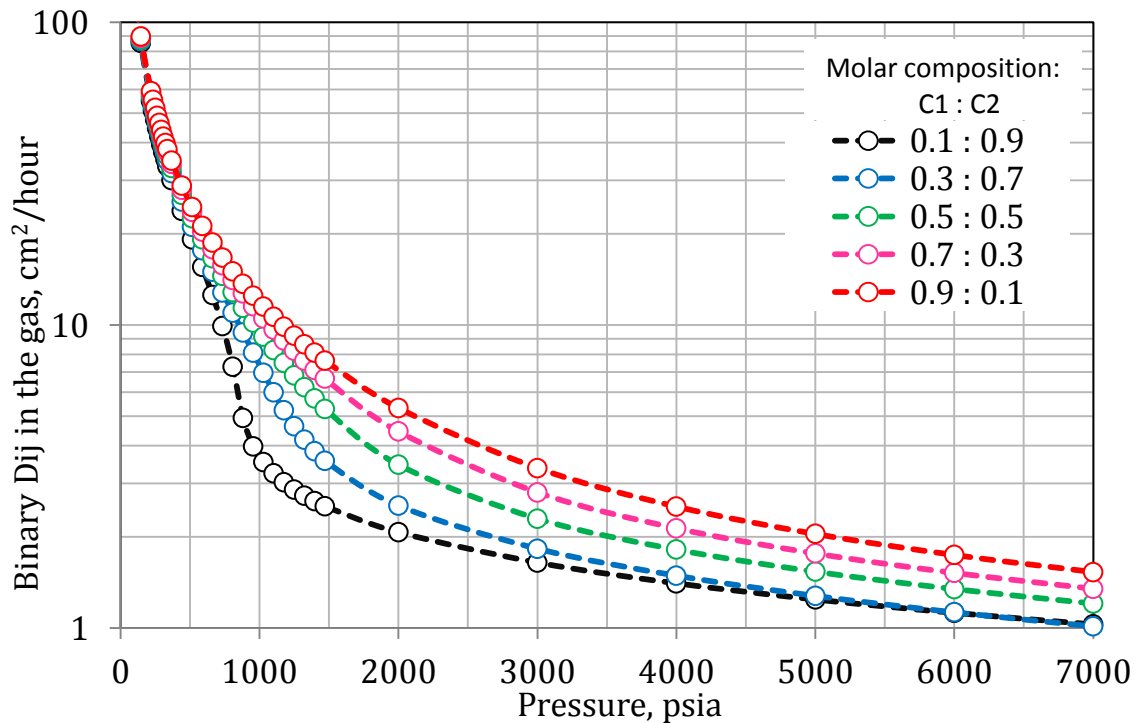


**Fig.3.4:** Diffusion coefficients for methane-ethane system for different compositions as a function of pressure. Temperature  $T=90^{\circ}\text{F}$

---

Calculation results for the molar density – pressure diagrams of methane-ethane system for five different mixture compositions are presented in Fig 3.3. At low pressures and up to about 500 psia, the mixture molar density is mainly independent of composition, what caused by ideal mixing in the methane-ethane system. As the pressure increases, the gas compresses and eventually (at just over 700 psia) the mixture molar densities diverge significantly and great effects of composition could be noted. A plausible explanation for this difference is nonideal mixing in the methane-ethane system. Intermolecular forces strongly affect the volumetric behaviour of the gas mixture, as ethane critical point is approached ( $P=707$  psia and  $T=90^{\circ}\text{F}$ ). In the near-critical region of ethane, as a pressure rises the mixture behaves differently and even a small increase in pressure causes a large increase in the density of the supercritical phase (Fig.3.3). This effect is essentially pronounced for the mixtures composed mainly of ethane ( $C_2$ ). In the same time, the molar density increases almost linearly with pressure as the methane ( $C_1$ ) concentration dominates in the mixture. Well far beyond critical region ( $P>5000$  psia), the effect of composition on molar density drops off, since volumetric properties of highly compressed gas mixtures became similar.

The diffusion coefficients obtained from predicted mixture molar density and employing extended Sigmund correlation are shown in Fig 3.4. The main trend is that the diffusion coefficients decrease with (1) increasing pressure and (2) increasing mole fraction of the heavier component ( $C_2$ ). An increase in pressure at constant composition leads to a decreased diffusion coefficient because of increased intermolecular forces and increased density, resulting in molecular motion reduction. This effect is qualitatively accounted by the Sigmund correlation, as can be seen from the Fig.3.4.

The predicted data indicates that at low pressures the diffusion coefficients are invariant with respect to composition and essentially identical. However, in the near- and over-critical region the diffusion coefficient decreases substantially, as the mole fraction of ethane in the mixture methane-ethane increases (Fig.3.4). The amplitude of difference between diffusion coefficients for «extreme» compositions is one order

of magnitude in the near-critical region. Therefore, diffusivity at constant pressure and temperature can be very sensitive to composition variation.

To predict diffusion coefficients using Sigmund correlation, one should note that Sigmund approximation is a unique function of the reduced mixture density, consequently the key parameter is the mixture molar density, which depends on mixture composition. The effect of composition may be rather modest at low and moderate pressures, however at higher pressures it can be dramatic, resulting in significant divergence of diffusion coefficients for the particular cases.

The commercial compositional reservoir simulator Eclipse 300, which is widely used in the reservoir engineering, include/comprise two diffusion models, where diffusion flux induced by either the concentration or chemical potential gradient. Both models support the effective diffusivity model and allow to set  $N_c$  diffusion coefficients, assuming them constant (where  $N_c$  – number of components).

Under the progress of simulation of diffusion process, the mixture composition changes gradually. Composition changes may cause the mixture to behave very differently as the pressure is raised. The gas nonidealities with concomitant effect on the system molar density may come important, as it was shown earlier (Fig.3.3-3.4). Consequently, the effective diffusion coefficients strong dependency of molar density is an uncertainty which might introduce a consistent error to simulation results, when diffusion coefficient is assumed to be constant all the simulation time.

In order to model diffusivity flux using Eclipse 300 simulator, a single and unique diffusion coefficient is required for each component. To predict diffusion coefficients employing Sigmund correlation, mixture molar density is required, which, in its term, is a strong function of composition. Uncertainty in proper molar density estimation has effect on magnitude of diffusion coefficient, which maybe significant in some cases. Therefore, question of appropriate composition to obtain mixture molar density arises.

The reasonable assumption could be is taking into account the mixture reduced density detected for intermediate composition at given constant pressure and

temperature. However solution now introduces some unknowing errors into predicted results.

For this study diffusion coefficient were determined for the «Base» mixture, composed of 50% mole fraction of  $C_1$  and 50% -  $C_2$ . Fig. 3.5 present molar density variation with pressure range up to 7000 psia at constant temperature  $T=90^{\circ}\text{F}$ . The considering mixture PVT properties were predicted by SRK EOS using PhazeComp Software. As describe in the chapter 2.3, diffusion coefficients were calculated from the extended Sigmund correlation and given in Figure 3.6 as a function of reduced molar density.

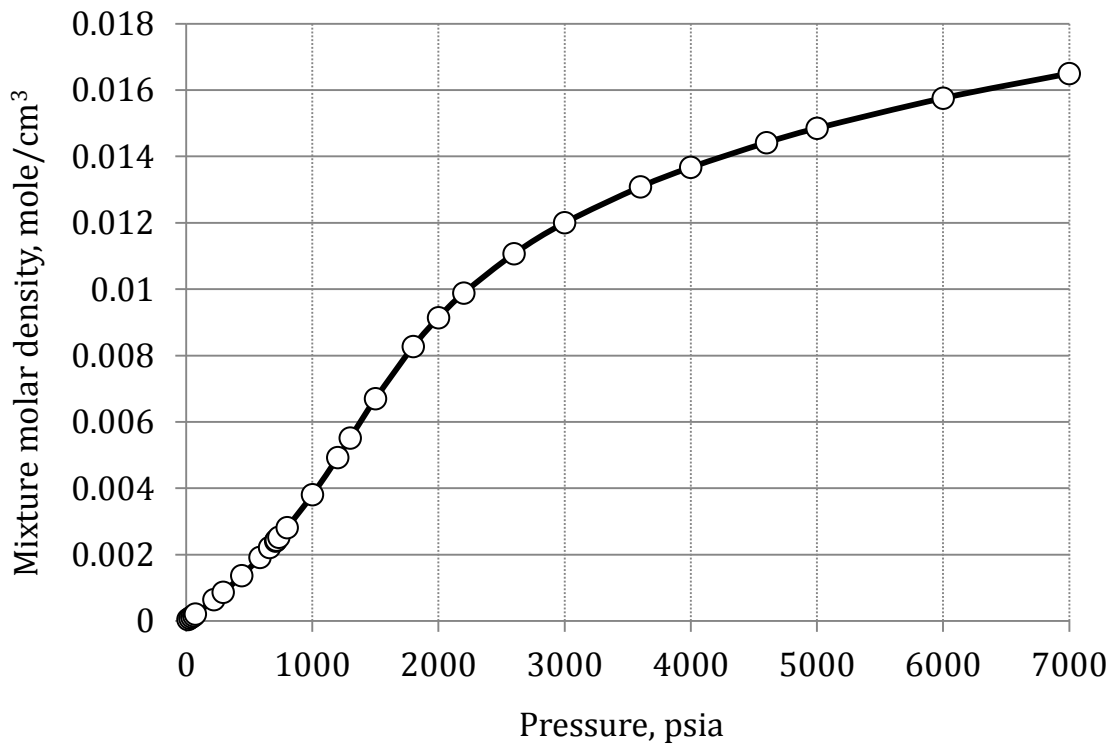


**Fig.3.5:** The molar density for 50% $C_1$ :50% $C_2$  mixture as a function of pressure.  
 $T=90^{\circ}\text{F}$ .

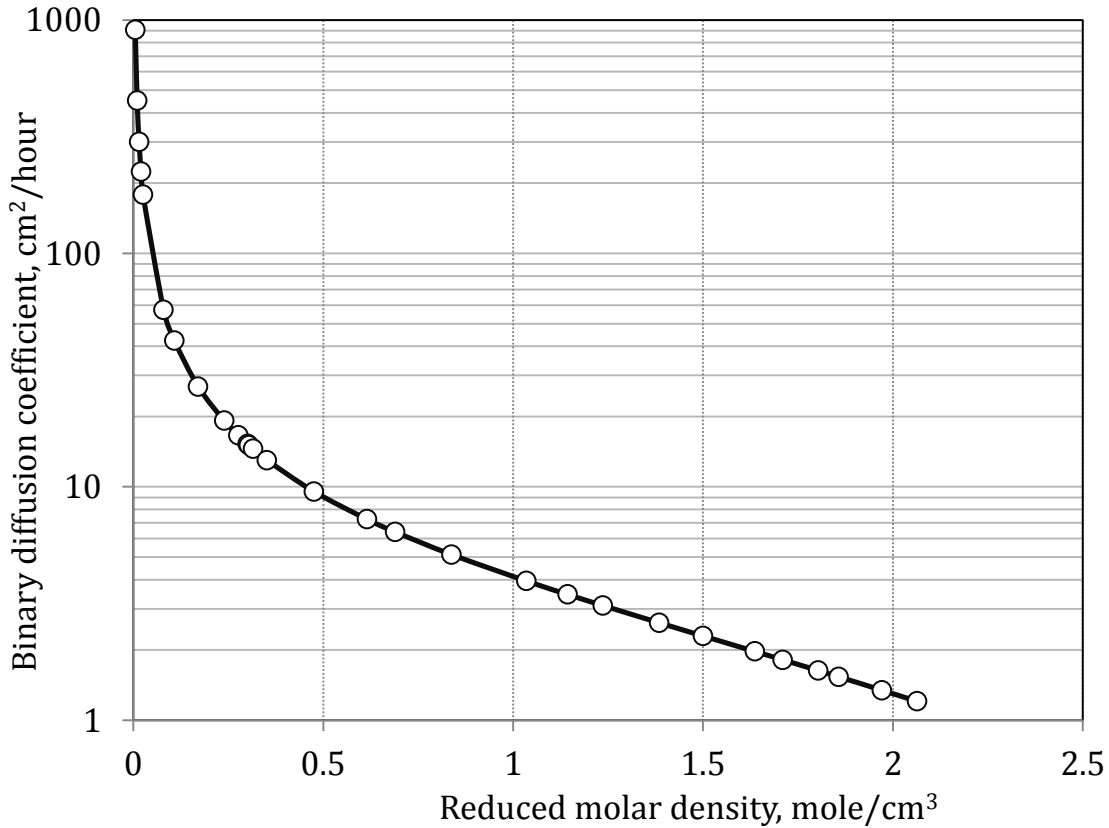


**Fig. 3.6:** Diffusion coefficients for 50% $C_1$ :50% $C_2$  mixture.  $T=90^{\circ}\text{F}$ .

### 3.2 Eclipse 300 Model description

We examine a diffusion process in the porous media, considering mixing in the binary system composed of  $C_1$  and  $C_2$  components. The commercial compositional simulator Eclipse 300 with fully implicit solution method was used for simulation study. In all the cases, the system is assumed to be isothermal. The study was restricted to diffusion in the single gas phase, unless the cross-phase diffusion was under investigation.

#### Geometry and dimensions

The model domain is a fully implicit 1D Cartesian model with 0.5, 25 and 0.25 cm of total length in x, y and z-direction respectively. Dimensions of the model are decided arbitrary. However, the domain thickness was purposely chosen to be very small ( $D_z=0.25\text{cm}$ ), so that gravity effect is excluded.

This model use one grid number along x-and z-direction ( $N_x=N_z=1$ ), while the grid optimum number in horizontal direction ( $N_y$ ) is equal 100 and its adjustment is explained in the Grid sensitivity section (Chapter 3.3). The model domain presented as 1D porous media of total length 25cm, where gases initialized such that  $C_1$  saturates one half of the domain (left side) and  $C_2$  saturates the second half. A snapshot of the domain at initialization state is shown in Fig.3.7. Counter-current diffusion starts at the initial  $C_1$ - $C_2$  contact at the middle of the domain (12.5cm).

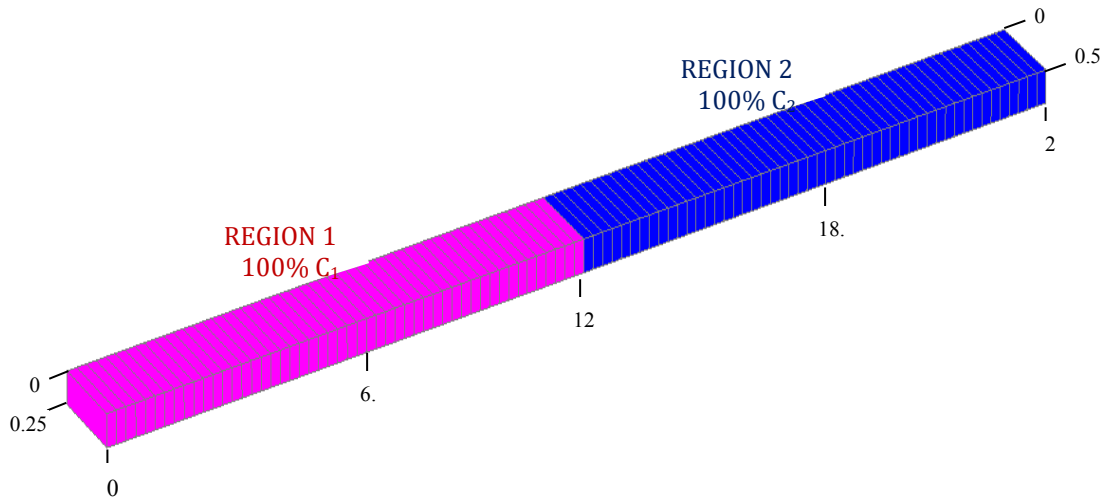


**Fig.3.7:** The model set-up with total dimensions (in cm).

Diffusivity model.

Eclipse 300 allows diffusion within both the oil and gas phases with specified diffusion coefficients. More importantly, it supports two diffusion models. In the first model, diffusion is driven by concentration gradient:

$$J_i = -cD_i \frac{\partial x}{\partial d} \dots\dots\dots(3.1)$$

In the second model, diffusion is driven by the gradient of chemical potential and in terms of component fugacity can be rewritten as a following form:

$$J_i = -cD_i^a \frac{\partial(\ln(f_i))}{\partial(\ln(x_i))} \frac{\partial x_i}{\partial d} \dots\dots\dots(3.2)$$

Therefore, there are two possible ways of specifying diffusion coefficients:

- Classical Fickian diffusion coefficients  $D_i$  defined by keywords *DIFFCOIL* and *DIFFGAS* for oil and gas phase respectively;
- Activity corrected diffusion coefficients  $D_i^a$  defined by keywords *DIFFAOIL* and *DIFFAGAS* for oil and gas phase respectively.

For horizontal flow in isothermal system relationship between diffusion coefficients can be written as:

$$D_i = D_i^a \frac{\partial \ln(f_i)}{\partial \ln(x_i)} \dots\dots\dots(3.3)$$

A consistent inter-comparison of two diffusion fluxes due to concentration and chemical potential gradient is one of the main goals of this study. Within framework of simulation study, we will set identical diffusion coefficients for both diffusivity models. Thus, any difference in diffusivity performance between two models will be induced by only diffusivity driven mechanism.

Both models support the effective diffusivity model, what allowing to set diffusion coefficients for  $C_1$  and  $C_2$  separately, assuming them constant throughout whole run time. The Sigmund correlation (Eq.2.12), which has been used to calculate diffusion coefficients, is a unique function of mixture molar density. Since it independent of relative proportions of two components, for methane-ethane binary system diffusion coefficients for both components are equal  $D_{C1}=D_{C2}$ .

#### Rock and Fluid properties

Porosity is constant throughout the model and the value is equal to 50%. Permeability was introduced to be equal 200 mD, unless convection effect is excluded. The rock compressibility is set to be zero, thus we have constant and equal pore volume for both initialization regions. The oil-gas relative permeabilities were set as a straight lines as shown in Fig.3.8. No capillary pressure was present in the system.



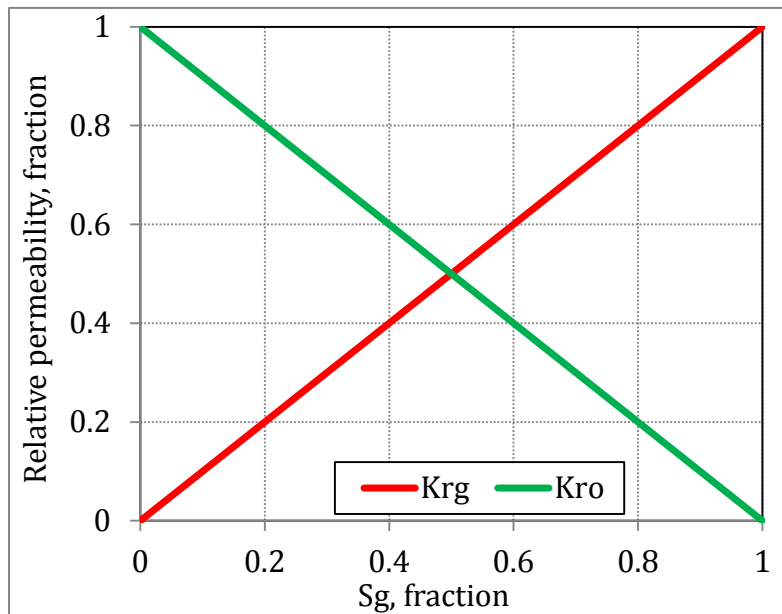


**Fig.3.8:** Oil and gas relative permeability

### The EOS description

A 2-component Soave-Redlich-Kwong (SRK) cubic equation of state (EOS) is used in numerical simulator. The EOS properties of the components were predicted by SRK EOS using PhazeComp PVT Software and are summarized in Table 3.2.

| Component      | MW     | Pc, psia | Tc, K  | Tb, K  | AF    | Vc<br>cm <sup>3</sup> /mol | Vshift | Zc    |
|----------------|--------|----------|--------|--------|-------|----------------------------|--------|-------|
| C <sub>1</sub> | 16.043 | 667.03   | 190.56 | 111.98 | 0.011 | 98.6                       | -      | 0.286 |
| C <sub>2</sub> | 30.07  | 706.62   | 305.32 | 184.84 | 0.099 | 145.5                      | 0.0589 | 0.279 |

### Time specification

Simulation is run over a period of 115 hours. The first 10 time steps are forced to be 0.001 hour. The following 500 reports come after 0.01 hour, followed by another 500 reports 500 with time-step interval -0.02 hour. The most of the run time (100 hours) reports come each 0.05 hour until the end of simulation.

### 3.3 Grid sensitivity analyses

Current simulation studies are targeted at obtaining accurate assessments and predictions of diffusion process. However, accurately predicting any reservoir performance is a challenging issue. One of the sources of uncertainty which can seriously impact diffusion performance is spatial discretization of the model into grid blocks. Since the discretization error proportional to  $x^2$ , the smaller the grid blocks used, the smaller will be the error involved. For the same length/area/volume, the smaller the grid blocks, more number of grids one need to use. As a rule, with increasing number of grid blocks in the model the computing time increase as well. Therefore, it is crucial to have optimum grids number and distribution so that the model could be representative enough to meet the study objectives with the reasonable computing time.

A numerical grid sensitivity analysis was performed to evaluate its impact on diffusion performance. A fully implicit horizontal 1D Cartesian model was used as an experiment media. The objective of the study is to find the optimum number of grid blocks in y-direction (along the path of molecular motion), while number of grid in x- and z-direction is set to be one. Grid sensitivity analysis was performed at 707psia system pressure and temperature was set equal 90<sup>0</sup>F.

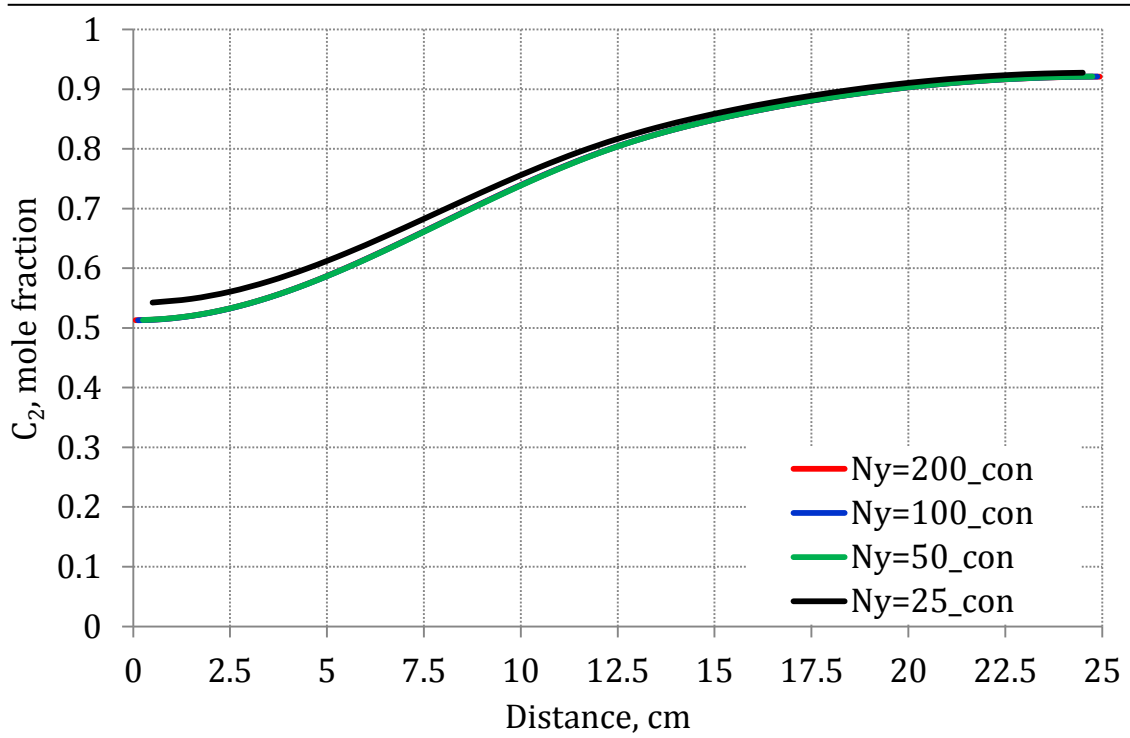
In  $N_y$  sensitivity, the Eclipse 300 simulation was run with  $N_x = 1$  and  $N_y = 1$ , while the  $N_y$  value is varied from 25 to 200. The simulation results are then compared to find the converged solution.

Fig. 3.11 and Fig. 3.10 show the comparison of  $C_2$  component distribution profile with increasing  $N_y$  values for concentration and chemical potential driven diffusion respectively. The simulation results presented for the time 10 hours after initialization of diffusion. As the number of grid in y-direction increase the results start to converge. However, the 1x25x1 ( $N_x \times N_y \times N_z$ ) grid resulted in a slightly faster diffusivity and does not follow the concentration profile of the other cases (Fig. 3.9, Fig. 3.10).

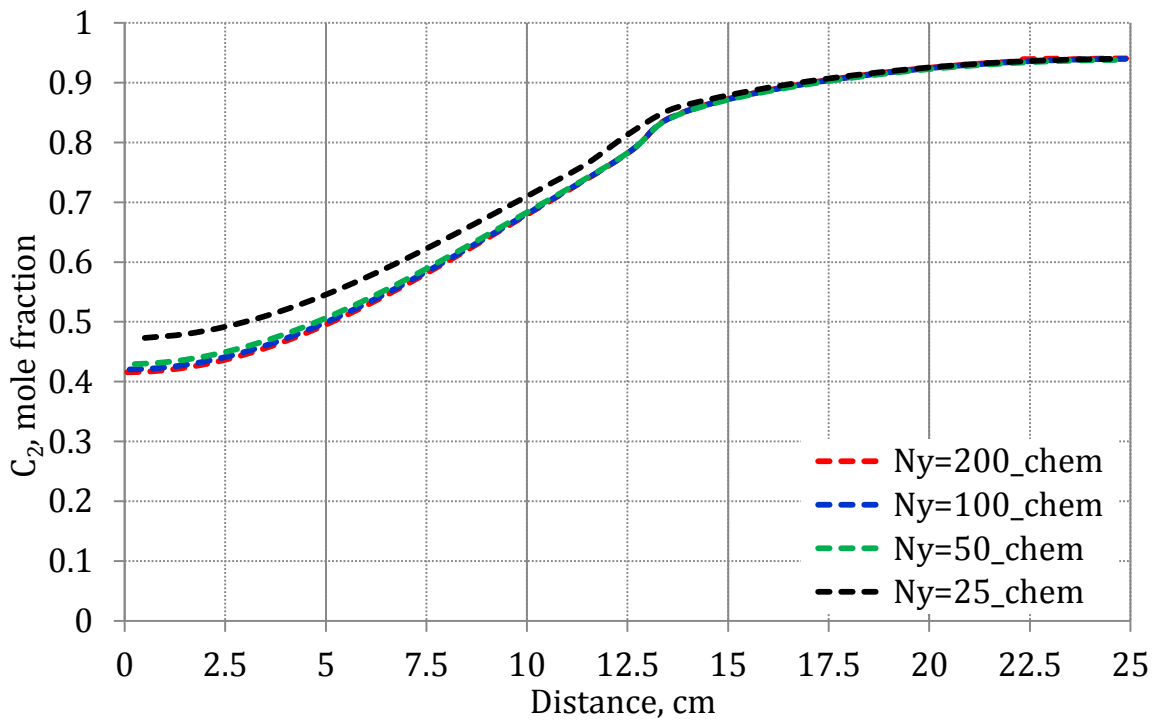
$C_2$  distribution profile for  $N_y = 100$  and  $N_y = 200$  is in close agreement, for both concentration and chemical potential driven diffusion models. Thus it could be concluded that with  $N_y = 100$  we already have a converged solution. The next step is to observe how CPU time varies with different grid models.

Table 3.3 provides the summary of simulation results: grid number, grid dimension and CPU time. For this generic model, it was observed that the CPU time increases as the grid number increases for both diffusivity models. CPU time for  $N_y = 100$  grid is less than  $N_y = 200$  by almost 1.5 times. Since simulation results for both grid models are in close agreement, a model with shorter CPU time is always preferable, since a large number of simulation cases will need to be run. For future work in this study,  $N_y = 100$  will be used in the model to perform diffusion experiments.

| TABLE 3.3: COMPUTING TIME SUMMARY |       |       |                |       |       |                       |                |                          |
|-----------------------------------|-------|-------|----------------|-------|-------|-----------------------|----------------|--------------------------|
| Model size                        |       |       | Grid dimension |       |       | Number of grid blocks | CPU time, sec  |                          |
| Lx, cm                            | Ly,cm | Lz,cm | Dx,cm          | Dy,cm | Dz,cm | NX*NY*NZ              | Concentr model | Chemical potential model |
| 0.5                               | 25    | 0.25  | 0.5            | 0.125 | 0.25  | 1*200*1               | 111.96         | 120.95                   |
| 0.5                               | 25    | 0.25  | 0.5            | 0.25  | 0.25  | 1*100*1               | 78.5           | 86.38                    |
| 0.5                               | 25    | 0.25  | 0.5            | 0.5   | 0.25  | 1*50*1                | 69.39          | 75.5                     |
| 0.5                               | 25    | 0.25  | 0.5            | 1     | 0.25  | 1*25*1                | 67.83          | 70.28                    |



**Fig. 3.9:**  $C_2$  distribution profile at time  $T=10$  hours. Concentration diffusivity model



**Fig. 3.10:**  $C_2$  distribution profile at time  $T=10$  hours.  
Chemical potential diffusivity model

### 3.4 Automated model post-processing

Before we unfold the results from current study and discussing them in detail, we would like to make a description of utilised Pipe-It project architecture and simulation results post-processing. Main elements composing a Pipe-It project are Resources, Connectors, Processes and Composites. The resources are mainly input and output files and can be any file stored on the hard disk or network that contains information related to a quantity. A process is an operation performed on a Resource which results in the production of another Resource. A process represents a launched application; It can be an integrated Pipe-It application, or any third party software, which possible to be executed from a command line (Excel, PhazeComp, Eclipse, etc.). The connectors link Resources to Processes and the over way round. Linkz is a built-in feature within Pipe-It, providing an intuitive graphical interface (GUI) to access input and output information located in Resources. User can “link” to the different types of information such as numbers, text, vectors, or matrices. The Pipe-It Runner engine creates the order of applications launching according to how the connectors are designed. The composites allow grouping several Resources and Processes into a single element, providing more clear visualization of the Pipe-It project structure (Petrostreamz, 2013).

To perform diffusivity experiments, the Pipe-It project was divided into four modules (Fig.3.11). The first one is in charge of pre-calculation of diffusion coefficients. The second one is responsible for Eclipse 300 model initialization. The last two modules represent post-processing of simulation results.

The “Diffusion coefficients” composite structure is quite simple and consist of two steps calculations, employing PhazeComp PVT software and Excel (Fig.3.12). The “Eclipse\_300 MODEL” composite includes two diffusivity models, based on concentration and chemical potential driven mechanisms; and its primary function is to initialize and execute both models using Eclipse 300 compositional simulator (Fig.3.13).

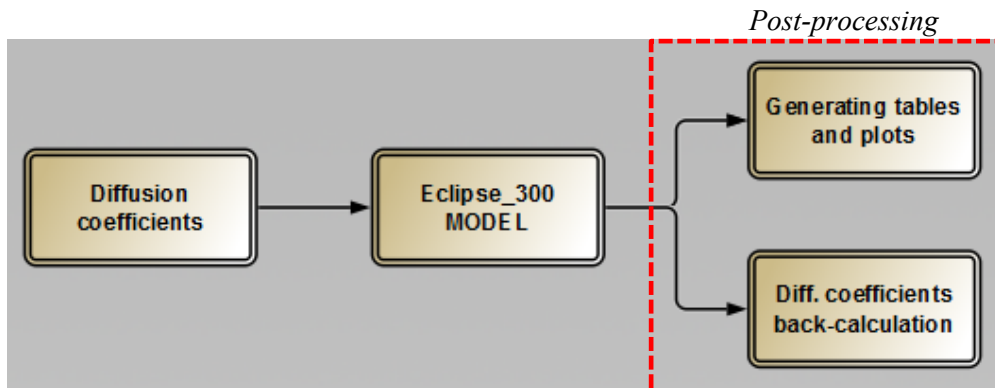


**Fig.3.11:** Pipe-It project architecture comprising four parts

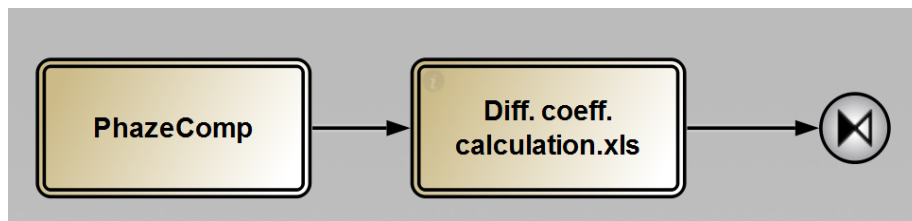


**Fig.3.12:** The "Diffusion coefficients" composite structure

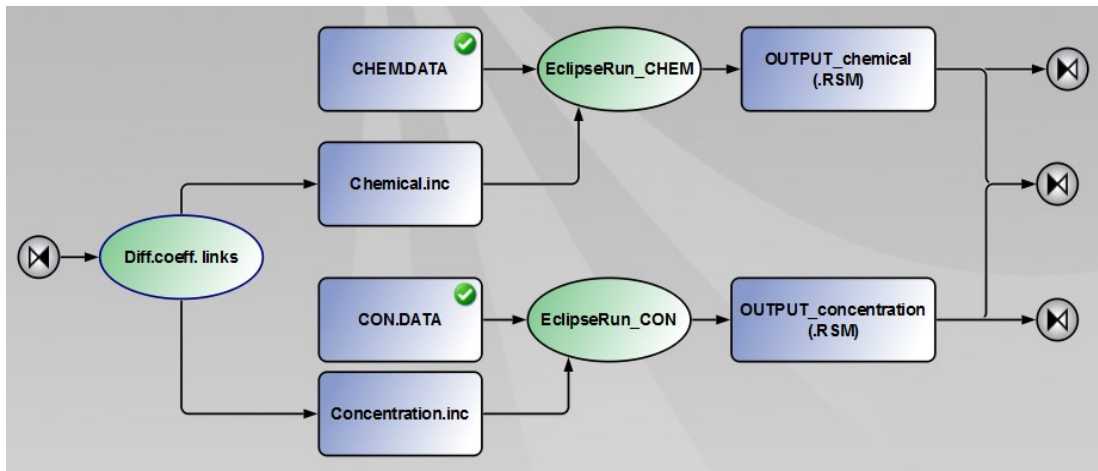
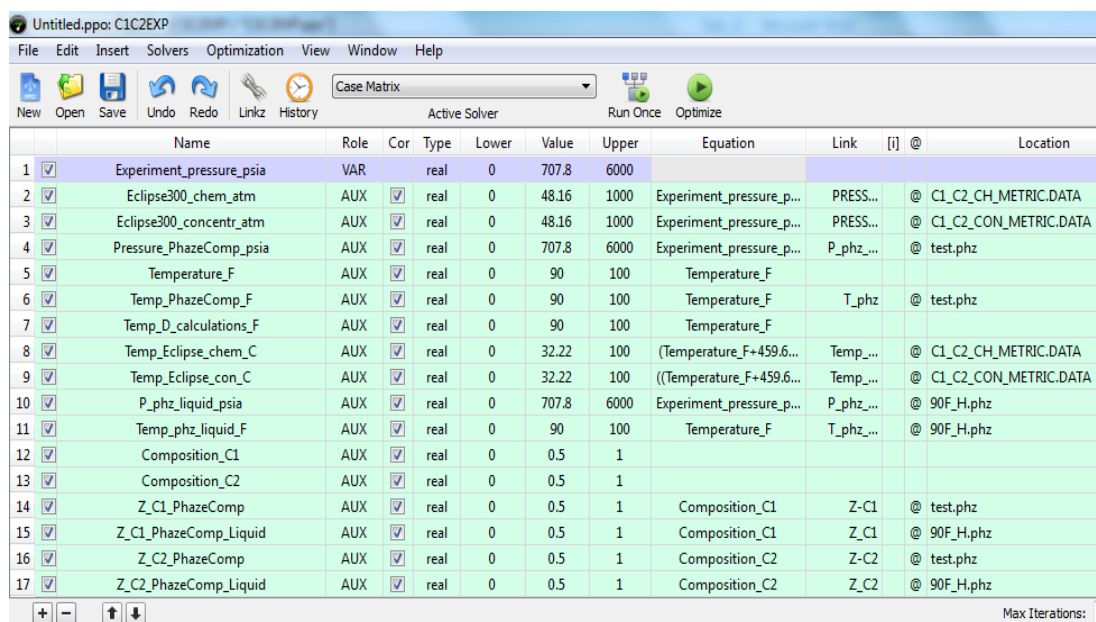


**Fig.3.13:** The "Eclipse300\_MODEL" composite structure

The main experiment properties such as pressure, temperature, mixture composition and media permeability must be assigned for every new experiment initialization. All these properties are defined in the PhazeComp and Eclipse 300 input files. The same properties were assigned as variables in the Optimizer module of Pipe-It (Fig. 3.14).

Several links have been created using Linkz feature, so that all the variables in processes input files could be updated with new experiment values automatically. The optimizer module updates values of variables in the PhazeComp and Eclipse 300 input files consecutively.

The Pipe-It simulator first executes composite called “Diffusion coefficients” using new pressure, temperature and composition values. The resulting output from this composite contains values of diffusion coefficients for vapour and liquid (if it exists for a given pressure-temperature condition) phases. Once the diffusion coefficients for  $C_1$  and  $C_2$  component are obtained (which are basically equal), Pipe-It simulator start running the “Eclipse\_300 MODEL” composite in manner hereinafter mentioned. The Maplinkz application updates diffusion coefficients inside Eclipse 300 Data files for both concentration and chemical potential gradient driven diffusion. As mentioned in the chapter 3.2, diffusion coefficients are entered equal for both diffusivity models, and they defined in the include files named as “Concentration.inc” and ”Chem.potential.inc” in accordance to the diffusivity model. Pipe-It runs Eclipse models with those values. Experiment pressure and temperature in the Eclipse Data files updated by Optimizer.



The screenshot shows the Pipe-It Optimizer interface with a table of optimization variables. The table has columns for Name, Role, Cor, Type, Lower, Value, Upper, Equation, Link, [i], @, and Location. The variables are listed as follows:

|    | Name                     | Role | Cor                                 | Type | Lower | Value | Upper | Equation                 | Link     | [i] | @ | Location              |
|----|--------------------------|------|-------------------------------------|------|-------|-------|-------|--------------------------|----------|-----|---|-----------------------|
| 1  | Experiment_pressure_psia | VAR  |                                     | real | 0     | 707.8 | 6000  |                          |          |     |   |                       |
| 2  | Eclipse300_chem_atm      | AUX  | <input checked="" type="checkbox"/> | real | 0     | 48.16 | 1000  | Experiment_pressure_p... | PRESS... |     | @ | C1_C2_CH_METRIC.DATA  |
| 3  | Eclipse300_concentr_atm  | AUX  | <input checked="" type="checkbox"/> | real | 0     | 48.16 | 1000  | Experiment_pressure_p... | PRESS... |     | @ | C1_C2_CON_METRIC.DATA |
| 4  | Pressure_PhazeComp_psia  | AUX  | <input checked="" type="checkbox"/> | real | 0     | 707.8 | 6000  | Experiment_pressure_p... | P_phz... |     | @ | test.phz              |
| 5  | Temperature_F            | AUX  | <input checked="" type="checkbox"/> | real | 0     | 90    | 100   | Temperature_F            |          |     |   |                       |
| 6  | Temp_PhazeComp_F         | AUX  | <input checked="" type="checkbox"/> | real | 0     | 90    | 100   | Temperature_F            | T_phz    |     | @ | test.phz              |
| 7  | Temp_D_calculations_F    | AUX  | <input checked="" type="checkbox"/> | real | 0     | 90    | 100   | Temperature_F            |          |     |   |                       |
| 8  | Temp_Eclipse_chem_C      | AUX  | <input checked="" type="checkbox"/> | real | 0     | 32.22 | 100   | (Temperature_F+459.6...  | Temp...  |     | @ | C1_C2_CH_METRIC.DATA  |
| 9  | Temp_Eclipse_con_C       | AUX  | <input checked="" type="checkbox"/> | real | 0     | 32.22 | 100   | ((Temperature_F+459.6... | Temp...  |     | @ | C1_C2_CON_METRIC.DATA |
| 10 | P_phz_liquid_psia        | AUX  | <input checked="" type="checkbox"/> | real | 0     | 707.8 | 6000  | Experiment_pressure_p... | P_phz... |     | @ | 90F_H.phz             |
| 11 | Temp_phz_liquid_F        | AUX  | <input checked="" type="checkbox"/> | real | 0     | 90    | 100   | Temperature_F            | T_phz... |     | @ | 90F_H.phz             |
| 12 | Composition_C1           | AUX  | <input checked="" type="checkbox"/> | real | 0     | 0.5   | 1     |                          |          |     |   |                       |
| 13 | Composition_C2           | AUX  | <input checked="" type="checkbox"/> | real | 0     | 0.5   | 1     |                          |          |     |   |                       |
| 14 | Z_C1_PhazeComp           | AUX  | <input checked="" type="checkbox"/> | real | 0     | 0.5   | 1     | Composition_C1           | Z-C1     |     | @ | test.phz              |
| 15 | Z_C1_PhazeComp_Liquid    | AUX  | <input checked="" type="checkbox"/> | real | 0     | 0.5   | 1     | Composition_C1           | Z_C1     |     | @ | 90F_H.phz             |
| 16 | Z_C2_PhazeComp           | AUX  | <input checked="" type="checkbox"/> | real | 0     | 0.5   | 1     | Composition_C2           | Z-C2     |     | @ | test.phz              |
| 17 | Z_C2_PhazeComp_Liquid    | AUX  | <input checked="" type="checkbox"/> | real | 0     | 0.5   | 1     | Composition_C2           | Z_C2     |     | @ | 90F_H.phz             |

**Fig.3.14:** Outline of Pipe-It Optimizer used to set up optimizations

Post processing is represented by composite named «Diff. coefficients calculation» and based on determination of diffusion coefficients from diffusion experiments using Eclipse 300 simulator. We used Sigmund methodology for diffusion experiment interpretation (chapter 2.4). In order to accomplish all the necessary calculations certain data must be provided. MapLinkz application is used again to access required values from Eclipse output files and link them to the Excel file sheets, where calculations are carried out. (RSM and PRT). Once case is executed and all information is available, an intuitive GUI will generate tables and display plots for properties of our particular interest, what easily allows us to make a comparison of diffusivity performance induced by composition and chemical potential gradients (Fig.3.15). The built-in application called txt2str converts a delimited text files, such as Eclipse .RSM output file, into a Streamz format. The plots for pressure, molar density, fugacity and component mole fraction profiles are generated directly from those Streamz files, combining data from both diffusivity models. Then plots automatically saved on the hard disk as .plot files and will be updated after each model execution. A great number of diffusion experiments, with different pressure-temperature-composition values, are performed using Pipe-it project. For every new experiment initialisation, the modules inside the project were executed all other again. The Pipe-It exclusive features/capabilities and built-in applications used to obtain and extract data from simulation resulting output files, allowed to save time and avoid lots of manual copy and paste work that could be time consuming.

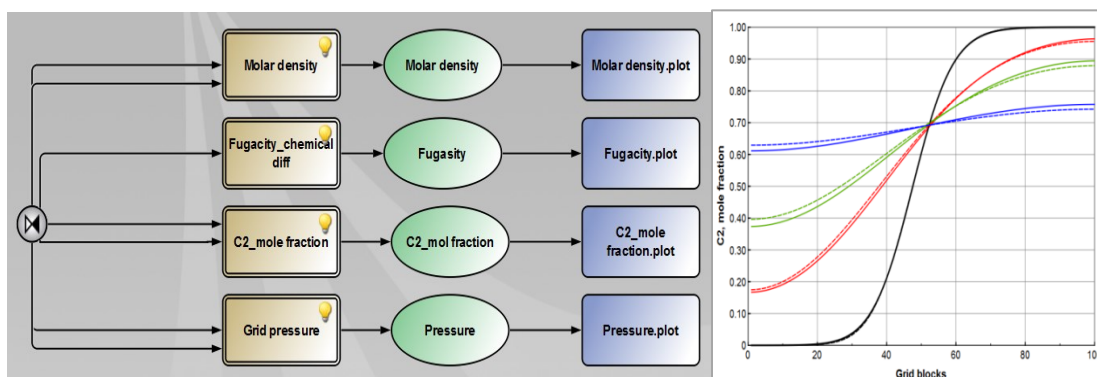


**Fig.3.15:** The "Generating tables and plots" composite structure.

Plotting streamz files within Pipe-It.



## Interpreting simulated diffusion experiments

### 4.1 Low pressure simulation results

At low pressures the diffusion coefficients are inversely proportional to pressure; that is, the diffusion coefficient times the mixture molar density gives a constant value. Plot of calculated diffusion coefficients for  $C_1$ - $C_2$  mixture is given in Fig 4.1, demonstrating that the density-diffusivity product at low pressure is essentially a constant.

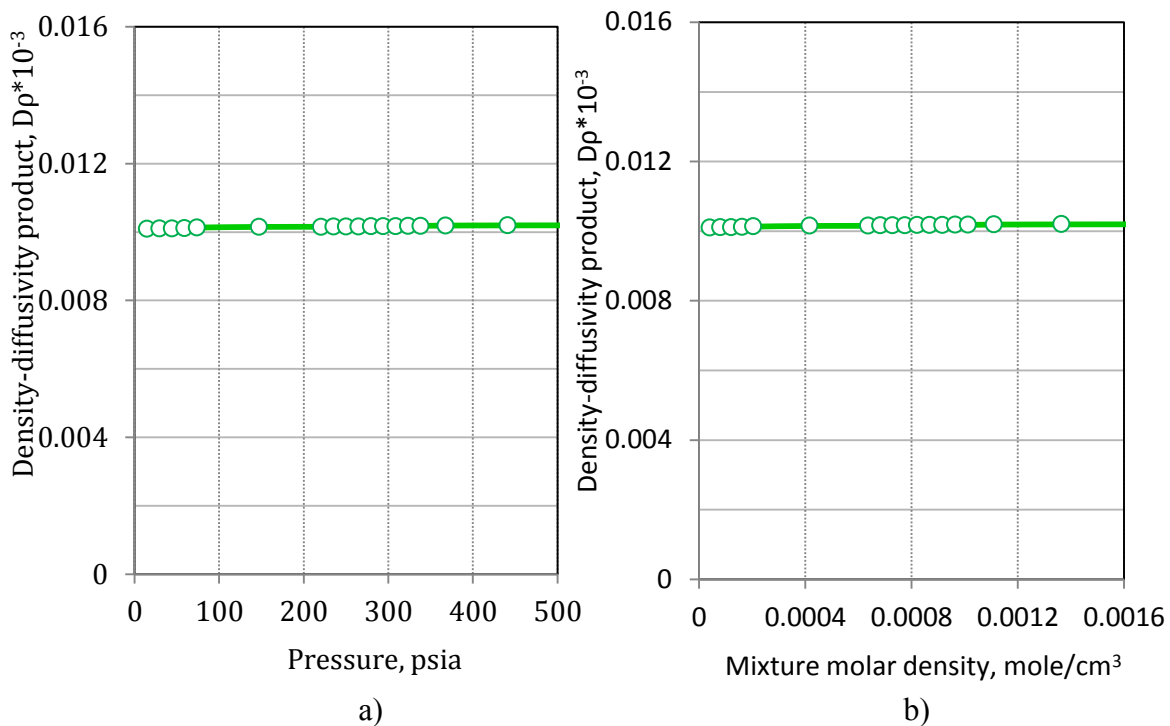


**Fig.4.1:** Density-diffusivity product of  $C_1$ - $C_2$  mixture at  $T=90^{\circ}\text{F}$  as a function of:

a) pressure, b) mixture molar density

The low pressure cases were run at constant temperature  $T=90^{\circ}\text{F}$  using Eclipse 300 model and Pipe-It project. Simulation results for initialization pressure equal 1 atm and 5 atm are shown in Figs. 4.2 -4.4, demonstrating comparison of concentration and chemical potential driven diffusivities. Pressure profiles along the model length at different time steps are shown in Fig 4.2. Pressure trend stays steady and exhibits no pressure variation throughout whole run time. Fig.4.3 shows mole fraction-distance profile for  $\text{C}_2$  component at different time steps. Fig. 4.4 also presents  $\text{C}_2$  profiles, but plotted for selected grid blocks position as a function of time. It is clearly seen from the Fig.4.4 that time before  $\text{C}_2$  profile reached equilibrium distribution were 0.5 hours for model with pressure  $P=1\text{atm}$  and 2 hours for  $P=5\text{atm}$ . The diffusivity is always faster for the lowest pressure model, what is caused by higher diffusion coefficients at lower pressure.

Both diffusivity models, driven by concentration and chemical potential gradients, demonstrate particularly no difference in diffusion performance. Observation of simulation results (Figs. 4.2 -4.4) does not show any effect of diffusion driven mechanism: trends for both diffusivity models do overlap for all properties under our study. The reasonable explanation is that at low pressures predicted flows induced by concentration and chemical potential gradient become the same.

The chemical potential of given component is proportional to its fugacity:  $\mu \sim \ln(f)$ . In chemical thermodynamics, the fugacity of a real gas is an effective pressure which replaces the true mechanical pressure in accurate chemical equilibrium calculations. The ideal gas pressure and fugacity are related through the dimensionless fugacity coefficient  $\phi$ :

$$\phi_i = \frac{f_i}{x_i P} \dots\dots\dots(4.1)$$

Since at low pressure component fugacity tends to be equal ideal gas pressure  $f_i \rightarrow x_i P$ , we can write following simple transformations:

$$\frac{\partial \ln(f_i)}{\partial d} \rightarrow \frac{\partial \ln(x_i)}{\partial d} \rightarrow \frac{1}{x_i} \frac{\partial x_i}{\partial d} \dots\dots\dots(4.2)$$

Substituting Eq. (4.2) into equation for chemical potential driven flux gives following expression:

$$J_i = -cD_i^a x_i \frac{\partial \ln(f_i)_{T,P}}{\partial d} = -cD_i^a \frac{\partial x_i}{\partial d} \dots\dots\dots (4.3)$$

Within framework of the current study we assume  $D_i^a = D_i$  for all simulation runs, what leads to the equivalent flow expressions for both concentration and chemical potential gradient driven diffusion:

$$J_i = -cD_i \frac{\partial x_i}{\partial d} = -cD_i^a \frac{\partial x_i}{\partial d} \dots\dots\dots (4.4)$$

In summary, for low pressure cases, when mixture follows ideal gas law, fugacity and pressure are equal. Thus, we observe no difference in performance between the two diffusion models and flux equivalence at low pressures.

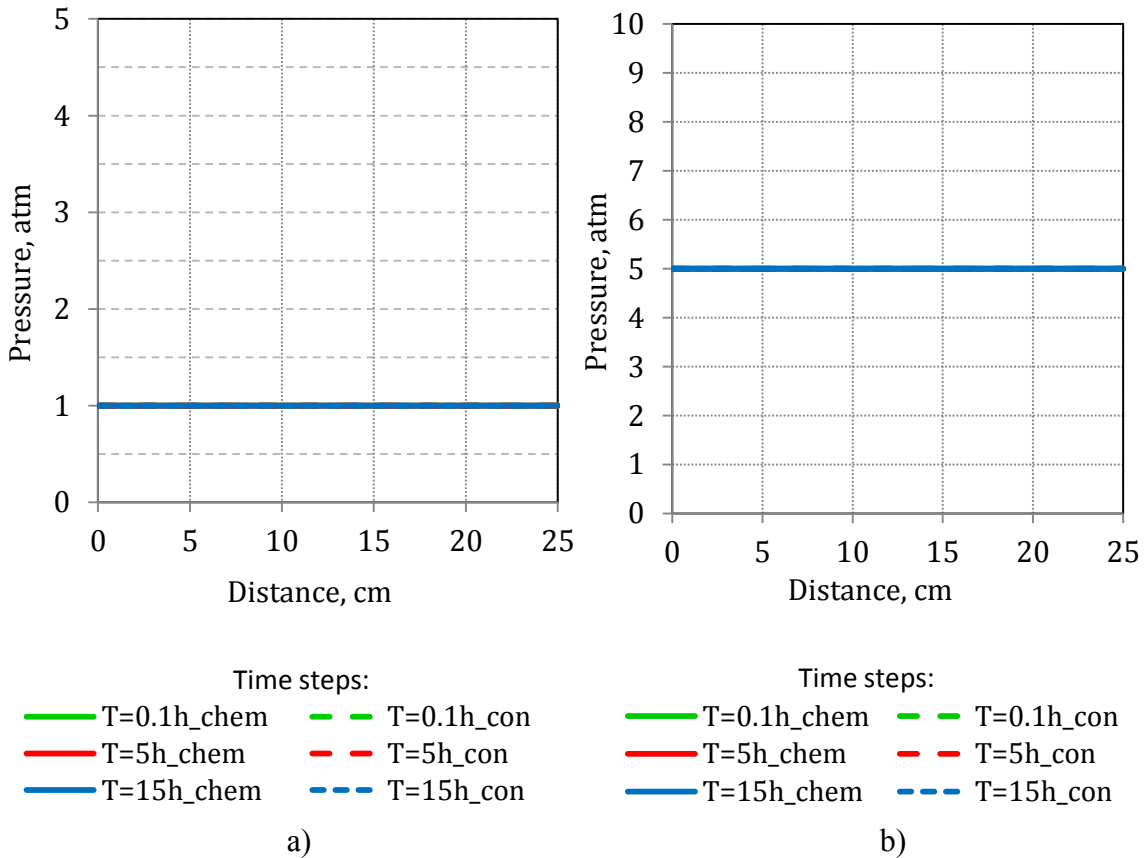


**Fig.4.2:** Pressure-distance profile at different time steps for initialisation pressure:  
 a)  $P_{init}=1atm$ , b)  $P_{init}=5atm$

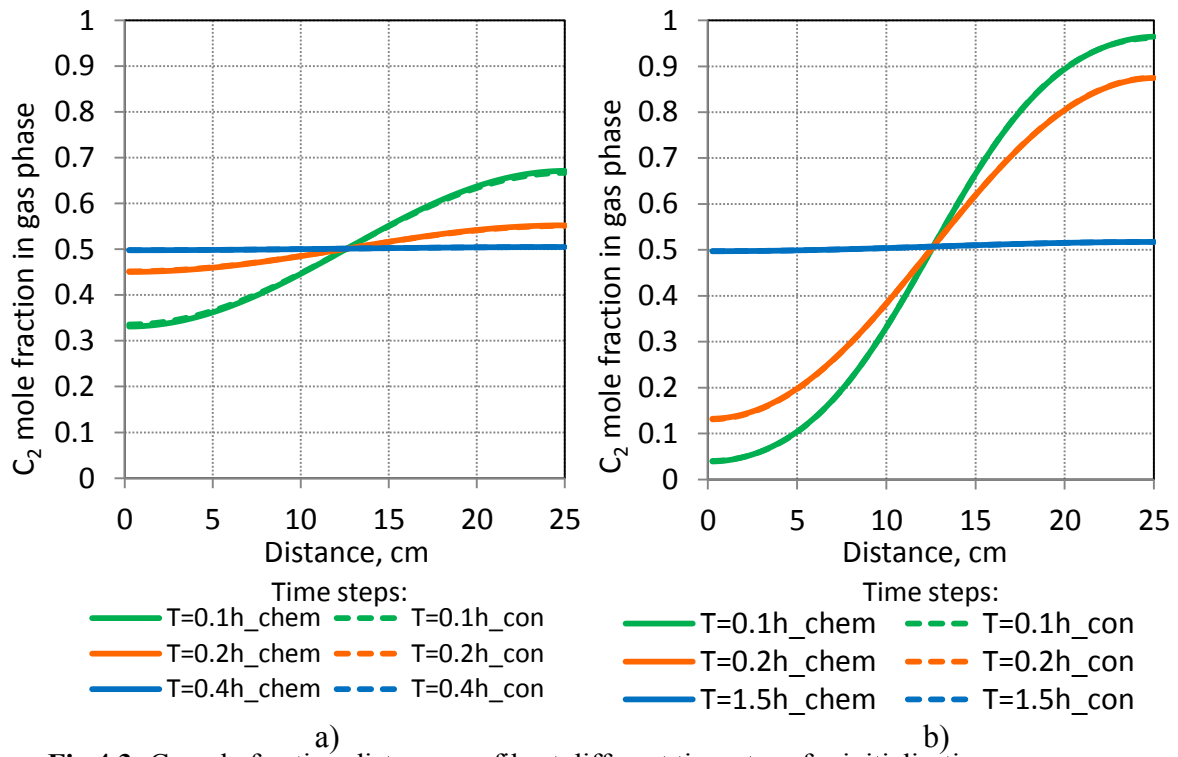


**Fig.4.3:** C<sub>2</sub> mole fraction-distance profile at different time steps for initialisation pressure: a) P<sub>init</sub>=1atm, b) P<sub>init</sub>=5atm

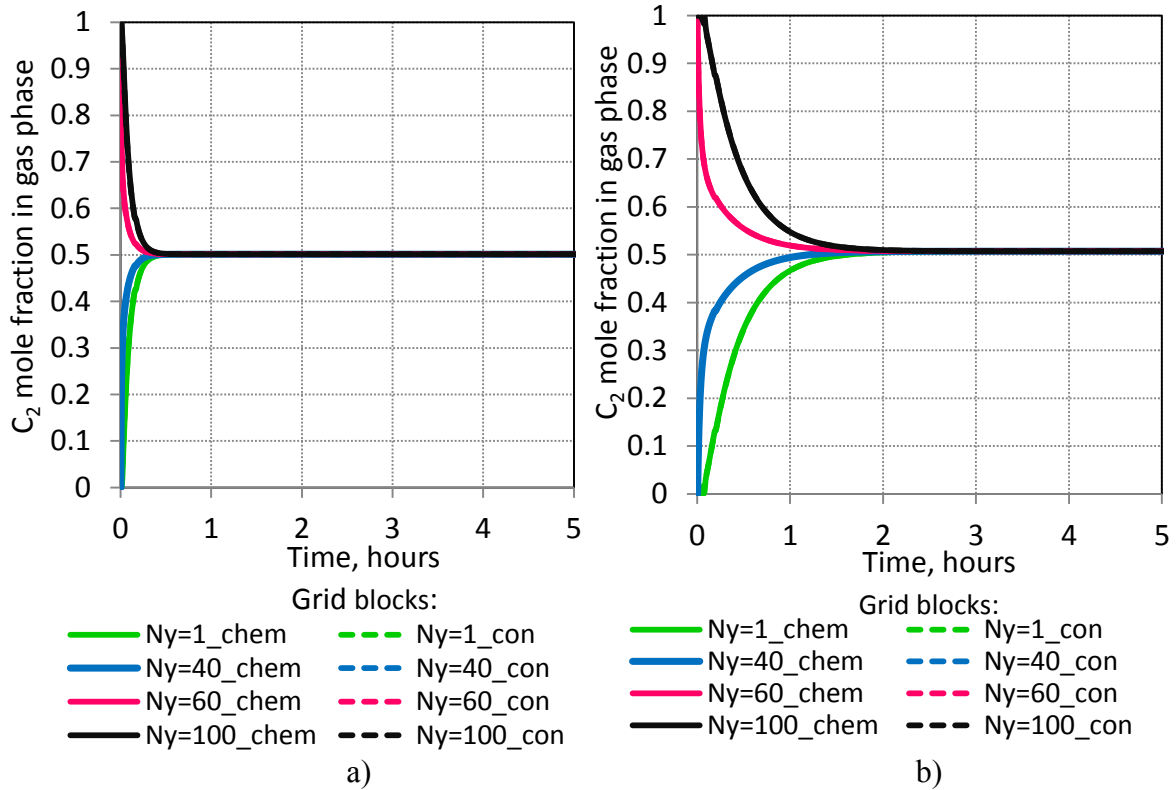


**Fig.4.4:** C<sub>2</sub> mole fraction in the grid blocks versus time for initialisation pressure: a) P<sub>init</sub>=1atm, b) P<sub>init</sub>=5atm

## 4.2 High-pressure simulation results

It is well known, that diffusion at elevated pressure deviates substantially from ideal gas law and fluid nonideality have a significant effect. In order to describe the transport properties of fluids a great number of simulation runs were performed, considering diffusive mixing in  $C_1$ - $C_2$  system at standard pressure and up to 7000 psia (along isotherm  $T=90^{\circ}\text{F}$ ).

The regions pore volume and molar concentration of  $C_1$  and  $C_2$  were taken from Eclipse output files and summarized in excel worksheet. As shown in Fig. 4.5, regions' pore volume stays equal  $0.7813 \text{ rcm}^3$  for pressure range covered in this study, because of zero rock compressibility set in the model. Thus, region 1 and region 2 pore volume, saturated with  $C_1$  and  $C_2$  respectively, is equal to volume of the gas, occupied given regions. The concentration variation with pressure exhibits different trends for  $C_1$  and  $C_2$  components (Fig.4.6). The  $C_1$  concentration increases almost linearly with pressure. Whereas,  $C_2$  component compresses linearly with pressure until ethane critical point is approached ( $P=707 \text{ psia}$ ). Near and over-critical region  $C_2$  concentration diverge dramatically from linear trend, resulting in significant difference between  $C_1$  and  $C_2$  concentration in the model.

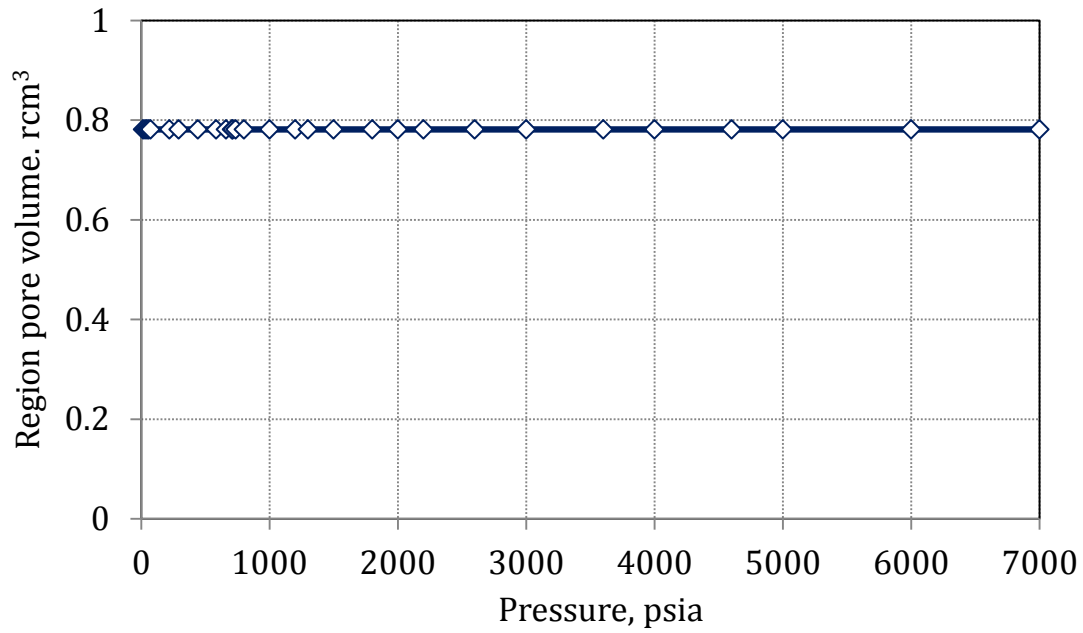


**Fig.4.5:** Region pore volume as function of pressure

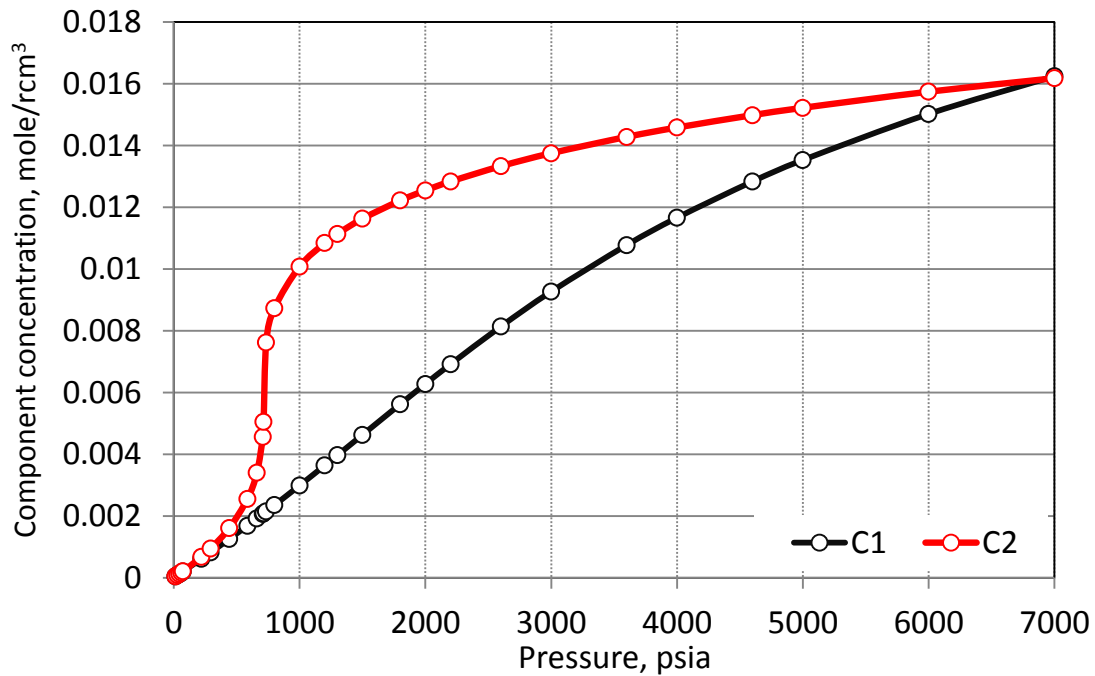


**Fig.4.6:** Component concentration as a function of pressure

---

For any new pressure initialization were performed, we consistently compared diffusive transport processes that are driven by fugacity or concentration differences. Thermodynamic behaviour of the pure species was under our particular interest.

The diffusivity flux of a component is assumed to be proportional to its chemical potential; and component in consideration is always diffuse down its own chemical potential gradient. As a rule, fugacity term is used, what logarithmically proportional to the chemical potential :  $\nabla\mu = \nabla\ln(f)$  . Therefore,  $\ln(f)$  as a function of component molar density has been quantified , in purpose to find a fair description of diffusive mass transport characteristic in the model based on chemical thermodynamics. Some simulation results are presented in Fig.4.7-4.8 for P=440 psia, Fig.4.9-4.10 for P=1200 psia and Fig.4.11-4.12 for P=2000psia. The component concentration profiles at different time steps were plotted together for both models, based on diffusivity due to concentration and fugacity (chemical potential) gradients.

At moderate pressure, fugacity gradient (or logarithm of the fugacities) is comparably proportionate to the concentration gradient profile for a given component (Fig. 4. 8). In other words, two different driven forces give quiet equivalent molecular motion across the whole range of compositional variation during diffusion. Fig. 4.7 (a,b) shows no difference in component distribution profiles for concentration and fugacity approaches to mass transport.

At elevated pressure, the fugacity gradients are no longer proportional to the concentration gradients, reflecting the departure from ideality of the mixture (Fig.4.10 and Fig.4.12).

Especially this effect is pronounced for ethane component, since it demonstrates the supercritical state behaviour under considered pressures P=1200 psia (Fig.4.10 b) and P=2000 psia (Fig.4.12 b). While approaching to a chemical equilibrium, fugacity gradient is almost uniform, but its concentration is not. Absence of sufficient fugacity gradients results in relatively slow diffusion driven by fugacity. Figs. 4.9 and 4.11 show concentration profiles for C<sub>1</sub> (a) and C<sub>2</sub> (b) component, displaying some delays in molecular transport where chemical potential used instead of concentration.

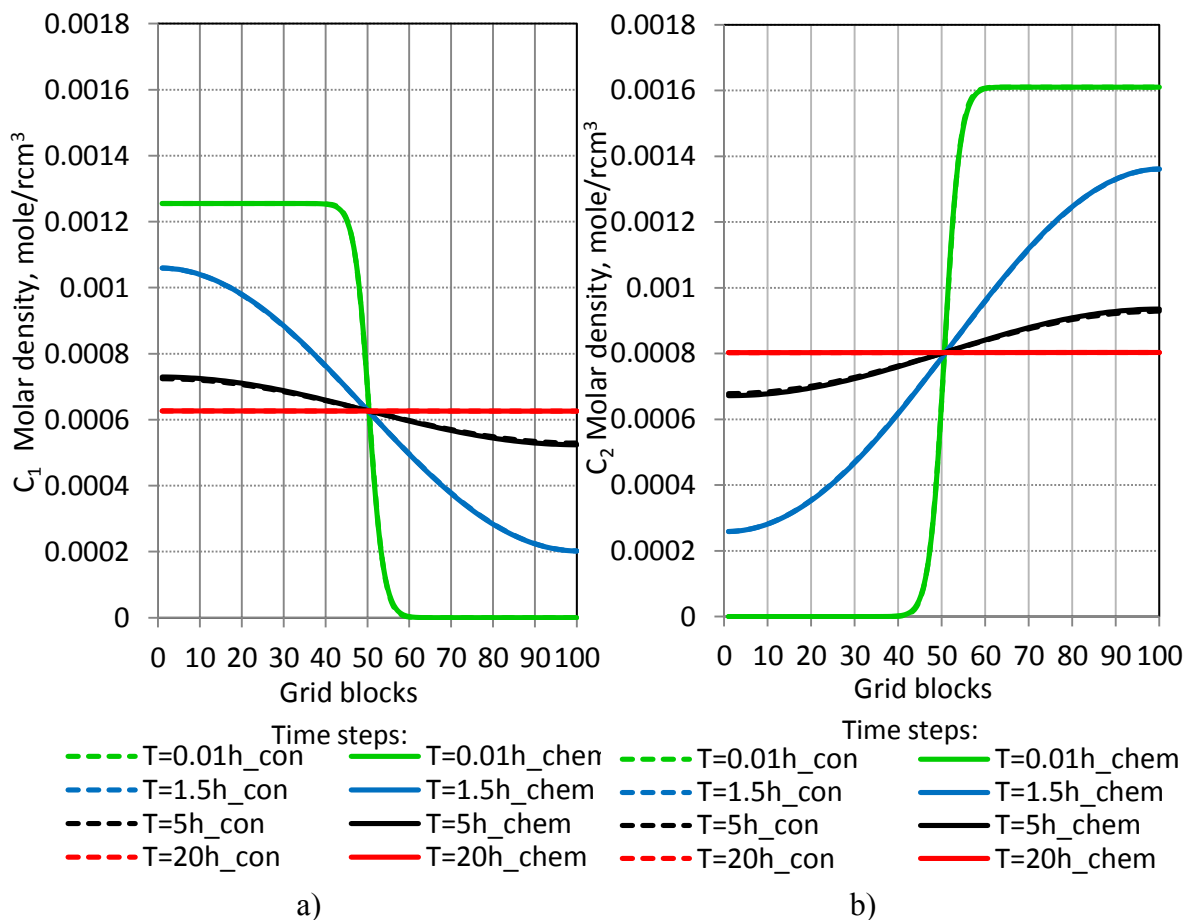


**Fig.4.7:** Concentration-distance profile at different time steps at P=440psia: a) C<sub>1</sub> b) C<sub>2</sub>.

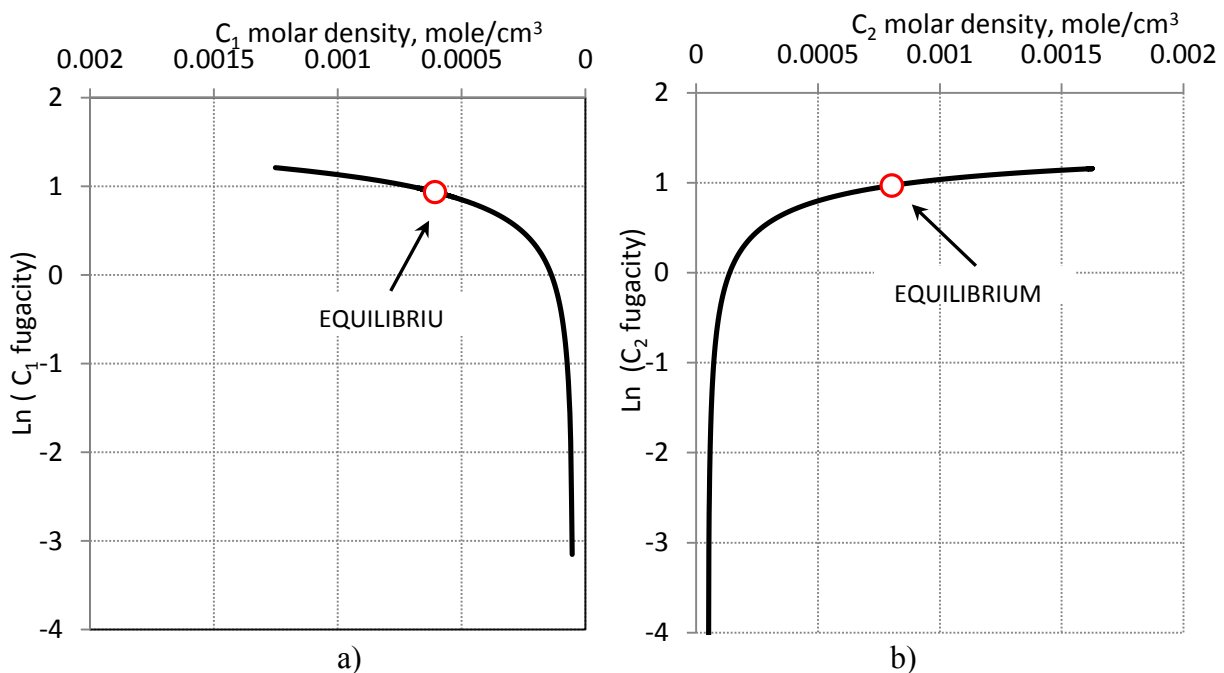


**Fig.4.8:** Ln(fugacity) as a function of molar density at P=440psia: a) C<sub>1</sub> b) C<sub>2</sub>



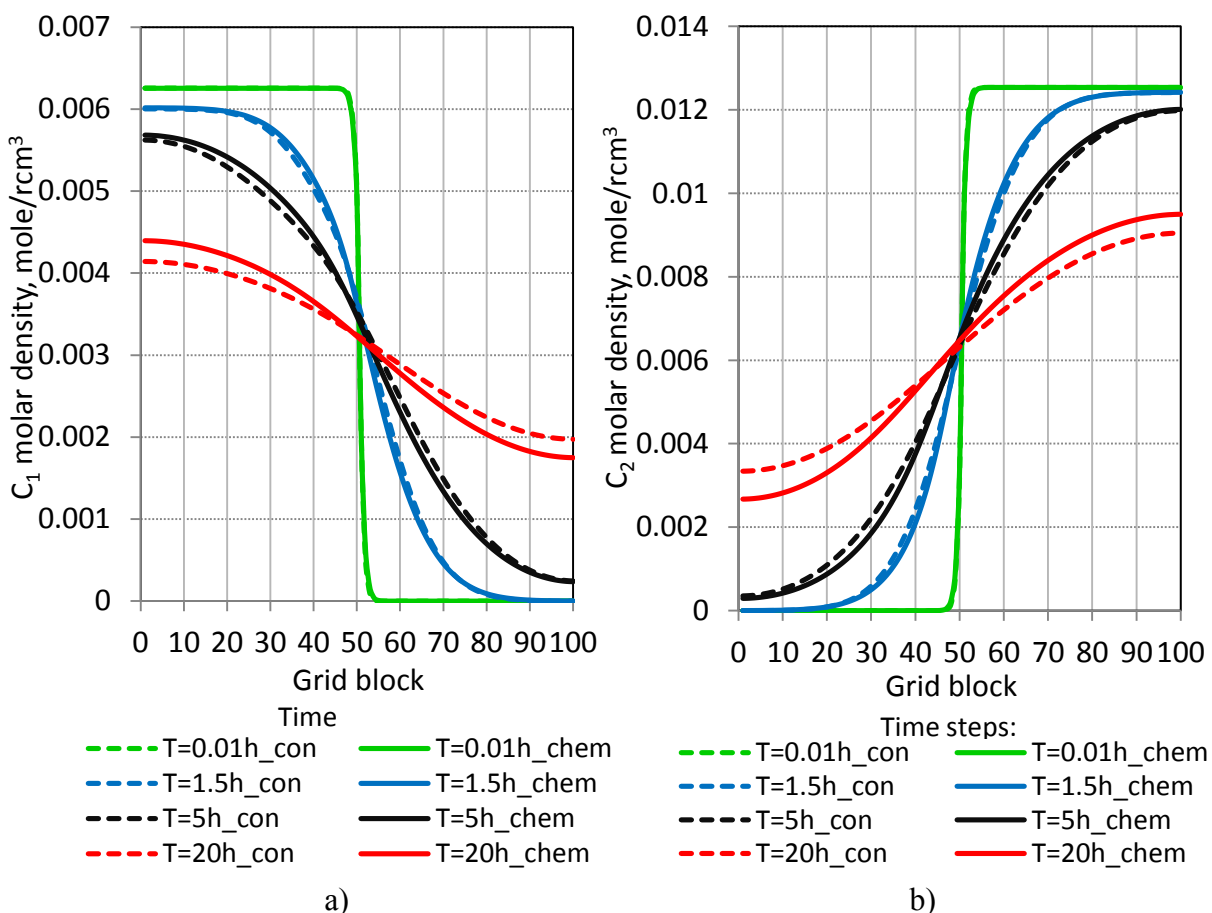


**Fig.4.9:** Concentration-distance profile at different time steps at P=1200psia: a) C<sub>1</sub> b) C<sub>2</sub>

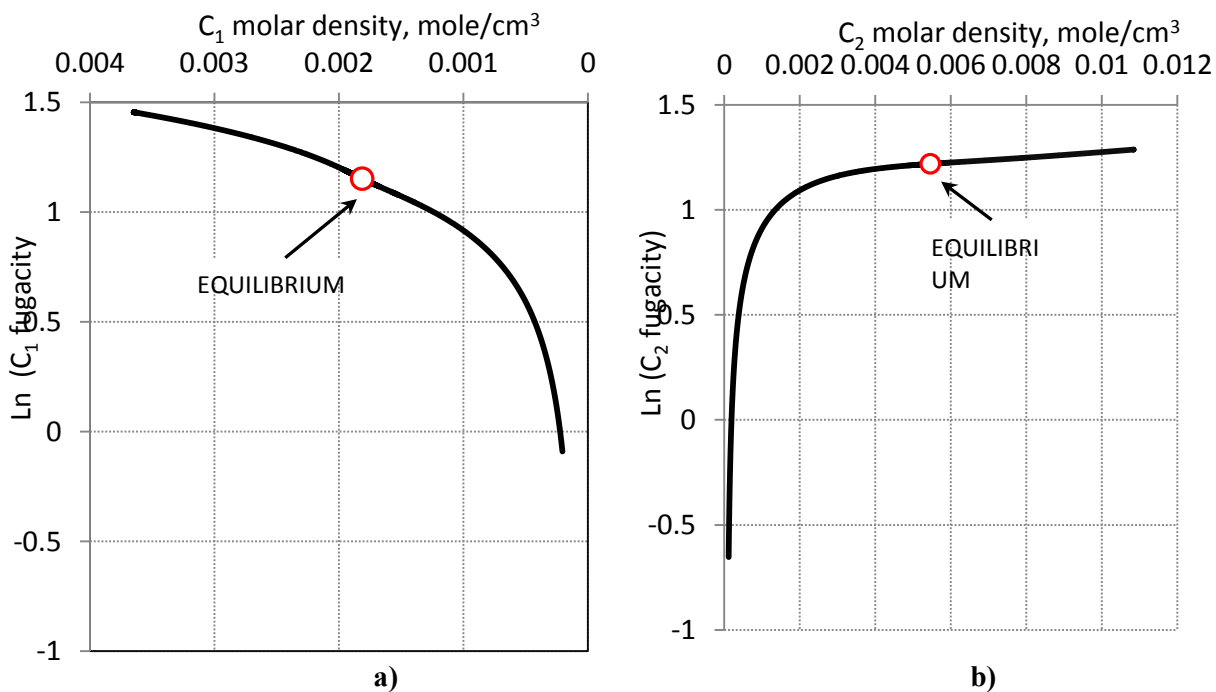


**Fig.4.10:** Ln(fugacity) as a function of molar density at P=1200psia: a) C<sub>1</sub> b) C<sub>2</sub>

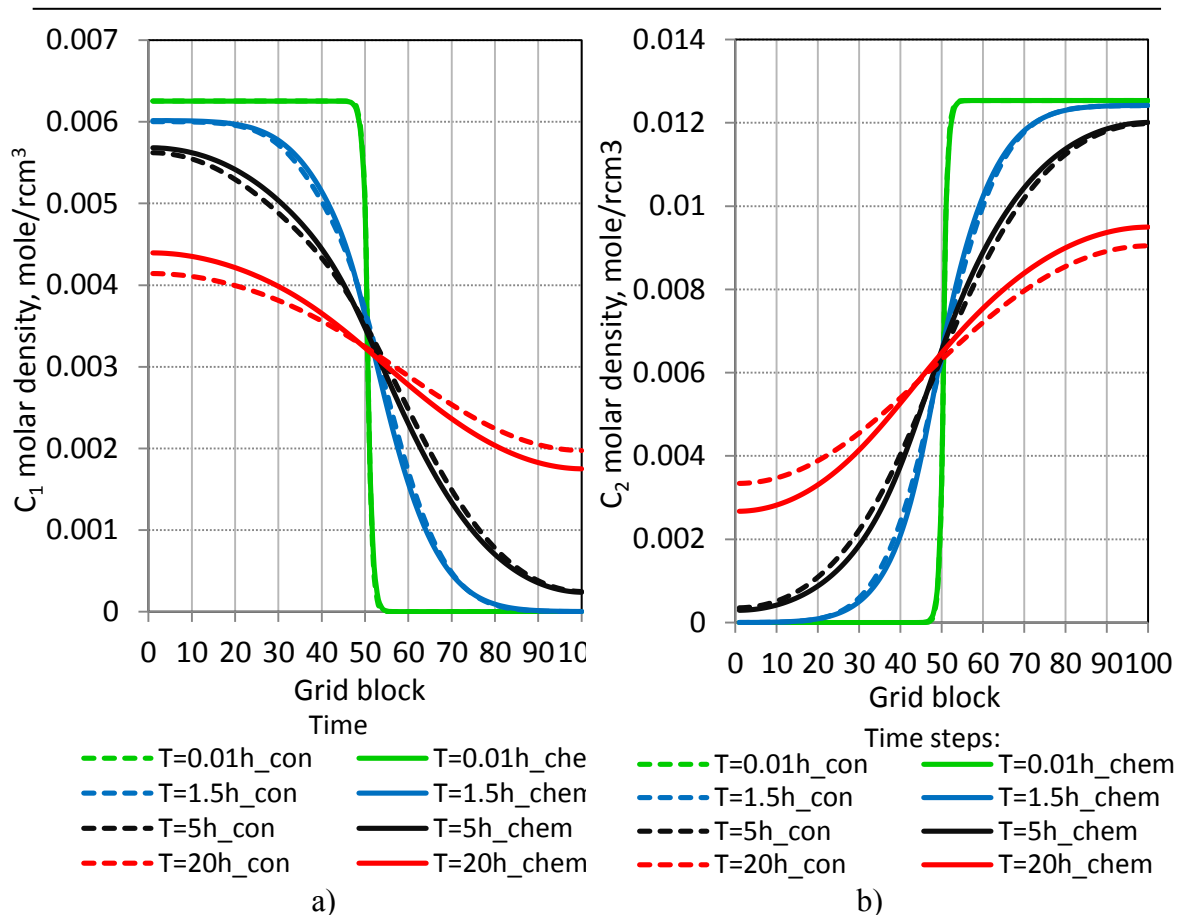


**Fig.4.11:** Concentration-distance profile at different time steps at P=2000psia: a)  $C_1$  b)  $C_2$ .

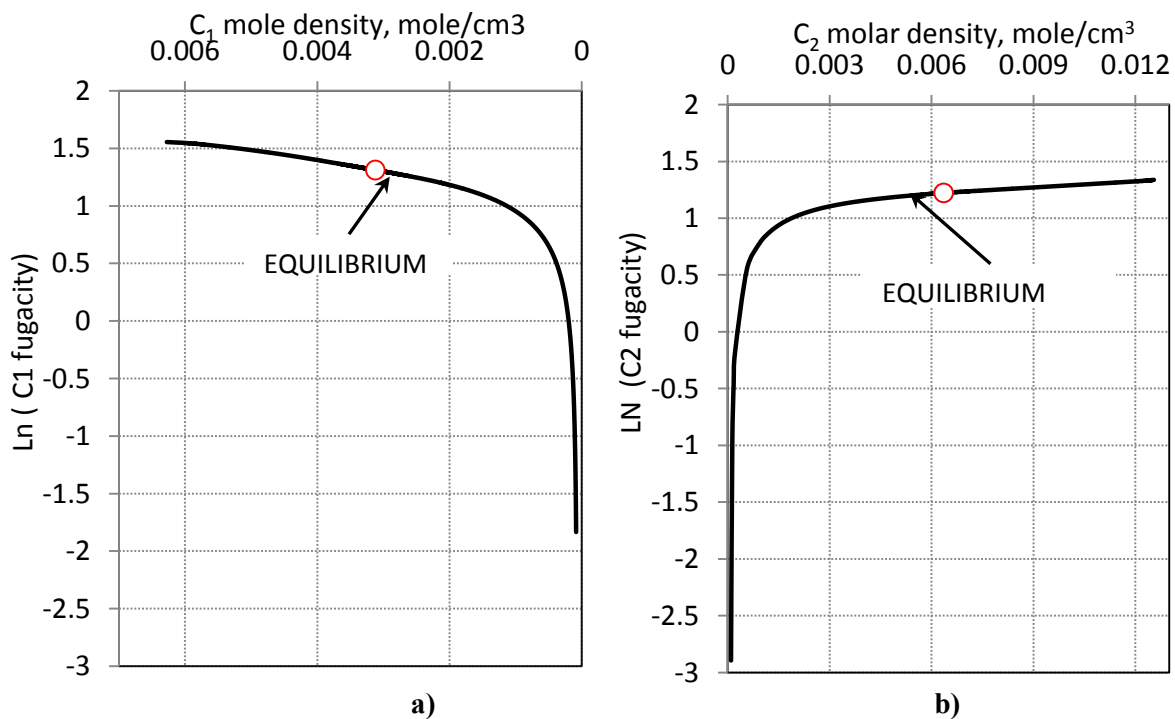


**Fig.4.12:**  $\ln(\text{fugacity})$  as a function of molar density at P=2000psia: a)  $C_1$  b)  $C_2$ .

---

### 4.3 Cross-phase diffusion

So far, we discussed molecular diffusion in single gas phase (intra-diffusion). Within one phase, as a rule, given component will diffuse from regions of high to low concentration or fugacity. The cross-phase diffusion that occurs at the gas-oil contact under non-equilibrium thermodynamic conditions is an important mechanism and requires proper modelling.

The purpose of this chapter is modelling of two-phase mixture and examination of its effect on diffusion performance driven by concentration and chemical potential gradients. To perform cross-phase diffusion experiment, model was initiated at pressure  $P=800$ psia and temperature  $T=73^{\circ}$ F. That pressure-temperature combination belong two-phase region for mixture composed of 0.15 and 0.85 mole fractions of  $C_1$  and  $C_2$  respectively ((Fig.3.1)  $C_1:C_2$  phase diagram). Thus, during diffusivity fluxes we do expect gas and liquid existence in some grid blocks with exact mixture composition indicated above.

Fig.4.14. shows  $C_2$  mole fraction in the gas phase profiles for three neighbouring grid blocks. A sketch of those three blocks is given in Fig.4.13. At some point liquid phase (or two-phase fluid) appears in the grid block NY=51 (Fig.4.15). Within one gas phase, concentration gradient is an adequate descriptor of diffusion “driving force” (as in Fick’s law) but between phases, concentration fails because of the phase discontinuity at interphase boundary. In case when the grid block saturated with gas (NY=50, NY=52 ) is adjacent to another grid block saturated with oil (NY=51), the gas-phase diffusion is almost interrupted (Fig.4.13). Thus, we observe cumulating  $C_2$  inflow in the grid NY=52 with no  $C_2$  outflow and cumulating  $C_2$  outflow from grid NY=50 with no  $C_2$  inflow (Figs.4.13-14).

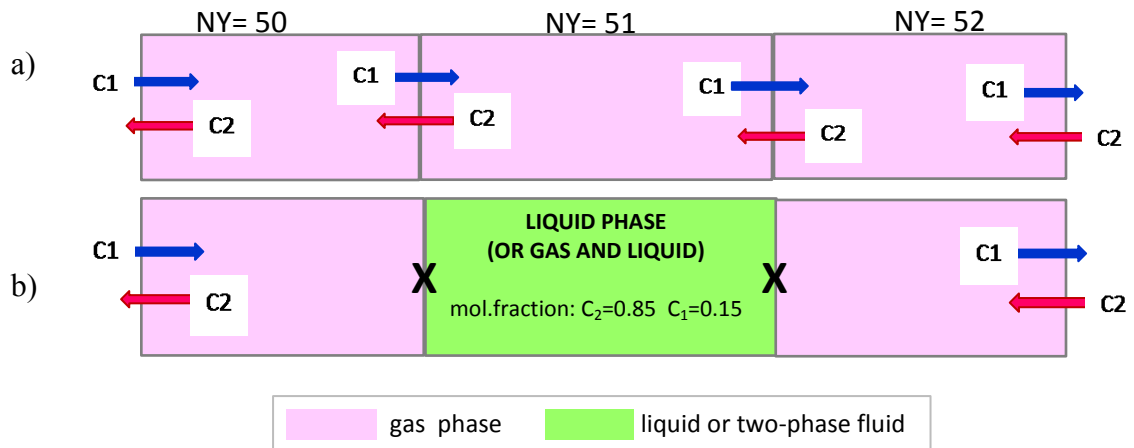


**Fig.4.13:** Schematics of:

a) intra-phase diffusion, b) phase discontinuity at interphase boundary

From the Figs.4.14-4.15 it is clearly seen, that existence of two phases in the grid block NY=51 has a temporary effect. From oil saturation profile (Fig.4.15) we can observe some gas presence in the grid block NY=51 (Soil $\neq$ 1), still enabling diffusive motion in the gas phase due to concentration gradients, with a much lower intensity though. Even a small change in composition of grid block NY=51 will move cell conditions out from the two-phase state, thus a single gas phase appeared again in the system. The other reason of short time period of liquid staying in the cell is that pressure increases with a time, moving cell condition out from two-phase region (Fig. 4.16).

The initiating of interphase mass transfer could be actualized by defining cross-phase diffusion coefficients, what a built-in feature in Eclipse 300. However there is no published work that suggests some approaches to calculate cross-phase mass transfer coefficients in a Fick's law-type diffusion. Therefore modelling mass transfer across phases using concentration driven diffusion may not have a sound basis.

The diffusivity model, based on fugacity gradients successfully describes cross-phase diffusion (Fig.4.14). The diffusion process is merely a manifestation of mixing, which tends to eliminate concentration gradients. The fugacity then is correct driving force to model interphase mass transfer, since diffusion always proceeds from high to low fugacity cross a phase boundary until chemical equilibrium is reached.

The simulation model has to be able to model the diffusion of oil and gas components within the oil and gas phase (intra-phase diffusion) as well as diffusion of components directly from the gas phase to the oil phase (cross-phase diffusion) from the sides. The concentration-based diffusion is not capable to model cross-phase diffusion because of the phase discontinuity at interphase boundary. The correct driving force is then fugacity since diffusion always proceeds from high to low fugacity cross a phase boundary.

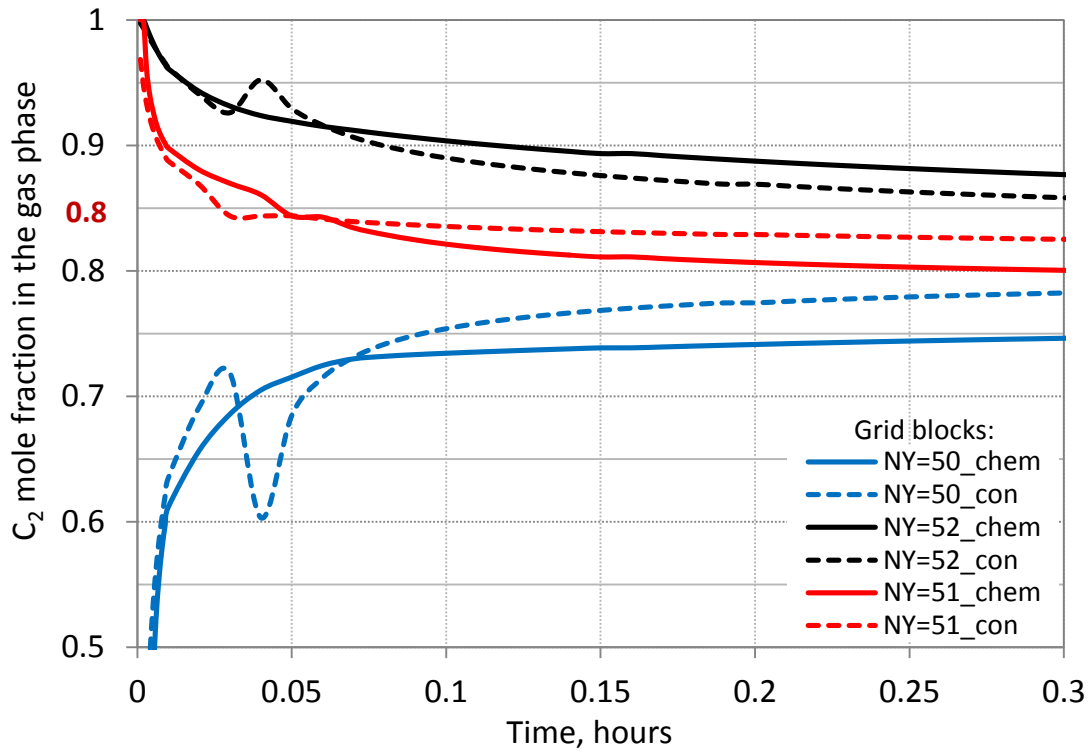


**Fig.4.14:** C<sub>2</sub> mole fraction profile as a function of time

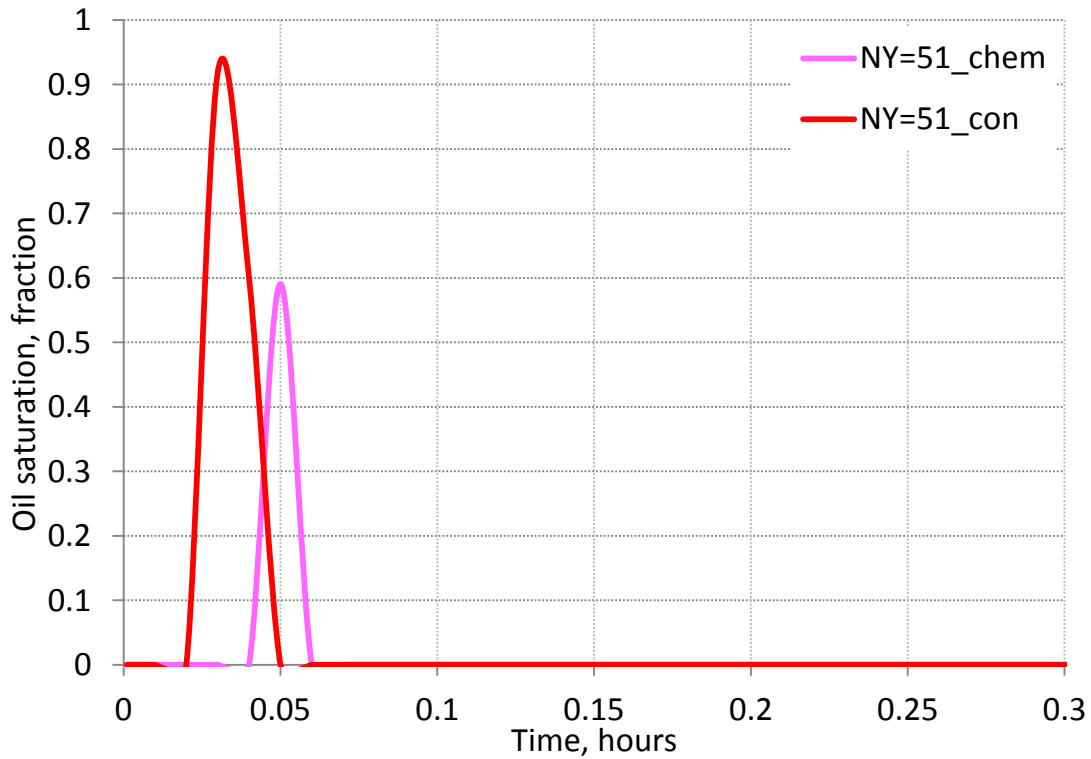


**Fig.4.15:** Oil saturation profile as a function of time for grid block NY=51

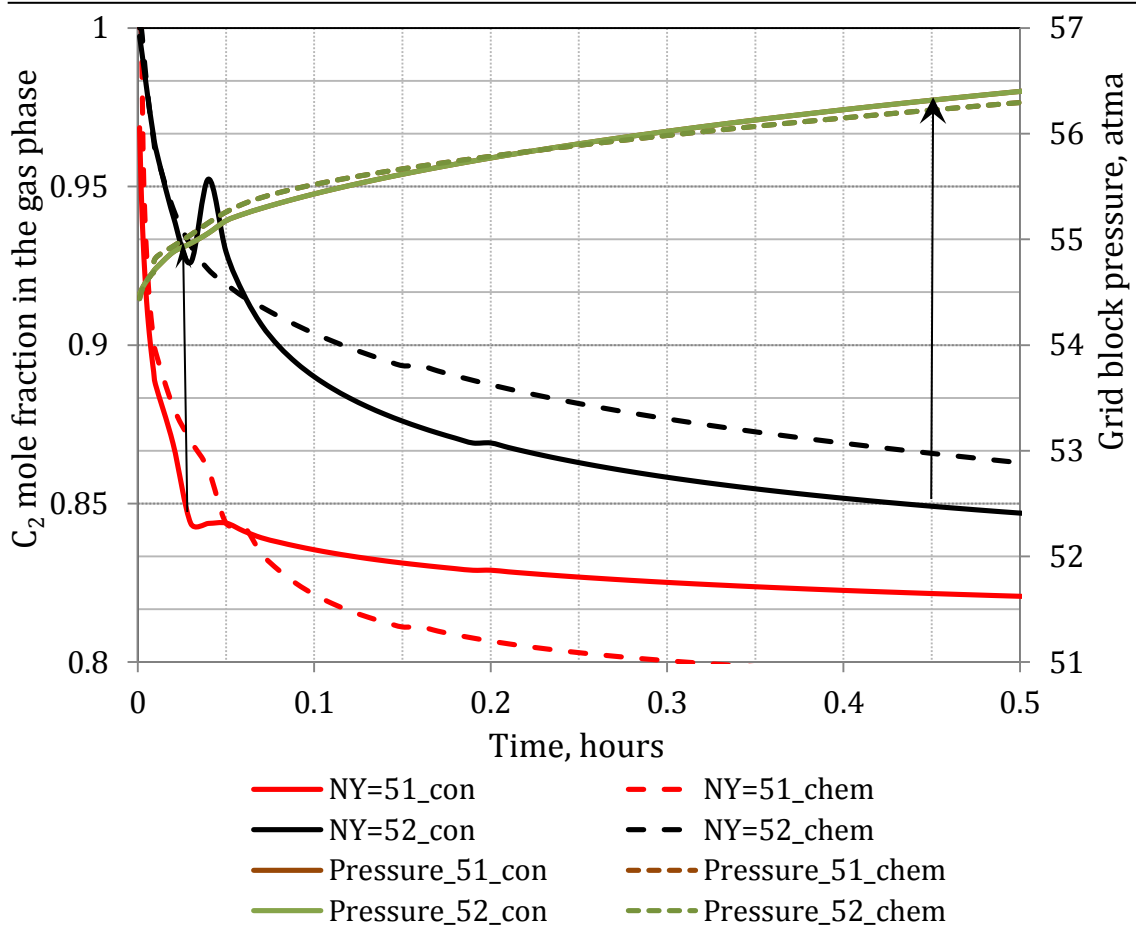


**Fig.4.16:** C<sub>2</sub> mole fraction and pressure profiles as a function of time

#### 4.4 The effect of convection on the diffusion process

The contribution of the pressure gradients, caused by molar density variation in the diffusion flux has often been neglected in the diffusion studies. Molar density (molar concentration) is a volumetric property, what gives the volume per mole:

$$\rho_m = \frac{n}{V} \dots\dots\dots(4.5)$$

The objective of this chapter is to examine the effect of molar density variation on diffusion flux. We consider diffusion with and without convection fluxes, in order to detect bulk flow contribution in total mass transport. To deactivate convection in the Eclipse 300 model, we set infinitely low medium permeability ( $k=10^{-6}$ mD). In the cases, where convection fluxes are included, media permeability is equal 200mD.

First, we modelled diffusion experiment at pressure  $P=73,48$  (5 atm), so that  $C_1$  and  $C_2$  component has equal molar densities (Figs.4.17a-4.18a). Fig. 4.19 and Fig.4.20 show mixture molar density and pressure profiles at different time steps for diffusion mixing without convection. The mixture molar density and pressure is essentially invariant during the diffusion process. Since initialisation pressure is rather low, fluid mixing from diffusion follows the ideal gas law. The mixture molar density stays stable and is independent of composition, what caused by ideal mixing in the methane-ethane system. The simulation results are the same with and without convection as expected (Figs. 4.19-4.22).

In the second example we consider diffusion in the same  $C_1$ - $C_2$  system at specific conditions ( $P=2000$ psia and  $T=90^{\circ}$ F), so that mixture molar density varies significantly during diffusion flux. Variation in mixture molar density occurs due to variation in mixture composition, what is expected because of components diffusive motion (Fig.4.17 b).



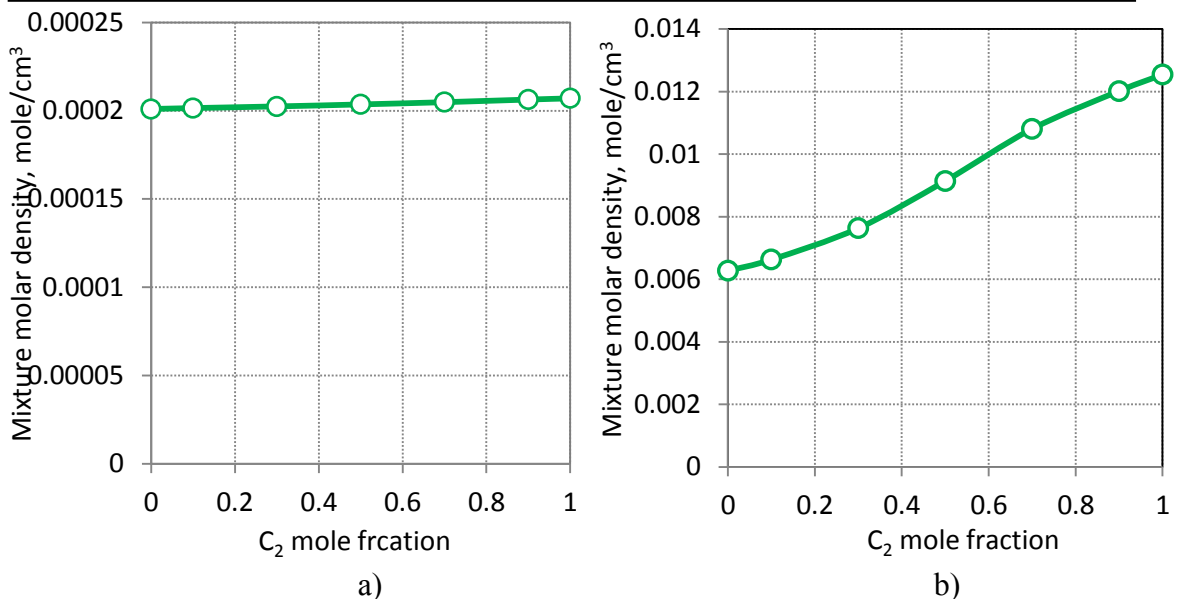


**Fig.4.17:** Mixture molar density variation with composition. C<sub>1</sub>-C<sub>2</sub> system at:  
a) P=73.48psia and T=90<sup>0</sup>F , b) P=2000psia and T=90<sup>0</sup>F

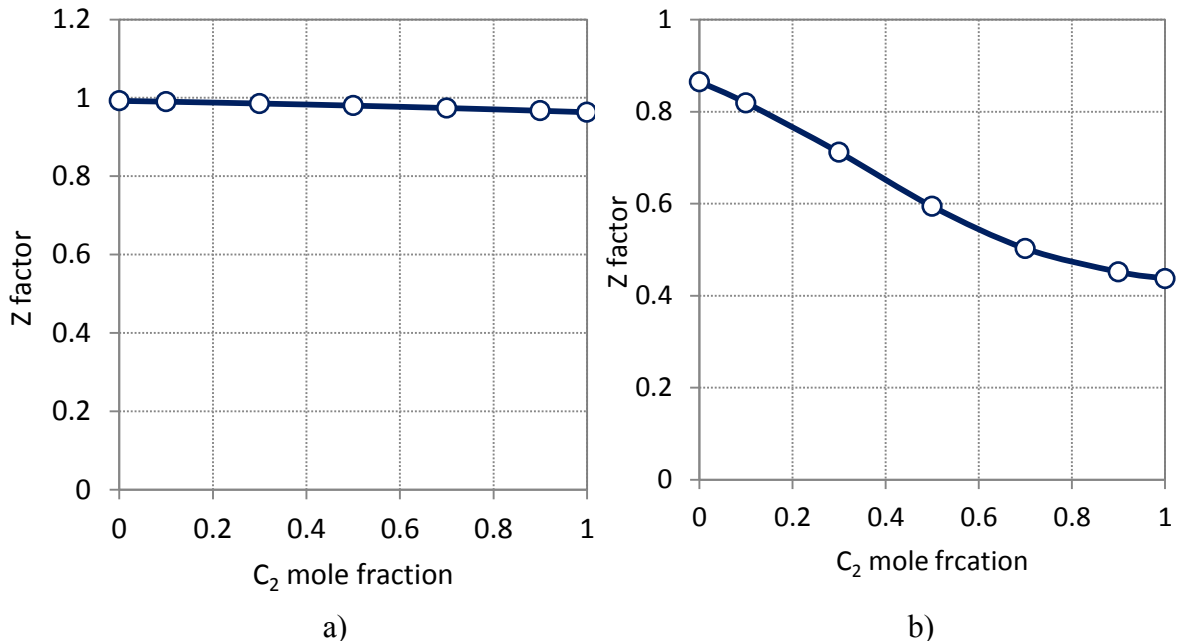


**Fig.4.18:** Mixture compressibility variation with composition. C<sub>1</sub>-C<sub>2</sub> system at:  
a) P=73.48psia and T=90<sup>0</sup>F , b) P=2000psia and T=90<sup>0</sup>F

Plots for mixture molar density and pressure profiles for different time steps are shown in Fig.4.23 and Fig.4.24 respectively for case without convection. The initial pressure is 2000psia (136 atm). This problem is not isobaric anymore because system is not ideal and follows the real gas law, including compressibility factor (Z):

$$\frac{n}{V} = \frac{P}{ZRT} = \rho_m \dots \dots \dots (4.6)$$

Z factor indicates a deviation from ideal gas behavior and is a strong function of composition (Fig.4.18b):

$$Z = f(T_r, P_r) \dots \dots \dots (4.7)$$

$$T_r = \frac{T}{T_{pc}}, P_r = \frac{P}{P_{pc}} \dots \dots \dots (4.8)$$

$$T_{pc} = \sum_{i=1}^N z_i T_{ci}, P_{pc} = \sum_{i=1}^N z_i P_{ci}$$

, where

$T_r, P_r$  – reduced temperature and pressure;

$T, P$  – temperature and pressure;

$T_{pc}, P_{pc}$  – mixture pseudocritical temperature and pressure;

$T_{ci}, P_{ci}$  – component critical temperature and pressure;

$z_i$  – mixture composition (mole fraction)

After diffusion initiated, counter-current diffusive motion at the initial C<sub>1</sub>-C<sub>2</sub> contact occurs, resulting in composition and, therefore, mixture molar density variations from the both side of the middle of the domain. The composition variation affects the fluid volumetric properties such as compressibility factor (Z) and molar density (inversely proportional to molar volume) (Figs.4.17b-4.18b).

In the absence of convection uniform pressure distribution can be honoured no longer due to significant Z factor oscillation. Thus, dramatic pressure fluctuations exist, caused by variations in gas volumetric behaviour and violation of initially balanced distribution of constituents (Fig.4.23).

The pressure gradients are often undetectable in most cases when convection is active and system has high permeability (Figs.4.25-4.26). Any pressure variation will create convection fluxes that will eventually readjust component distribution, so that to regain pressure balance. In this case high permeability makes molar density variation less pronounced, masking pressure gradients. The numerical solution therefore is a result of diffusion balanced with convection fluxes due to molar density variation.

The component diffusive flux related to chemical potential gradient is a weak function of its concentration. That is why diffusion characteristics are in a less degree affected by the variation in mixture molar density with composition.

It is obvious, that convective mass transfer will contribute greatly to diffusion fluxes when gas mixture molar density is a strong function of composition. The stronger that correlation effect, the more pronounced pressure «errors» and, consequently, bulk flow.

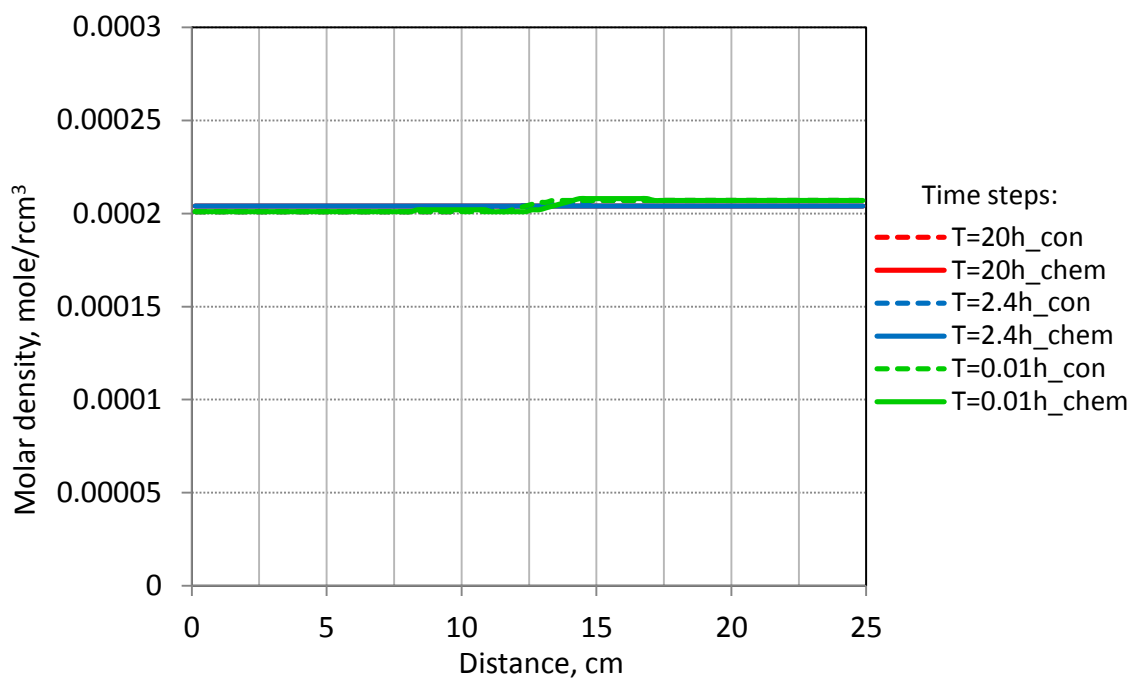


**Fig.4.19:** Molar density versus distance at different time steps.  $P_{init}=30\text{atm}$ .  
No convection

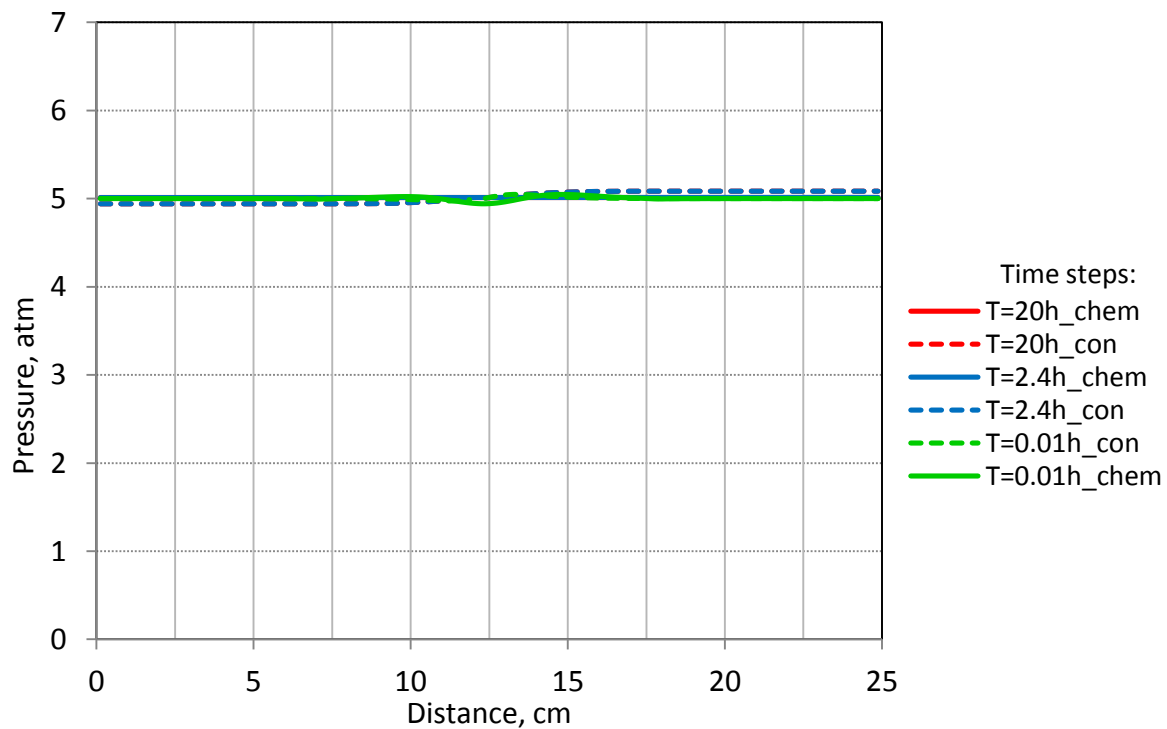


**Fig. 4.20:** Pressure versus distance at different time steps.  $P_{init}=30\text{atm}$ .  
No convection

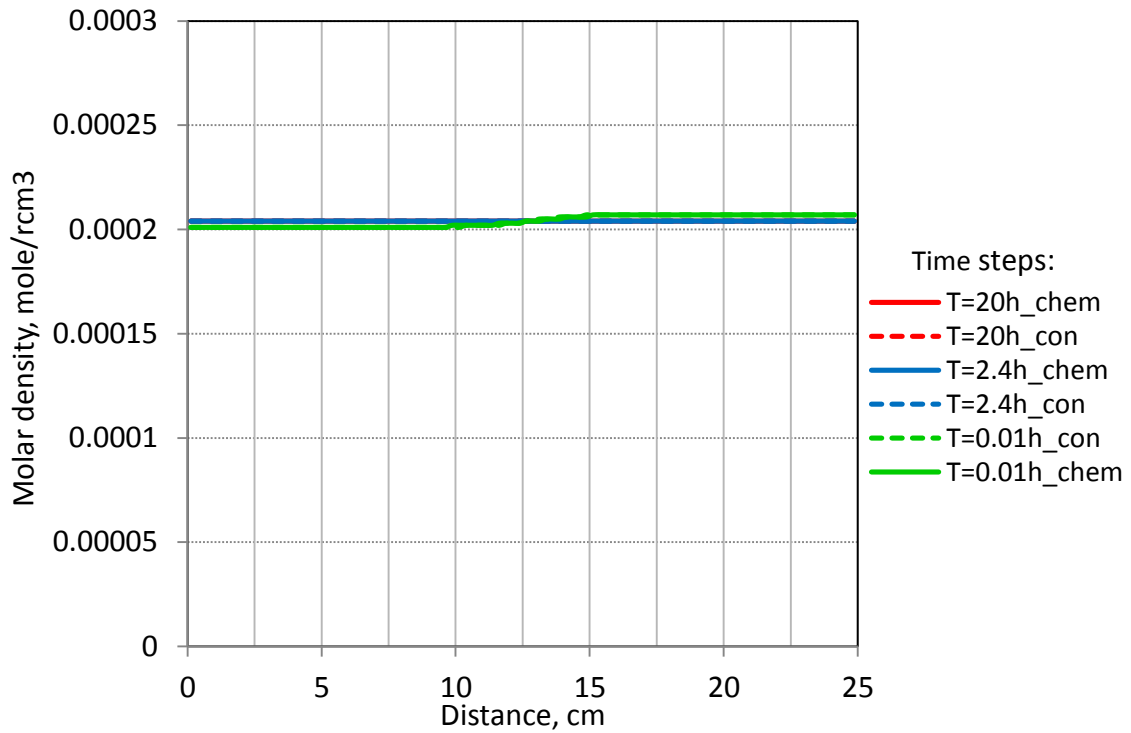


**Fig.4.21:** Molar density versus distance at different time steps.  $P_{init}=30\text{atm}$ .  
With convection

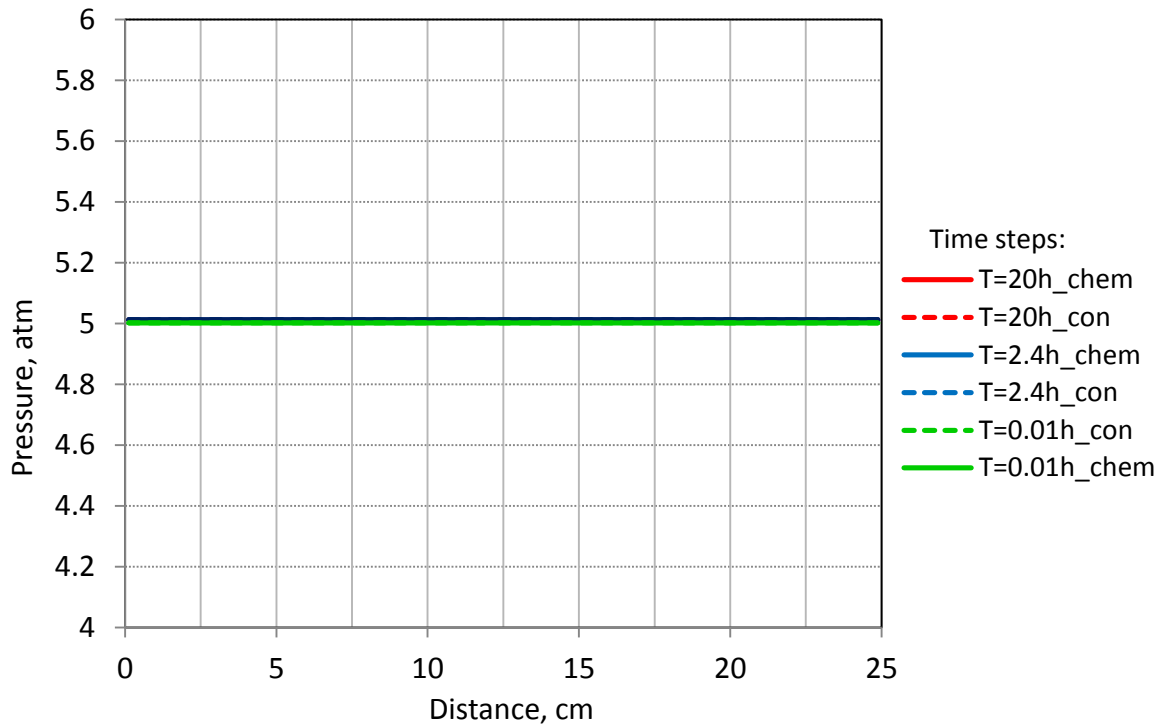


**Fig. 4.22:** Pressure versus distance at different time steps.  $P_{init}=30\text{atm}$   
With convection

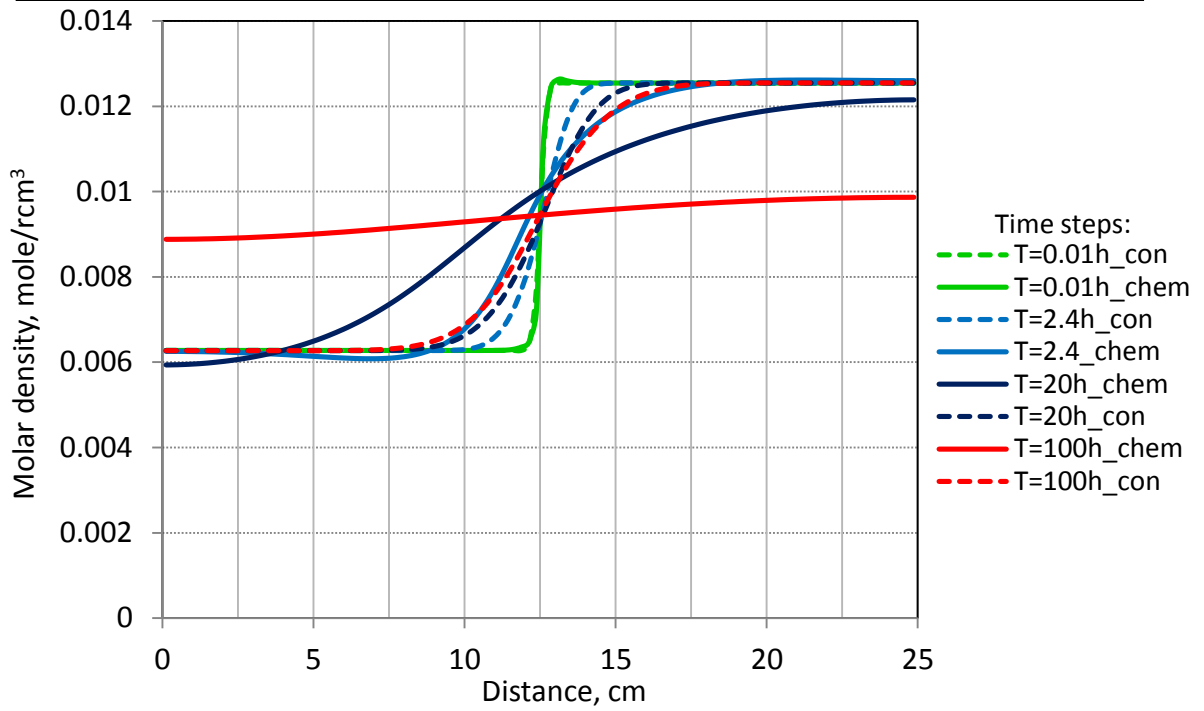


**Fig.4.23:** Molar density versus distance at different time steps.  $P_{init}=136\text{atm}$ .  
No convection

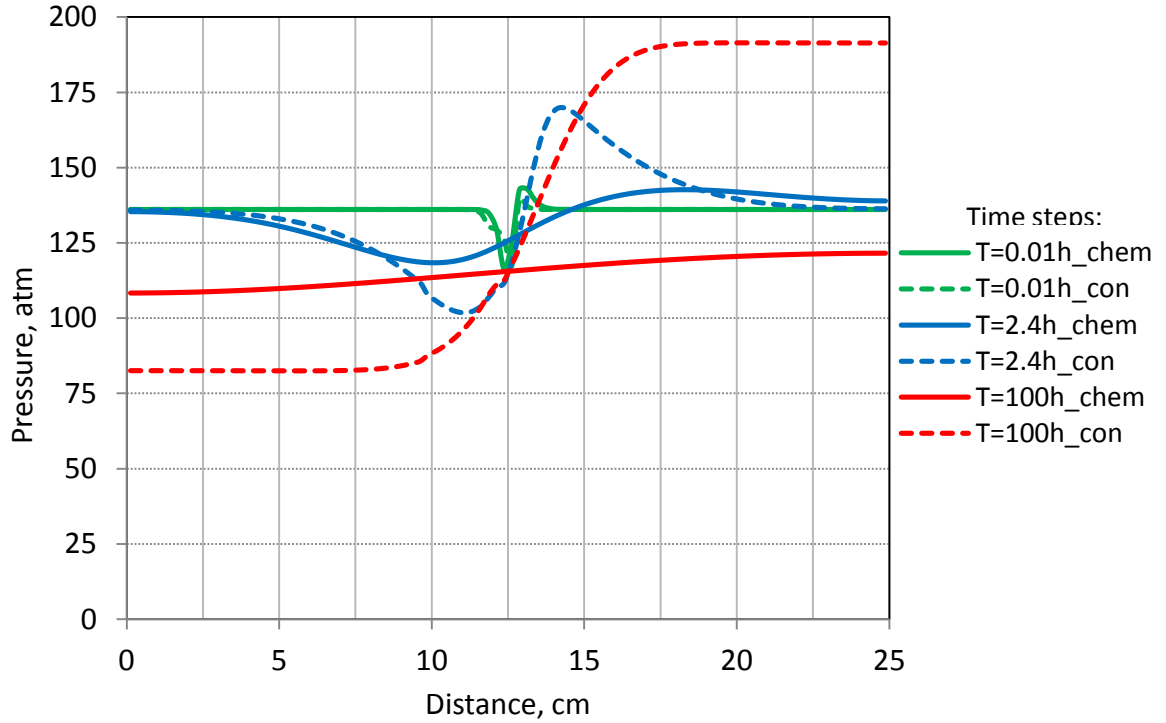


**Fig. 4.24:** Pressure versus distance at different time steps.  $P_{init}=136\text{atm}$ .  
No convection

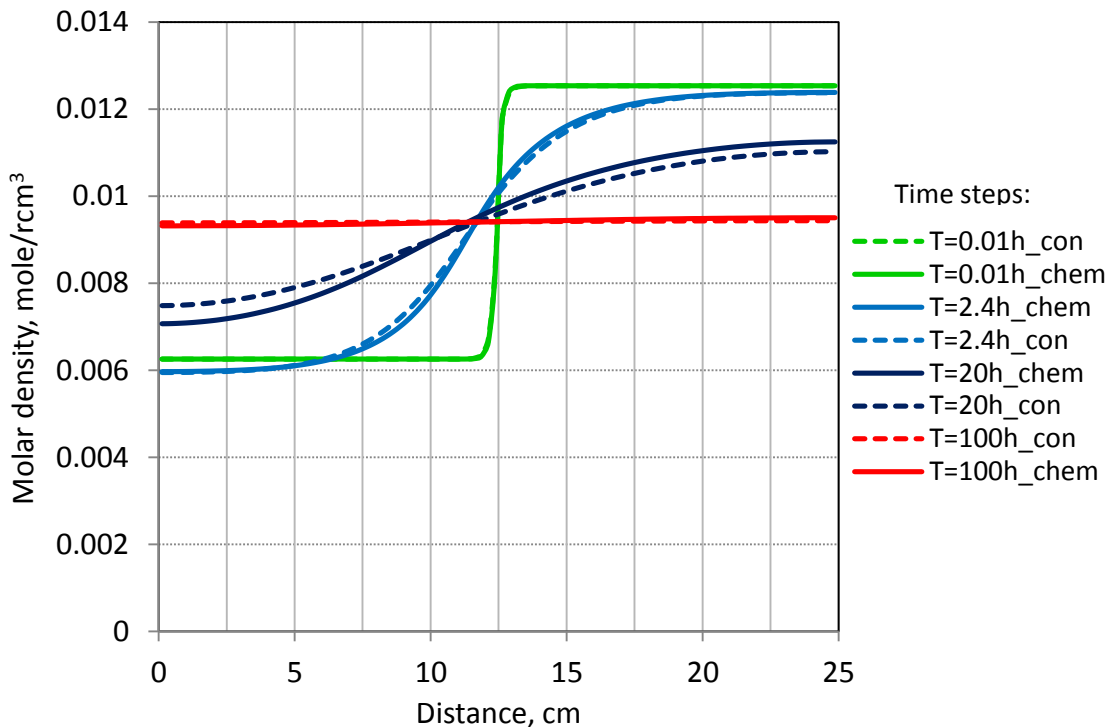


**Fig.4.25:** Molar density versus distance at different time steps.  $P_{init}=136\text{atm}$ .  
With convection

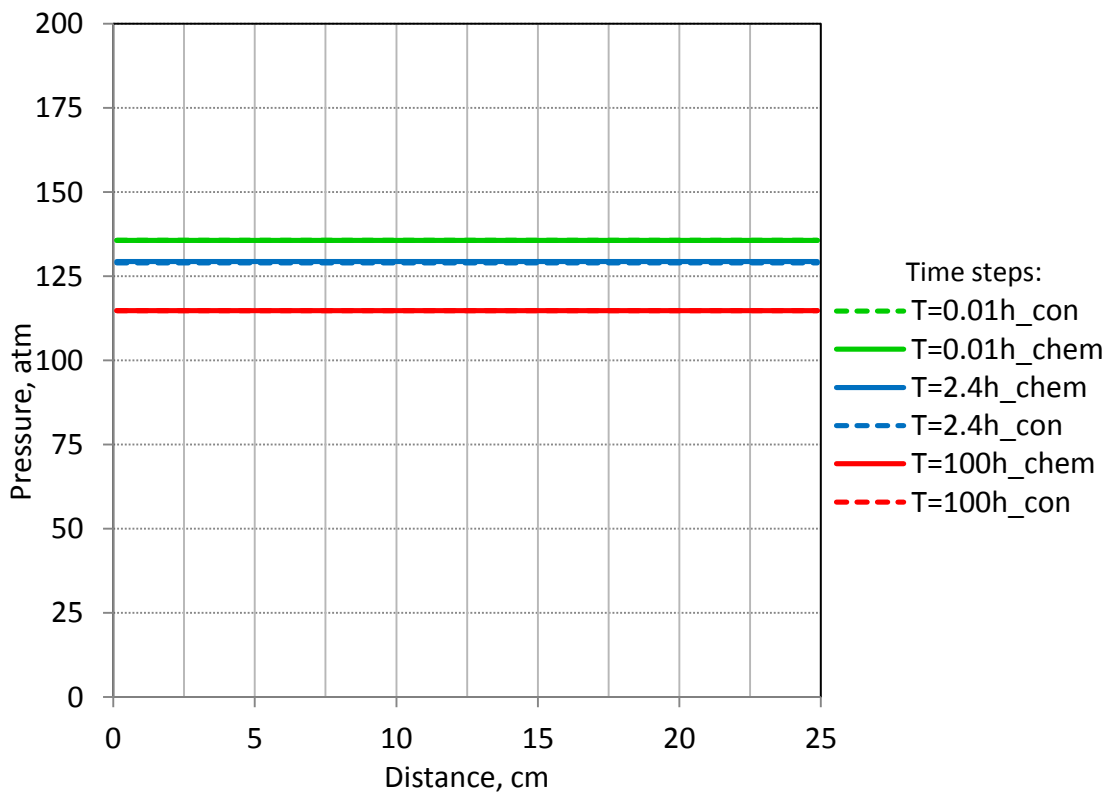


**Fig. 4.26:** Pressure versus distance at different time steps.  $P_{init}=136\text{atm}$ .  
With convection

---

## 4.5 Features of mass transfer and diffusion in the near-critical regions

Some hydrocarbon reservoirs contain near-critical fluid mixtures. Therefore, diffusion and species spatial distribution at the critical conditions are of special interest.

It is the aim of this chapter to examine diffusivity performance of binary mixture in the region around the critical point. Note that analyses we provide based on a very simple case, treating 1D diffusion in the  $C_1$ - $C_2$  binary system. In order to simulate diffusion experiments, the conditions were chosen so as to achieve critical behavior of mixture under our investigation.

Two pressure-temperature combinations were considered:

- $P=707\text{psia}$  and  $T=90^{\circ}\text{F}$  - near critical point of pure  $C_2$  fluid;
- $P=800\text{psia}$  and  $T=74^{\circ}\text{F}$  - asymptotically close to critical point of mixture composed of 0.15 and 0.85 mole fractions of  $C_1$  and  $C_2$  respectively.

### 4.5.1 Diffusion in the near critical region of pure ethane

At a given constant pressure-temperature combination ( $P=707\text{psia}$  and  $T=90^{\circ}\text{F}$ ) the strong deviation of system compressibility and molar density with variation in composition is observed (Fig. 4.27 (a,b)). The system molar density increase more than twice (2.22 times) as ethane mole fraction increase in the mixture and reach  $0.0046\text{ gmole/cm}^3$  for pure  $C_2$  fluid, while pure  $C_1$  molar density is only  $0.021\text{ gmole/cm}^3$ . Since intermolecular attraction of methane is weaker than that of ethane, methane is transferred by pure diffusion more rapidly than is ethane down to its concentration.

Fig.4.28 and Fig. 4.29 describe the concentration-time-distance behavior of the components  $C_1$  and  $C_2$  of a binary diffusing system. As shown in Fig. 4.30 pressure profile is equalized throughout the model, however general pressure trend with time is upward, caused by non-ideal mixing of methane-ethane system.



---

We already saw in chapter 4.4 that diffusion performance is affected much by mixture molar density variation, which may be a strong function of composition. Cross-current diffusive fluxes of  $C_1$  and  $C_2$  start in the middle of domain evoking composition changes in the nearest grid blocks and, consequently, mixture volumetric behavior. Sensible departure from initially equilibrated pressure occurs from the both sides of initial  $C_1$ - $C_2$  contact. An increased hydrostatic pressure will in fact be built up towards the region of increased  $Z$  compressibility, and pressure drop is expected towards less compressible mixture. This pressure gradient is relieved by a compensating bulk flow of  $C_1$  and  $C_2$  together, establishing a new uniform pressure distribution. The real convective movement in many cases itself undetectable (Figs.4.28-4.29).

However, existence of bulk flow can be demonstrated by plotting inter-block flow rates in the positive and negative directions (Figs.4.32, 4.36, 4.40). The component flux down its lower concentration or chemical potential is assumed to be positive (co-current flow), in the same manner, component flux opposing diffusive flow is treated like negative (counter-current flow).

Fig.4.32 and Fig.4.36 illustrate total transport rate of  $C_2$  molecules as function of time for  $N_Y=80$  and  $N_Y=100$  grid blocks respectively. Fig.4.40 shows  $C_1$  flow rates into- and out of  $N_Y=1$  grid block.

It is clearly seen from the graphs that in the early time steps matter transferred massively against its diffusion driving gradient. Convective rates of  $C_1$  and  $C_2$  are exactly adequate to produce the required counterbalancing bulk flow, which is aiming to compensate pressure imbalance.

Let us consider now inter-block mass transfer in the grid block  $N_Y=100$ . If we take closer look at Fig.4.33, we can detect here another sharp counter-current  $C_2$  flux occurred later on. This motion arises from exclusive volumetric behavior of pure  $C_2$  fluid in its critical region, which developed in the last few grid blocks on the right-side of the model (Fig.4.29)

The relationship between fluid compressibility factor and pressure is governed in Fig 4.35. The system pressure is not stable and increases with time. At some point of

pressure, ethane compressibility factor ( $Z$ ) decreases dramatically; what enforce additional molecular transfer from the neighboring grid blocks into the region with extremely compressed fluid. The reoriented motion of  $C_2$  is supplied in adequate quantity to compensate  $Z$  factor and, in the same time, equilibrate pressure throughout the media (Fig.4.34). As a reminder we refer to the real gas equation, describing relationship between gas volumetric properties:

$$\frac{n}{V} = \frac{P}{ZRT} = \rho_m \dots\dots\dots(4.9)$$

Indeed, highly concentrated fluid shows up at the right-side border of the media, where a critical phenomenon is observed (Fig.4.29). It is evident, that strong  $C_2$  bulk flow opposes natural diffusive flux, which is, most probably, count or little in this case. A more instructive illustration is perhaps components concentration profile with time in the last grid block  $NY=100$  (Fig4.32). As  $C_1$  concentration front reaches the grid block, ethane critical condition is maintained no longer. The mixture compressibility factor increases with increasing methane mole fraction in the grid block. Therefore, no further intake of  $C_2$  is required and even conversely the cell will get rid of extra molecules, so that to balance increasing compressibility. This forced bulk flow out from the cell intensifies the diffusive motion of  $C_2$  component in direction to its lower concentration or fugacity, in accordance with diffusivity force.

To ensure that  $C_2$  critical phenomena have local effect, we compared mixture volumetric behavior for other grid blocks in the model. Fig. 4.38-4.39 shows  $P/Z$  and mixture compressibility–pressure variation as a function of time for grid block  $NY=80$ . The critical phenomena pronounced much less, and  $Z$  factor does not exhibit extreme deviation. The reasonable explanation is that,  $C_1$  advancing front reached grid block earlier and ethane critical condition simply cannot be developed (Fig.4.36). On the left side of the model, initially saturated with methane, no critical effect is detected as expected. As approaching to the equilibrium, mixture compresses gradually with increasing  $C_2$  mole fraction, thus no collapse in volumetric behavior is observed (Fig. 4.42-4.43).

Contribution of diffusion driven force is more pronounced at high mixture molar density (right-side of the model) (Fig.4.29). The component diffusive flux related to chemical potential gradient is a weak function of its concentration. Fugacity stays almost invariant over wide range of concentration (Fig. 4.31 a,b). Absence of sufficient fugacity gradients results in relatively slow diffusion driven by fugacity. Generally speaking, the demonstrated numerical solution is a result of the total mass transport in the mixing system, including transfer of matter due to pure diffusion and transfer by convective movement (bulk flow). Existence of phenomenological critical region in the case of gas diffusion, stimulate some additional convective migration of components, aiming to readjust constituents distribution and pressure across entire porous media.

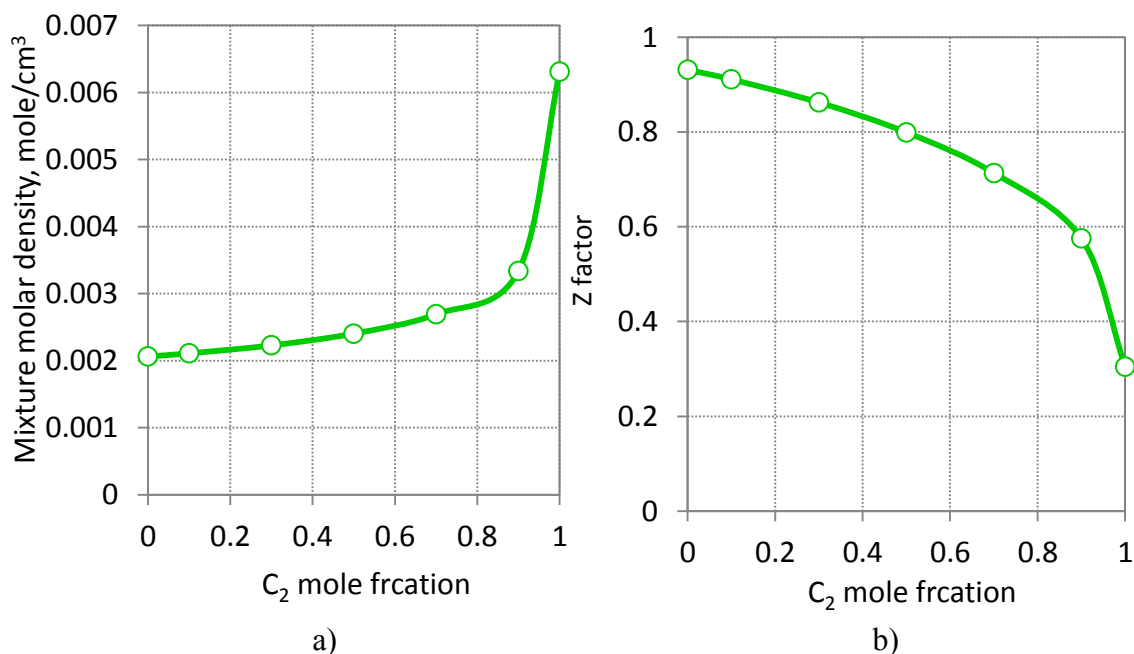


**Fig.4.27:** C<sub>1</sub>-C<sub>2</sub> system volumetric properties at P=707 psia and T=90<sup>0</sup>F:  
a)molar density; b) compressibility factor Z

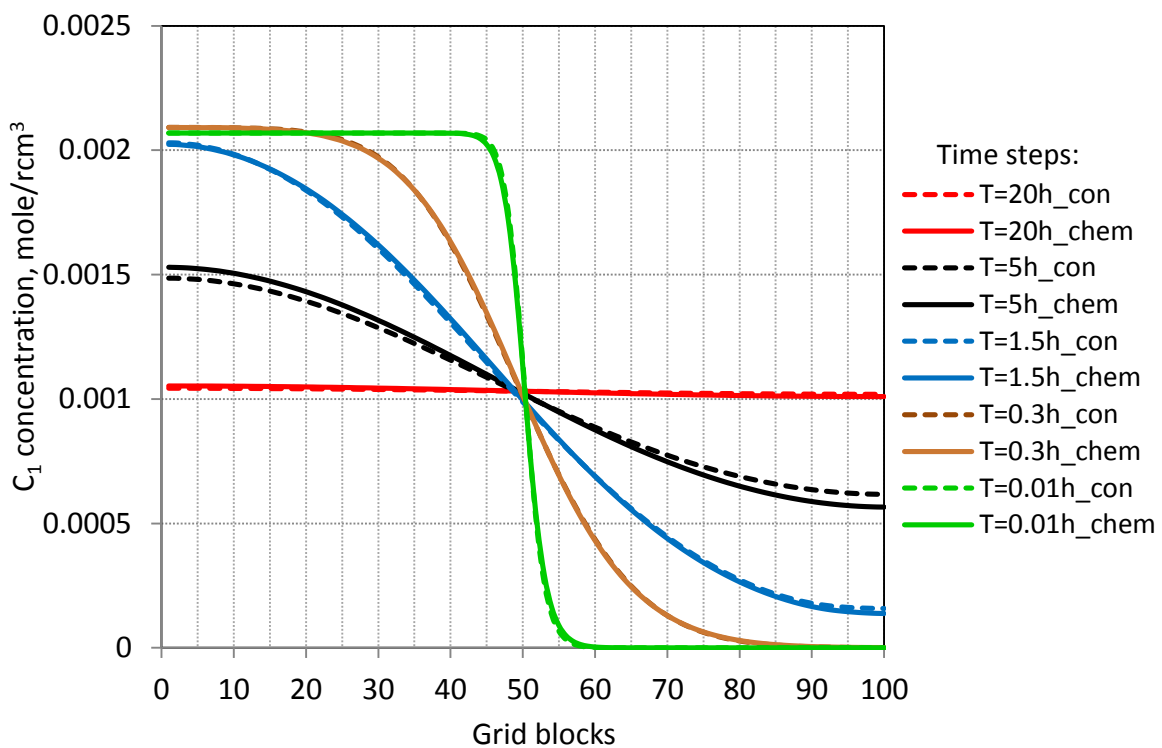


Fig.4.28: C<sub>1</sub> concentration-distance profile at different time steps at P=707 psia and T=90<sup>0</sup>F

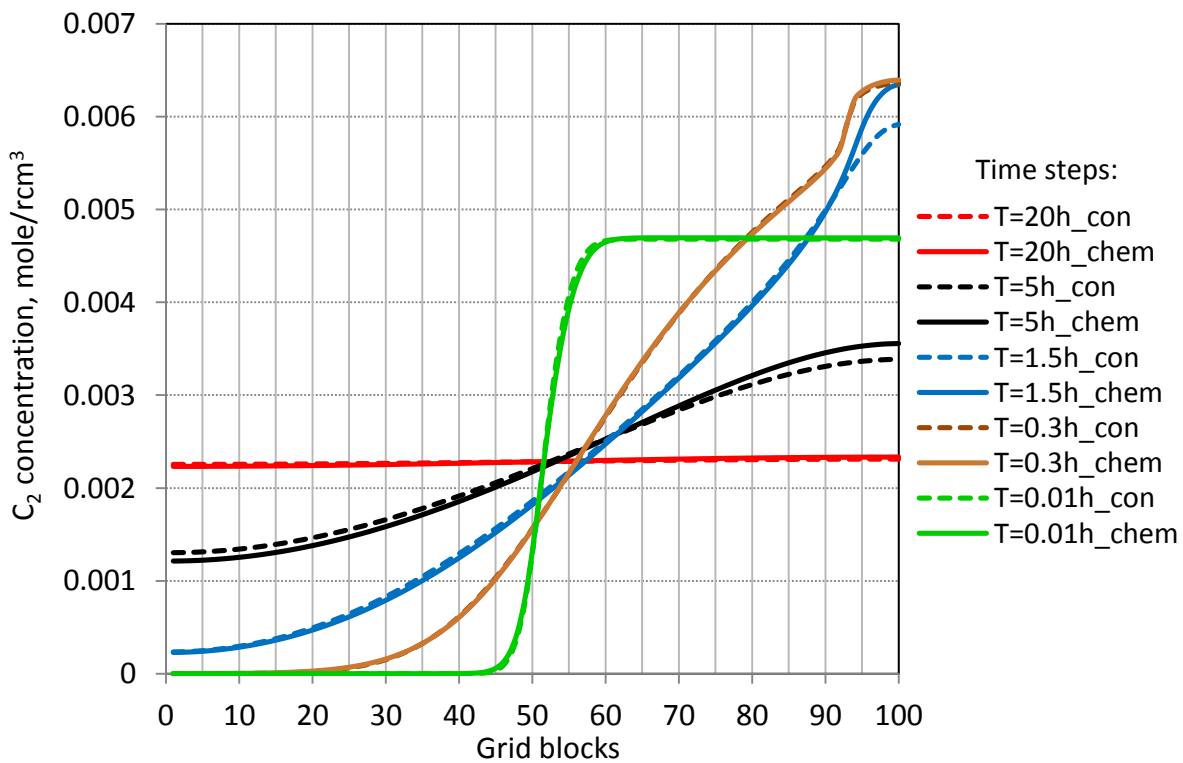


Fig.4.29: C<sub>2</sub> concentration-distance profile at different time steps at P=707 psia and T=90<sup>0</sup>F

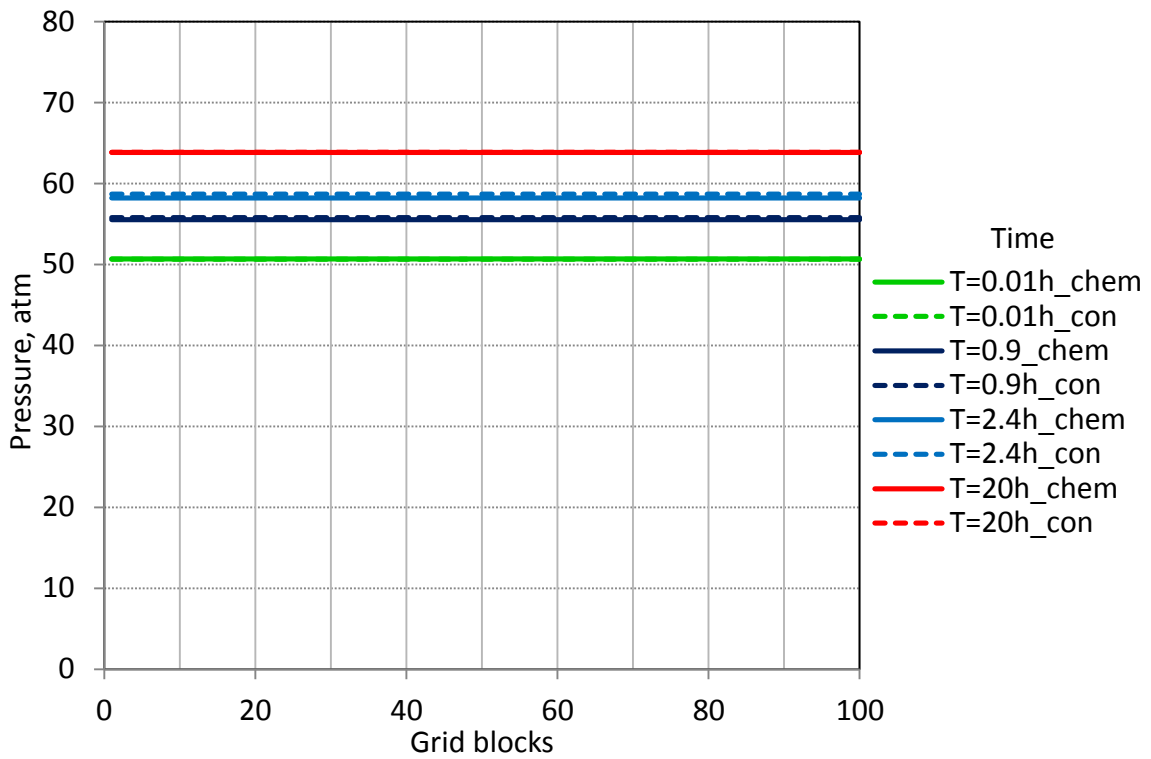


Fig.4.30: Pressure-distance profile at different time steps at  $P=707$  psia and  $T=90^{\circ}\text{F}$

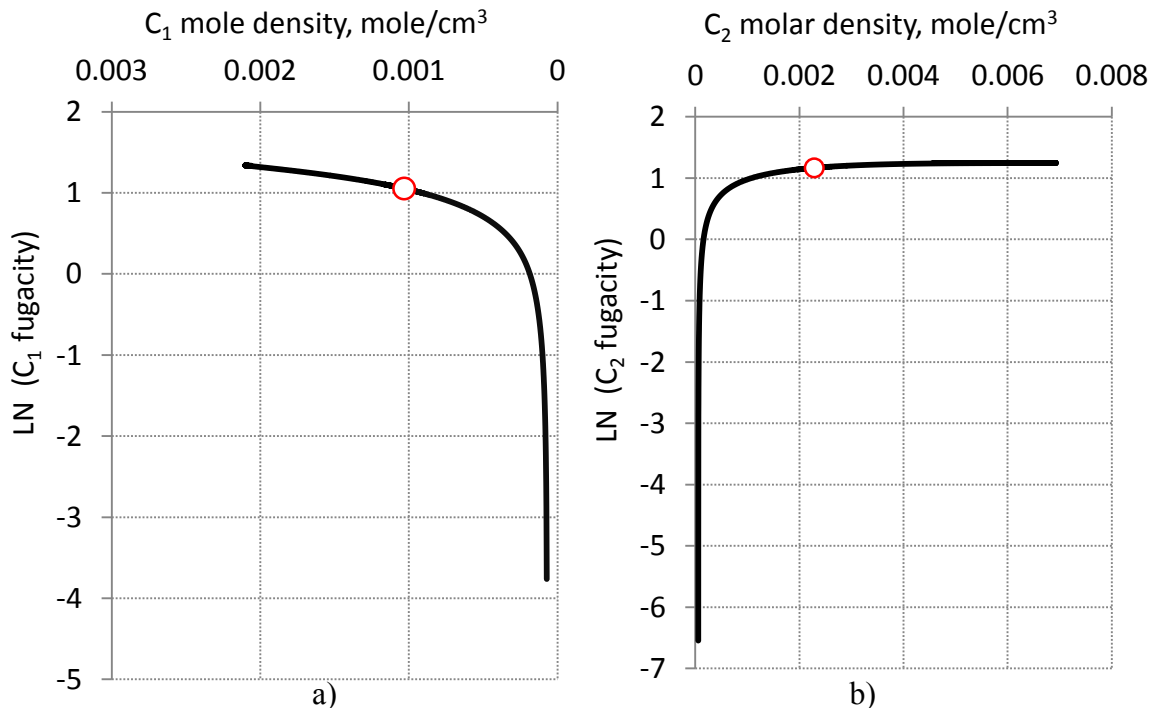


Fig.4.31:  $\text{Ln}(\text{fugacity})$  as a function of molar density at  $P=707$  psia and  $T=90^{\circ}\text{F}$ :

a)  $C_1$  b)  $C_2$

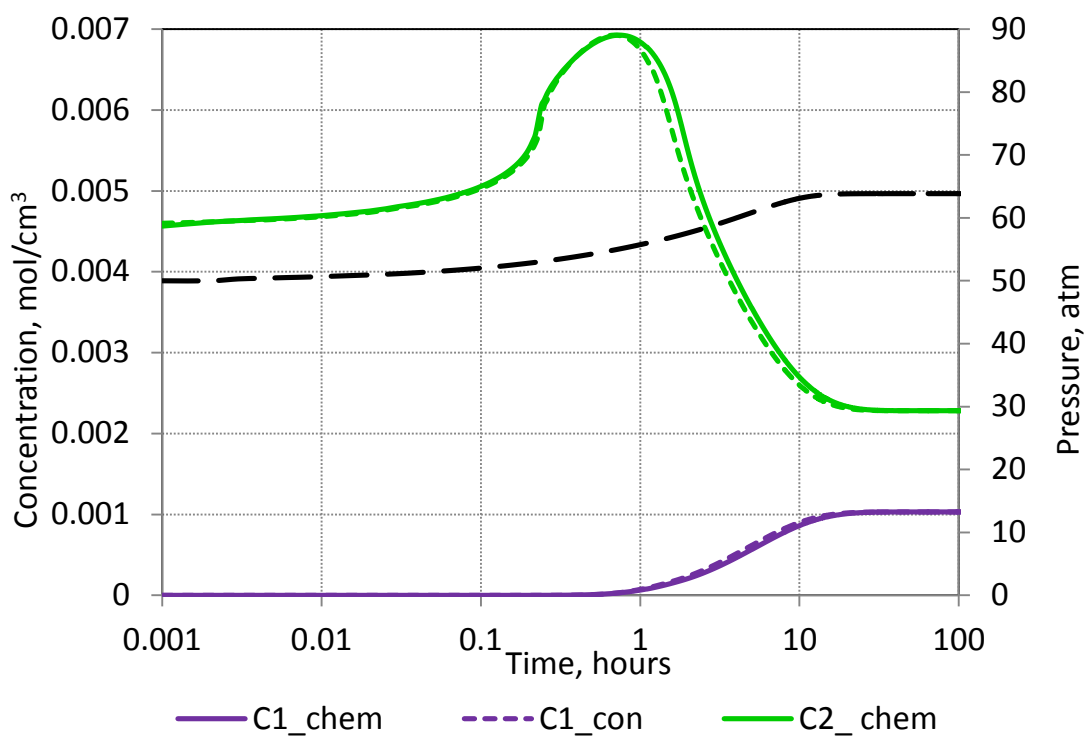


Fig.4.32: Concentration and pressure as a function of time. NY=100

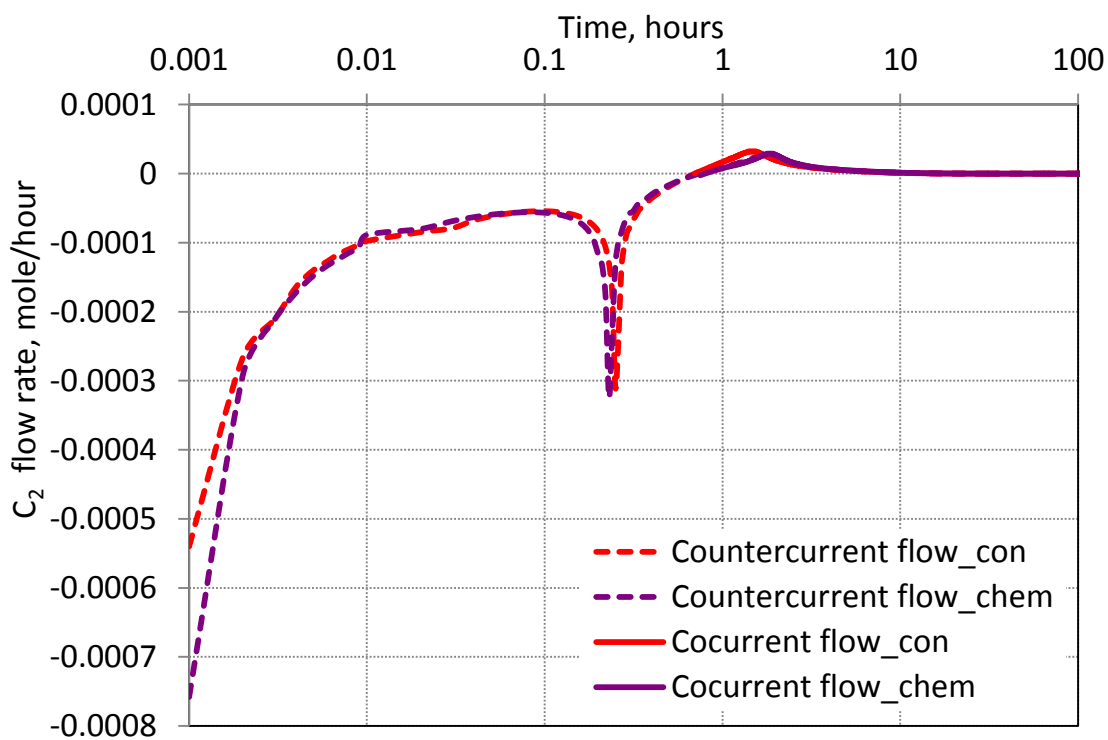
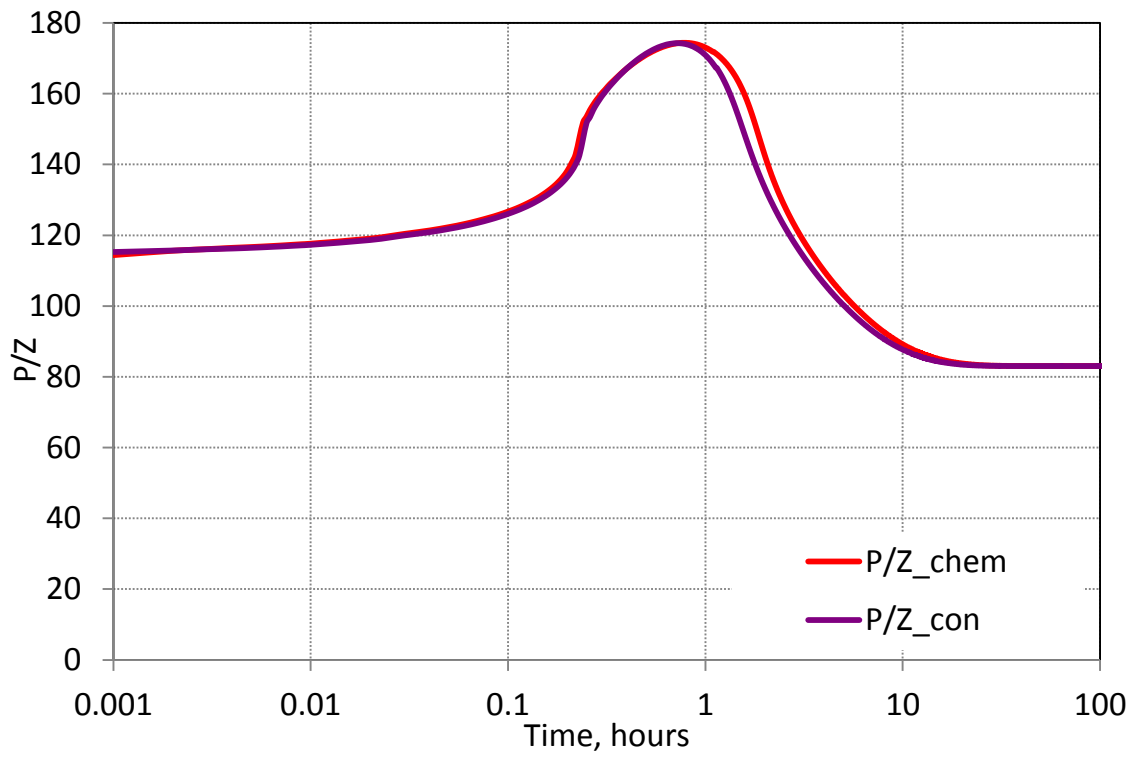
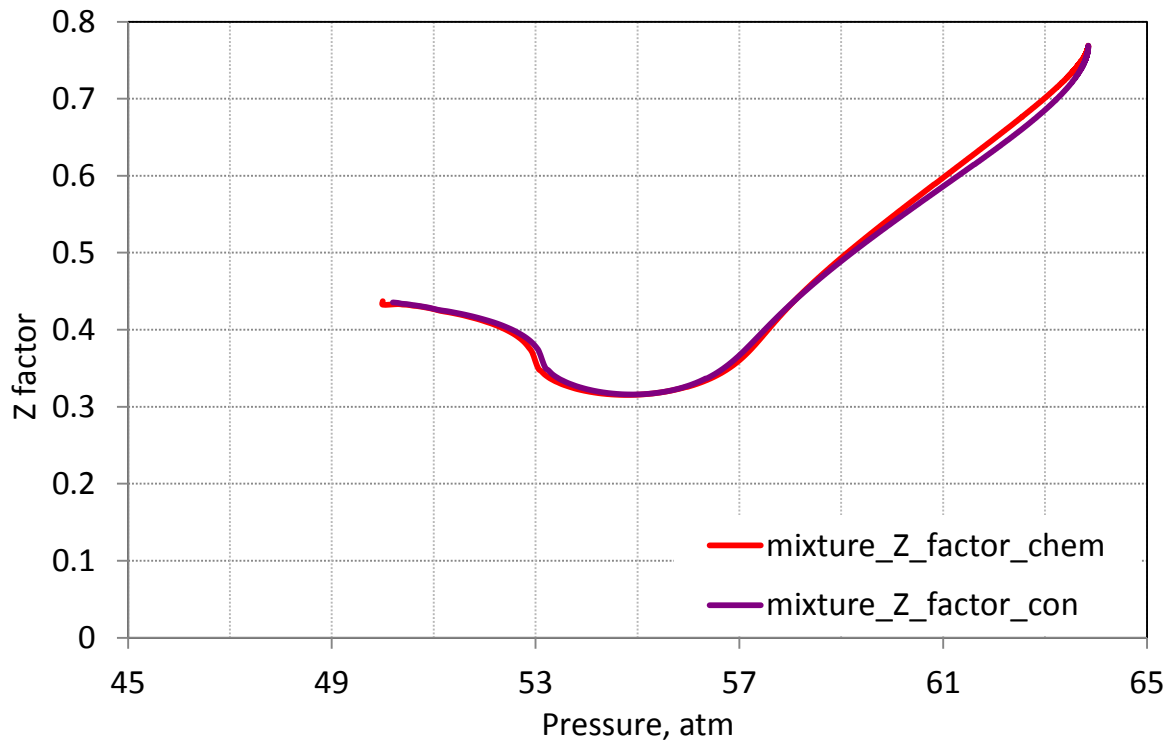


Fig.4.33: C<sub>2</sub> component inter-block flow rate. NY=100



**Fig.4.34:** P/Z ratio as a function of time. NY=100



**Fig.4.35:** Fluid compressibility as a function of pressure. NY=100

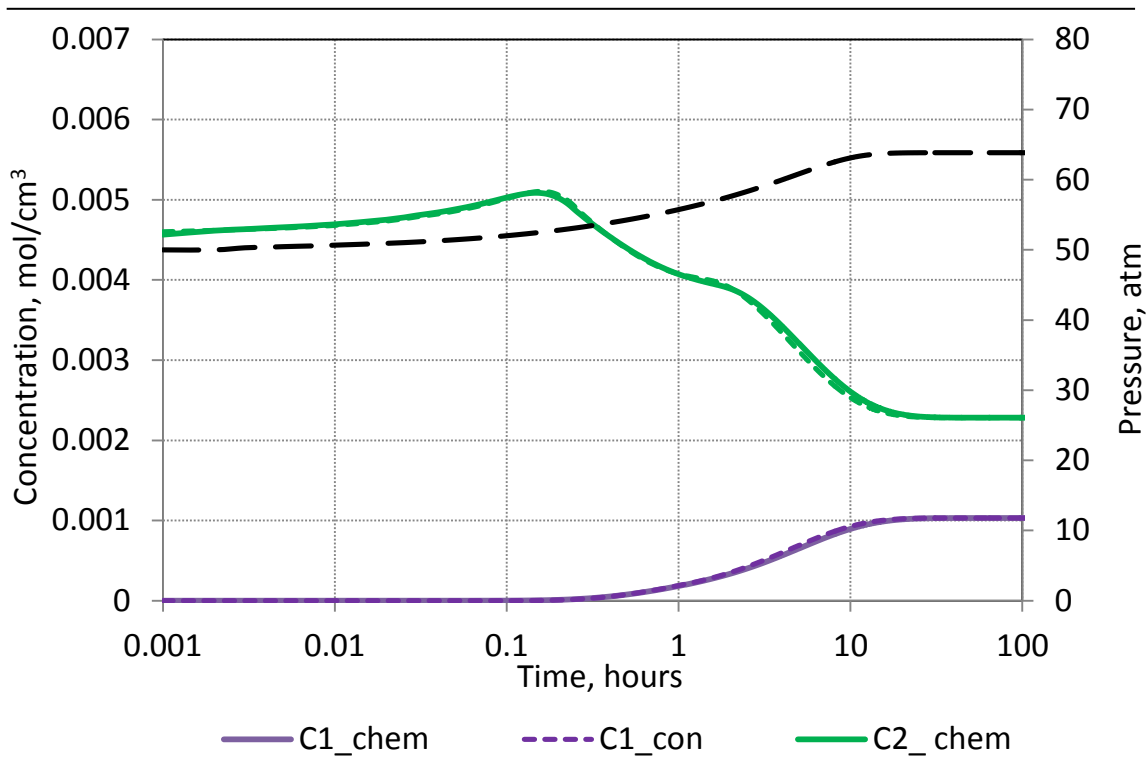


**Fig.4.36:** Concentration and pressure as a function of time. NY=80

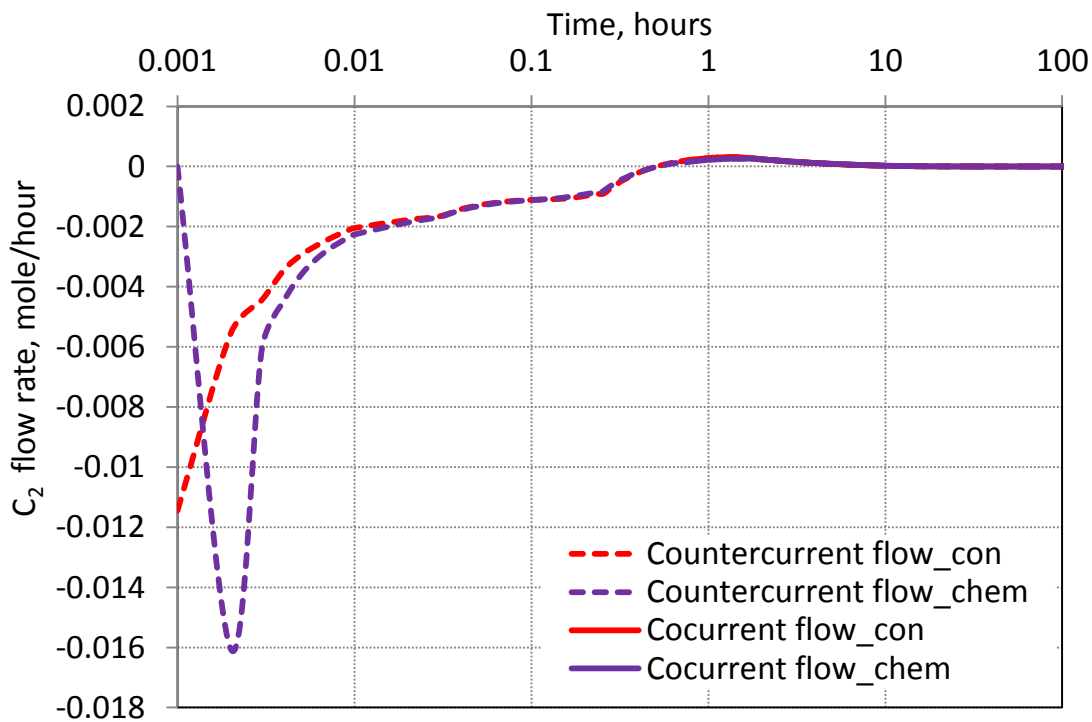


**Fig.4.37:** C<sub>2</sub> component inter-block flow rate. NY=80



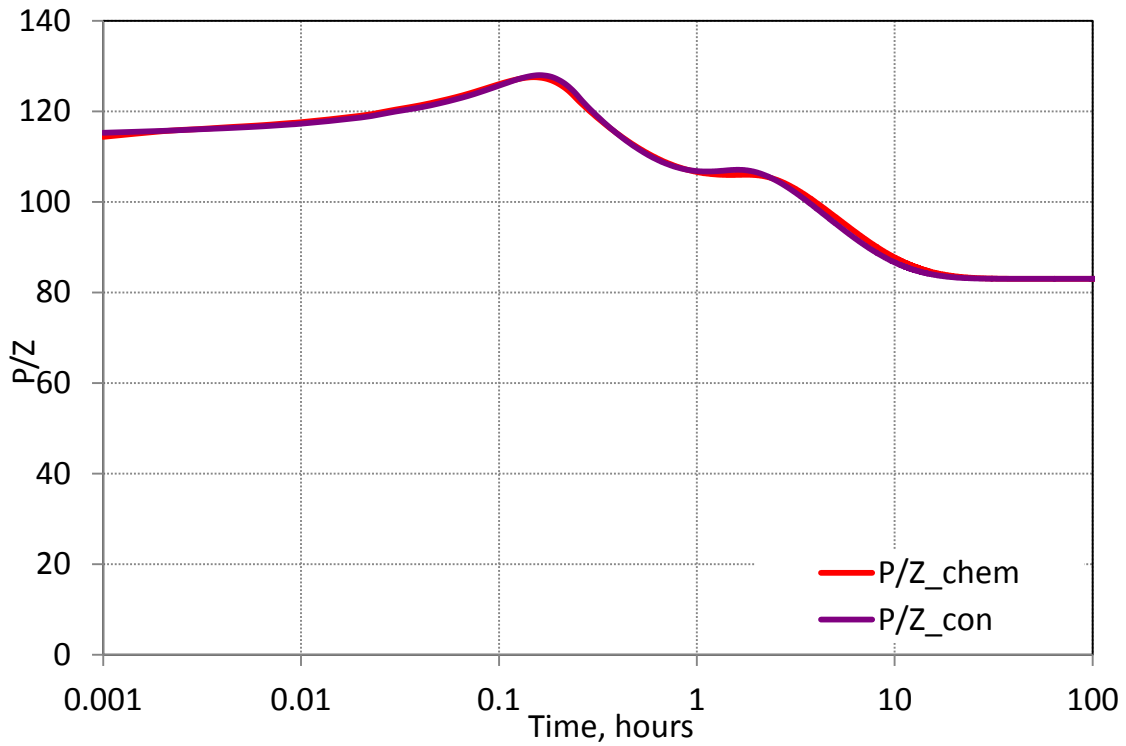


Fig.4.38: P/Z ratio as a function of time. NY=80

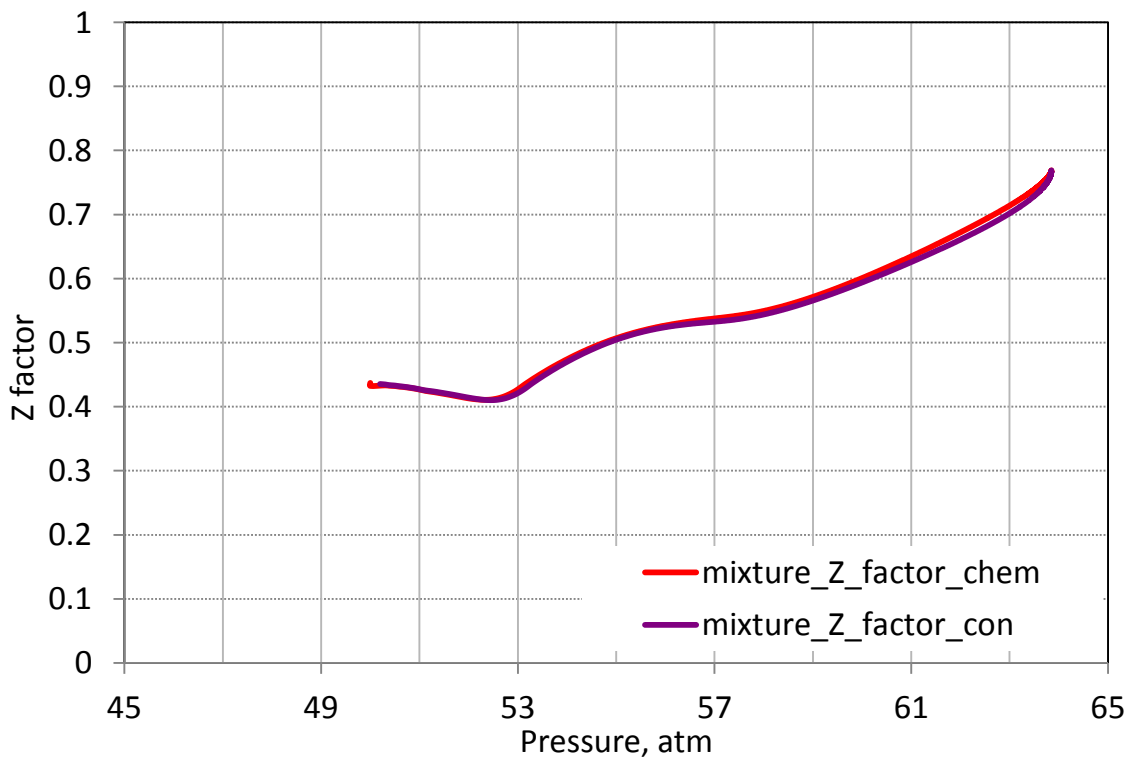
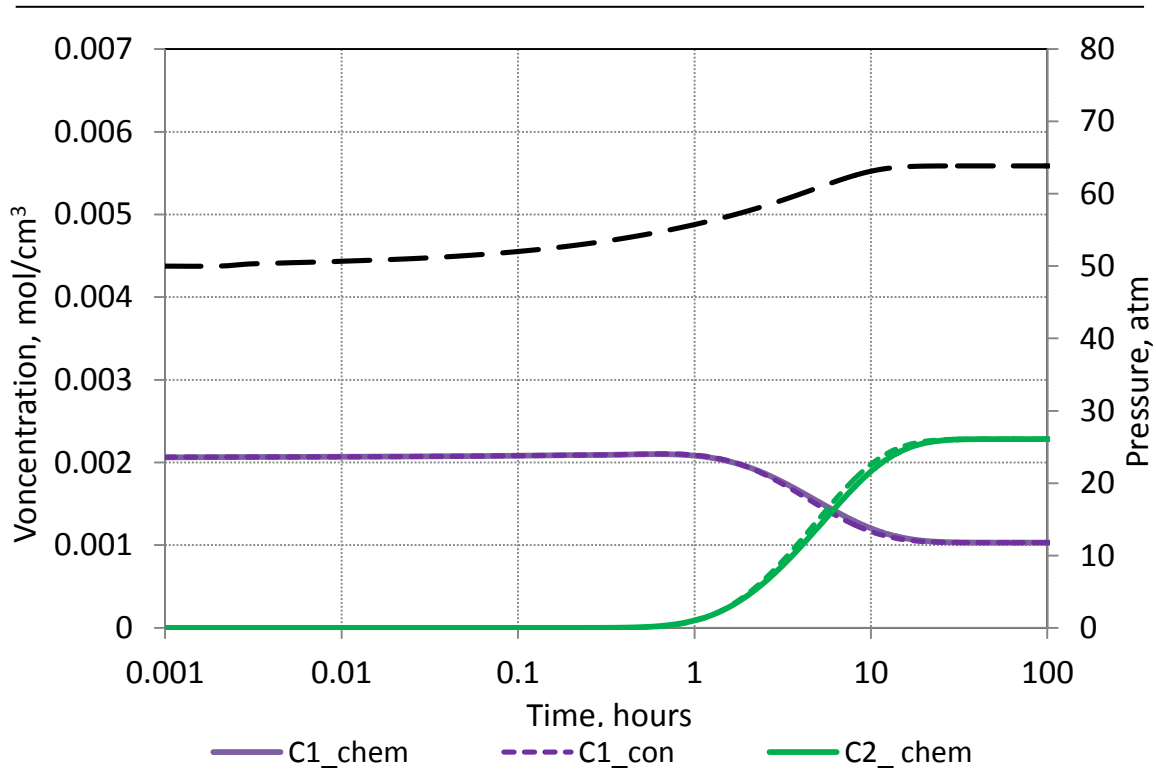
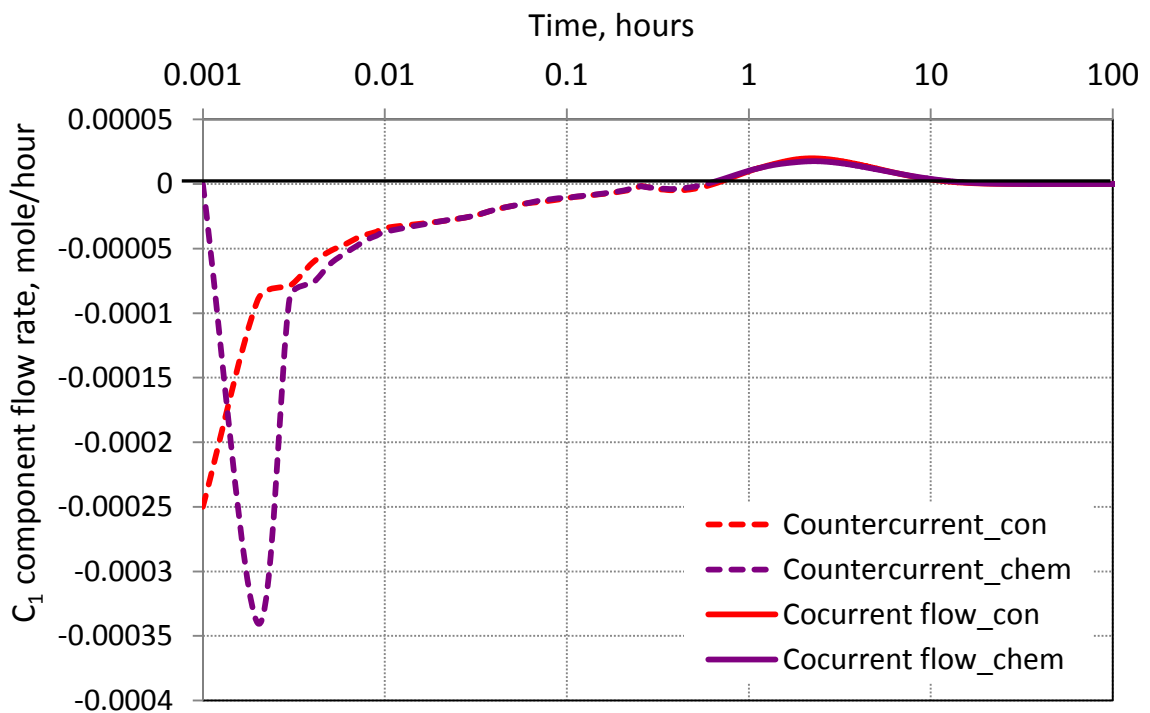


Fig.4.39: Fluid compressibility as a function of pressure. NY=80



**Fig.4.40:** Concentration and pressure as a function of time. NY=1



**Fig.4.41:**  $C_1$  component inter-block flow rate. NY=1

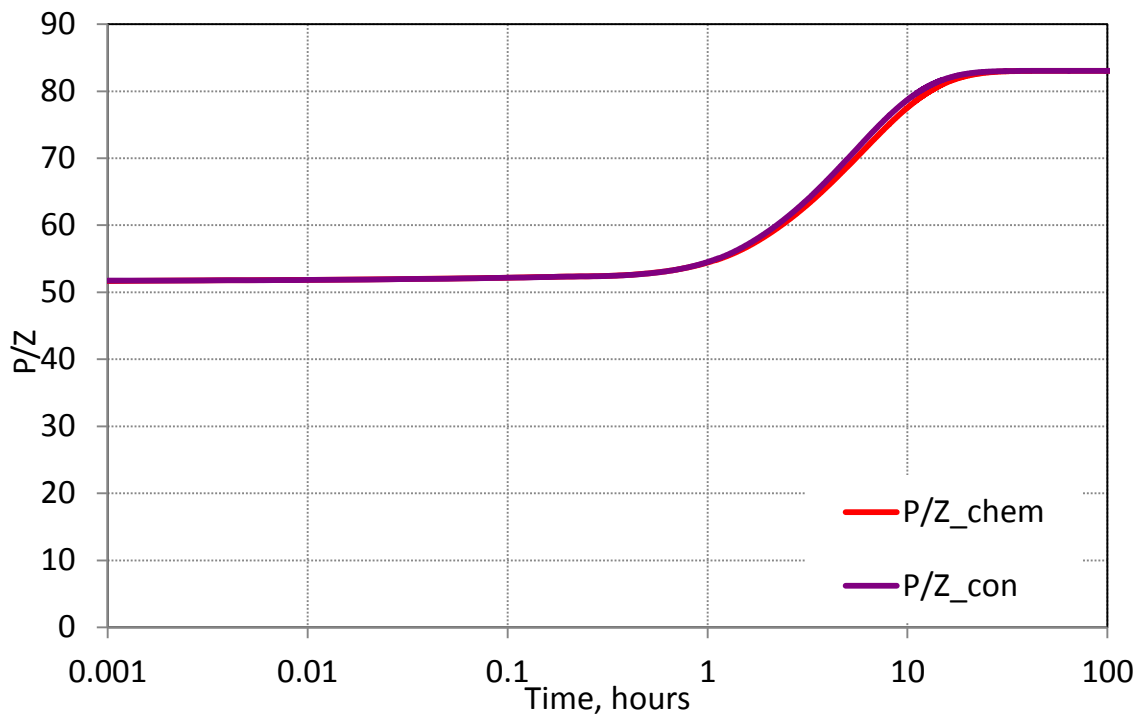


Fig.4.42: P/Z ration as a function of time. NY=1

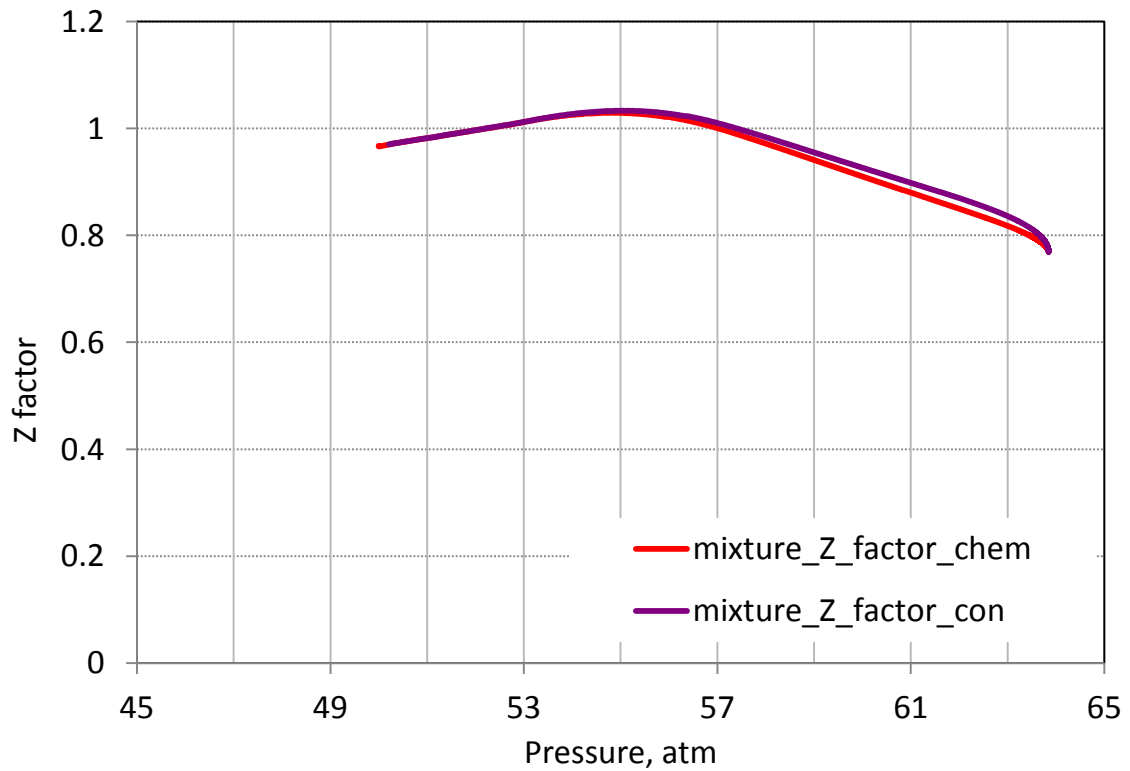


Fig.4.43: Fluid compressibility as a function of pressure. NY=1

---

#### 4.5.2 Diffusion in the methane-ethane mixture critical region

We also performed a simulation run at pressure-temperature condition specified as:  $P=800\text{psia}$  and  $T=73^{\circ}\text{F}$ . This combination is asymptotically close to critical point of mixture composed of 0.15 and 0.85 mole fractions of  $C_1$  and  $C_2$  respectively.

At specified pressure-temperature combination mixture molar density varies significantly with composition. The molar density of the mixture, composed of only ethane, is  $0.0106\text{ gmole/cm}^3$  and it goes down to only  $0.0025\text{ gmole/cm}^3$  for pure  $C_1$  fluid. It follows, that some convective bulk flow appears due to variation of molar density during diffusion flux.

We shall more concentrate on specific diffusive performance, caused by critical region. During diffusion flux the critical condition is expected to be developed at some grid blocks with mixture composition indicated above.

Fig.4.44 and Fig. 4.45 describe the concentration-time-distance and mole fraction-time-distance behavior respectively of  $C_1$  during diffusive mixing with  $C_2$ . The similar plots were built for  $C_2$  component and results are presented in Figs.4.46-4.47. We can observe unusual fluctuation in distribution profile of  $C_1$  component. The reason for this high divergence we can relate to the compositional effect in the grid blocks, where maximum deviation was noted. From the Fig.4.44 it is clearly seen that fluctuations appeared locally and exactly correspond to the area of critical composition: 0.15 and 0.85 mole fraction of  $C_1$  and  $C_2$  respectively (Fig. 4.45-4.47). We found out, that zone of divergence reside in the grid blocks  $NY=51$ ,  $NY=52$  and  $NY=53$ .

We will study diffusion performance driven by concentration gradient in the specified cells more precisely. At any given time step pressure is uniform across model. However mixture compress differently, due to various composition in the grid blocks. This was evidenced by plotting on the same graph values of  $Z$  factor as a function of pressure for three adjacent grid blocks:  $NY=51$ ,  $NY=52$  and  $NY=53$  (Fig.4.48a). A similar plot of fluid compressibility as a function of composition for the same selected grid blocks is shown in Fig. 4.48b. Figures demonstrate significant

---

disagreement in  $Z$  factor values for the same mixture composition, showing more compressible fluid in the grid block 51. This discrepancy most probably is due to higher pressure in the neighboring grid block at the moment when precisely defined critical composition is archived (Fig.4.49). Since system pressure increased,  $C_1$ - $C_2$  mixture, even at “critical” composition, is beyond its critical condition. Therefore, the critical phenomena in grid blocks 52 and 53 affect the fluid behaviour in a much lesser extent. The fluid compressibility ( $Z$  factor) increases as  $C_1$  mole fraction increases in the mixture. The critical composition effect combined with near-critical pressure gives a sharp rise of fluid compressibility in the cell NY=51 (Fig. 4.50). The compressibility factor growth is balanced by a compensating bulk flow of  $C_1$  and  $C_2$  together out of the grid block NY=51, so that to reduce number of moles in the given cell. Existence of convection can be demonstrated by plotting inter-block flow rates (Figs.4.51,4.52). The component flux down its lower concentration considered to be positive (co-current flow), component flux opposing diffusive flow is treated as negative (counter-current flow). At an early stage, first countercurrent bulk flows reflect the convective flows caused by pressure gradients due to molar density variation. After co-current fluxes were established in the system, the dramatic decline in diffusive rates appeared, suggesting that some countercurrent fluxes were introduced again. The simultaneous collapse of diffusive flow rates in all the cells exactly coincide in time with critical phenomena developed in cell 51. That observation makes us confident in describing them as compensating bulk flows, directed against true diffusive mass transfer. When critical composition is exceeded, pure diffusive flow will start to grow again.

By detailed analysis of simulation data it has been shown that in some special cases the diffusive mass transfer can be a result of diffusion itself and convective bulk flows. The direction of the bulk flows, created by pressure gradients or exclusive critical behaviour, can either intensify/accelerate or oppose diffusion fluxes. The magnitude of phenomenal convection is likely to be the specified problem dependant. However, one thing is clear: for accurate prediction or proper interpretation of diffusion experiments, employing traditional concentration-based formulation of diffusion (classical Fick’s law), one should take into account and preferably to size a phenomenon of bulk flow, what is affecting the total mass transport in the mixing system.

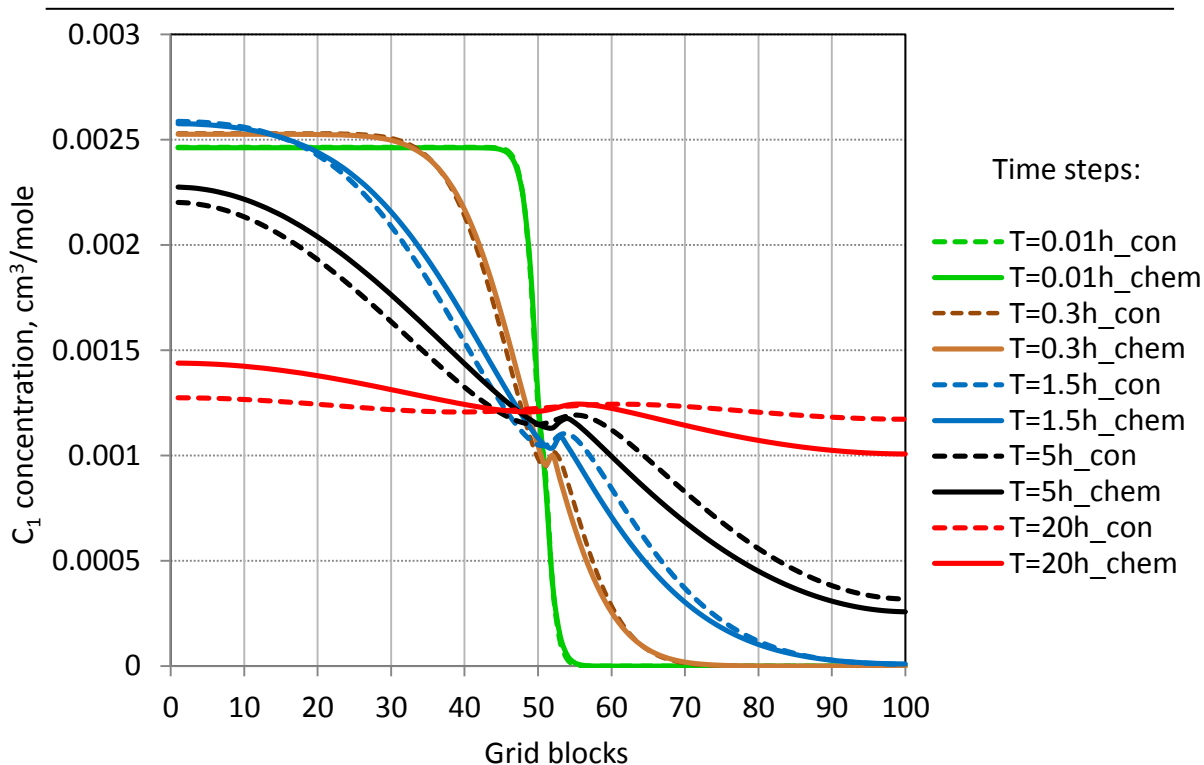


**Fig.4.44:**  $C_1$  concentration-distance profile at different time steps at  $P=800$  psia and  $T=74^\circ\text{F}$

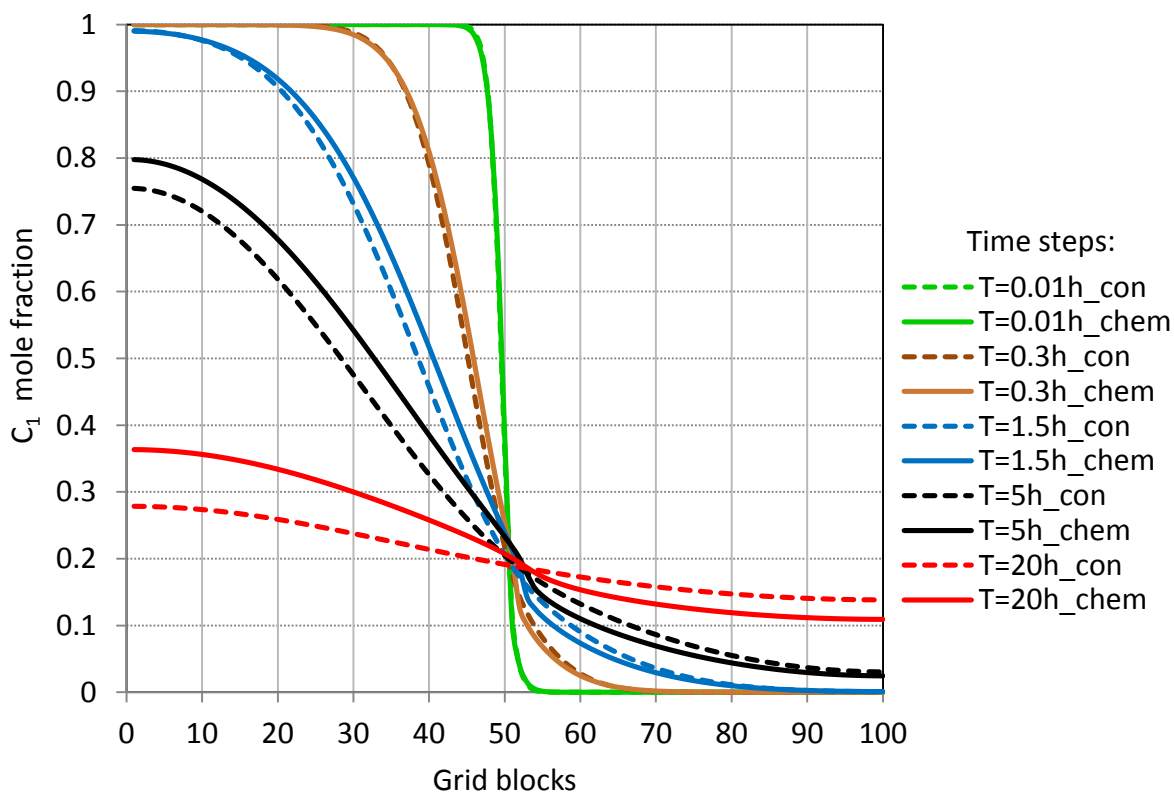


**Fig.4.45:**  $C_1$  mole fraction-distance profile at different time steps at  $P=800$  psia and  $T=74^\circ\text{F}$

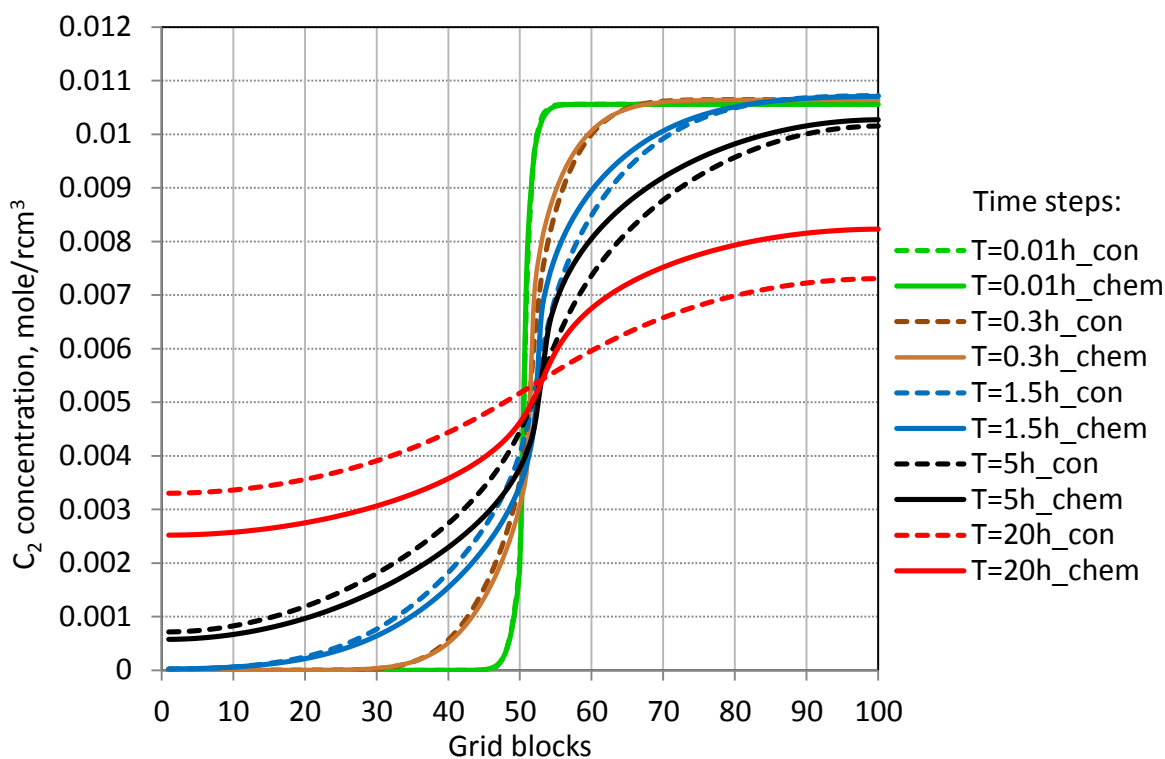


**Fig.4.46:**  $C_2$  concentration-distance profile at different time steps at  $P=800$  psia and  $T=74^{\circ}\text{F}$

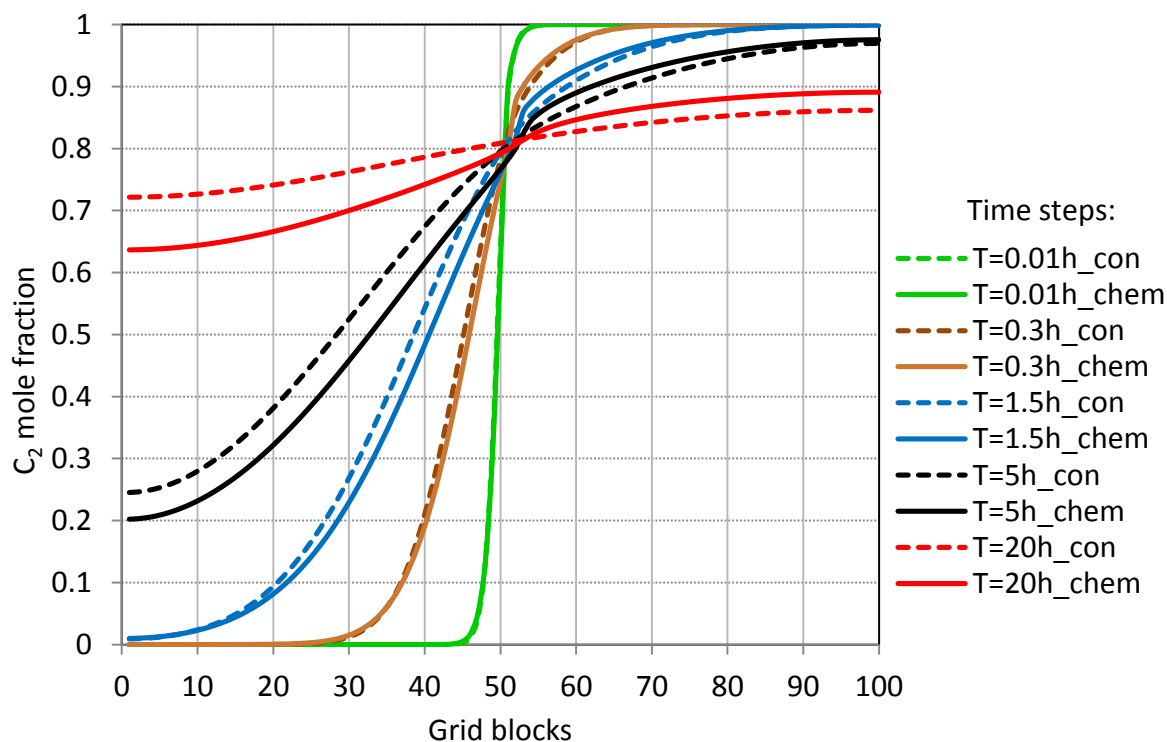


**Fig.4.47:**  $C_2$  mole fraction-distance profile at different time steps at  $P=800$  psia and  $T=74^{\circ}\text{F}$

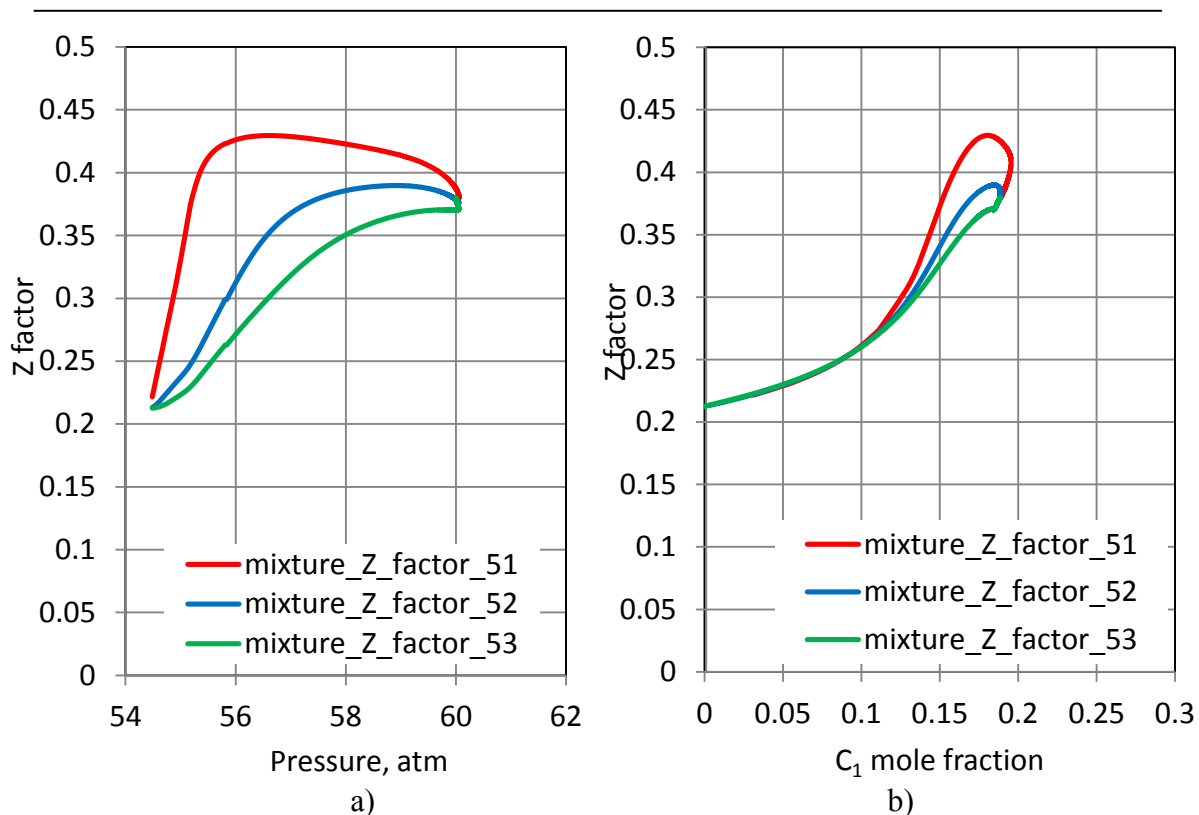


**Fig.4.48:** Z factor as a function of a) pressure, b) composition

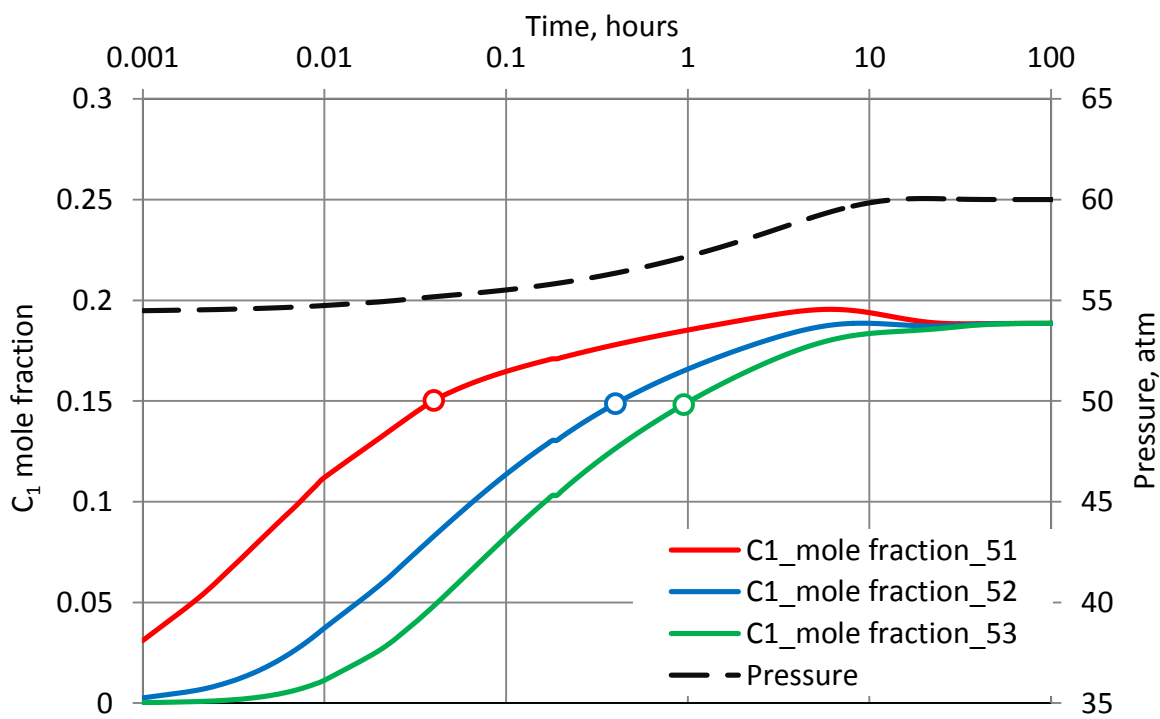
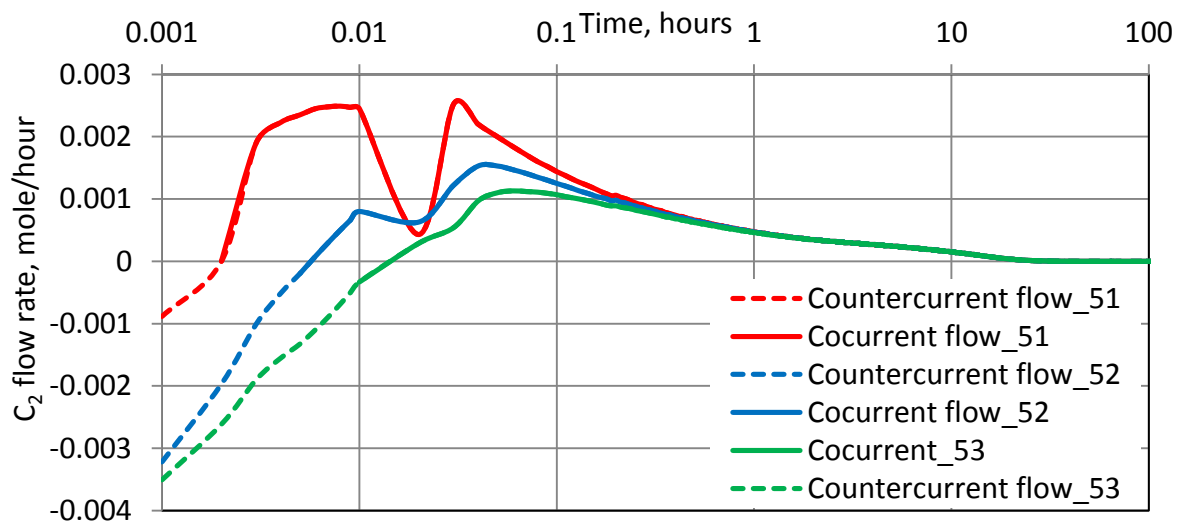
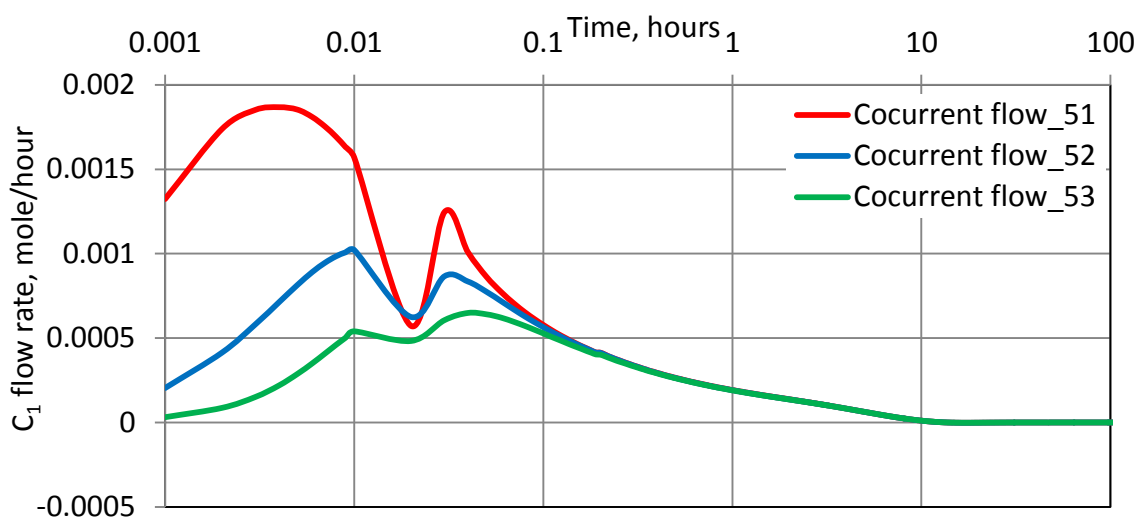
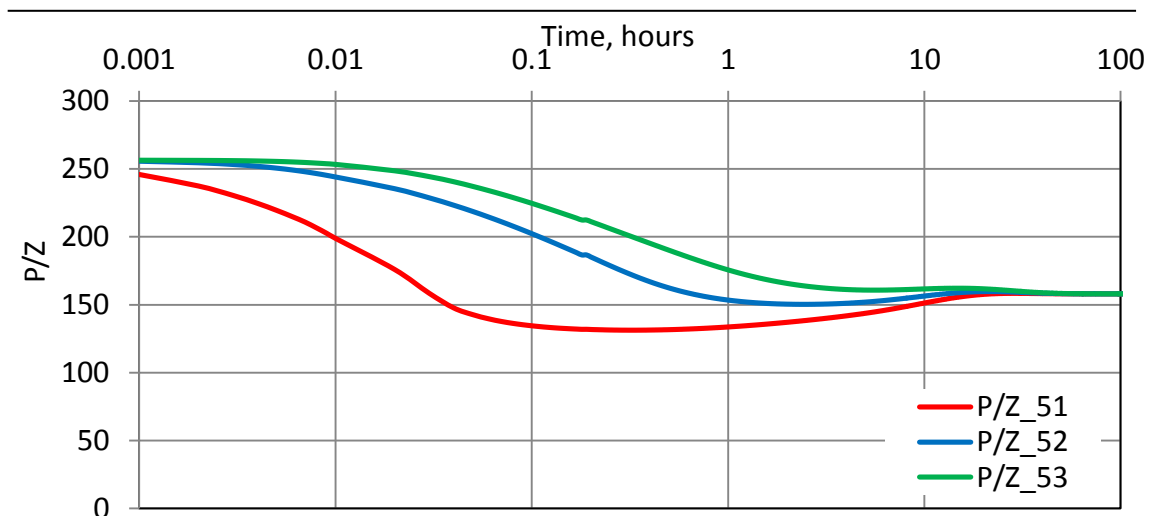


**Fig.4.49:**  $C_1$  mole fraction and pressure profiles as a function of time





---

## Diffusion coefficients determined from simulated diffusion experiments

---

Our objective in this chapter is to determine diffusion coefficients from diffusion experiments simulated in Eclipse 300. It is our intention to present follow up of this investigation with a discussion of the complex effect of convective bulk flow on real mass transfer coefficients.

It is to be recalled that modelling diffusion experiments in present work, employing simulator Eclipse 300, associated with following assumptions:

- Diffusive behaviour of  $C_1$ - $C_2$  binary system is described by one diffusion coefficient:  $D_{C1}=D_{C2}$ .
- For any initialisation pressure input diffusion coefficients were determined for the «Base» mixture, composed of 50% mole fraction of  $C_1$  and 50% - of  $C_2$  (employing Sigmund correlation);
- Diffusion coefficients (specified in the input data file) are constant over whole run time, assuming no variation with composition and molar density;
- We set identical diffusion coefficients for both diffusivity models using concentration or chemical potential as a driving force.

A great number of diffusion experiments were conducted, considering diffusive mixing in  $C_1$ - $C_2$  system at standard pressure and up to 7000 psia (along isotherm  $T=90^{\circ}\text{F}$ ). To estimate diffusion coefficients from simulation results we adopted procedure suggested by Sigmund, who conducted experiments of diffusion in the high-pressure dense gases (chapter 2.4). The geometry of the model, the time period elapsed and the average concentration change in each region may be used to measure

---

mutual diffusion coefficients from the simulation results (Eq.2.24-2.25). The determined diffusion coefficients from simulated experiments are compared to the theoretical values from empirical Sigmund correlation (Figs.5.1-5.2).

At low pressure experiment diffusion coefficients obtained from simulation results and input data (theoretical values) are in a good agreement. However at pressure just above 700 psia the system cannot be described with single diffusion coefficient any more. The different diffusion coefficients were obtained from simulation results and the reason is that  $C_1$  and  $C_2$  components diffuse with different mass transfer rates. If the mass transfer values obtained from simulated experiments were not contaminated with bulk flows the plots would overlap (Figs.5.1-5.2). The significant deviation in coefficients shows that  $C_1$  and  $C_2$  diffusion appears strongly dependent of molar density variation and consequent changes in mixture volumetric behavior.

This is confirmation that the total mass transfer during diffusive mixing is to be much more complicated mathematically and to be not simply driven by its concentration/chemical potential gradients as would be the case if molar density is independent on composition. The reversed bulk flows are undetectable in terms of conventional interpretation of diffusive experiments.

It is of our interest to note, however, that the actual molecular diffusion coefficients were not determined from simulated experiments, but the changes in average molar concentration of the components followed with time were registered. The conventional analysis of diffusion experiment does not take into account neither forced fluid reorientation, nor reversed bulk flows within the region of interest, created by pressure gradients or exclusive critical mixture behavior.

From observation of Fig.5.4 alone we can conclude, the deviation between  $C_1$  and  $C_2$  transfer coefficients and their fluctuations with time strongly affected by magnitude of convective fluxes (simulated diffusion experiment at  $P=707$ psia). Figs.5.5-5.6 show that bulk flows occurred in opposite direction to concentration/chemical potential gradients (counter-current flows) result in artificially slowed down diffusivity itself. The massive reversed convection of  $C_2$  yielded more tangible decrease of registered diffusion coefficients for  $C_2$  to compare with  $C_1$  (Fig.5.4).

---

It proved to be difficult to obtain definitive mass transfer values from pure diffusion that could be compared to the theoretical values from empirical correlation suggested by Sigmund. However we calculated a mean total mass transfer coefficient (averaged  $C_1$  and  $C_2$  mass transfer values) for each run for both diffusivity models and plotted results for density-diffusivity products together with theoretical values versus pressure as in Fig.5.3.

The diffusion coefficients were calculated for selected time period, so that the average dimensionless concentration change in both regions was between 0.15 and 0.25. The specific time frame may introduce sensible uncertainty in calculations, employing traditional concentration-based formulation of diffusion.

Diffusion coefficients depend on the time during which diffusion has been taken place. The concentration change by less than 25 % is referred to the early time steps, which characterize by pronounced convective flows (Fig.5.5-5.6). Thus mass transfer by pure diffusion is “contaminated” highly by reversed bulk flow, which contribution increase as increase variation of molar density with composition.

In order to illustrate the uncertainty introduced by the time selected to determine diffusivity rates, we plotted together dimensionless concentration change for  $C_1$  and  $C_2$  components with time for the diffusion experiment at  $P=707$ psia (Fig.5.7(a,b)). The plots indicate tendencies to different diffusion rates of  $C_1$  and  $C_2$  at the time steps when concentration changed less than 25%. Thus intrinsic  $C_2$  diffusion coefficients for the given time elapsed is lower by 30% than that for  $C_1$  (Fig.5.8 (a,b)), however later on their amplitudes converge. The actual reason is that  $C_2$  molecules transferred in reversed direction by convective motions have being greater than that of  $C_1$  (Fig.5.5-5.6). Consequently, it results in much slower total mass transfer of  $C_2$  in the direction of its concentration gradient.

In our numerical solution the input diffusion coefficient is time independent, whereas concentration gradients decrease with time, consequently diffusive fluxes slow down as system approaches equimolar spatial distribution. It is readily visible from Fig.5.4 that diffusion coefficients for  $C_1$  and  $C_2$  converge and decline together as the system approaching equilibrium. It becomes a problem to choose a representative time and mass transfer coefficient to represent the system in general.

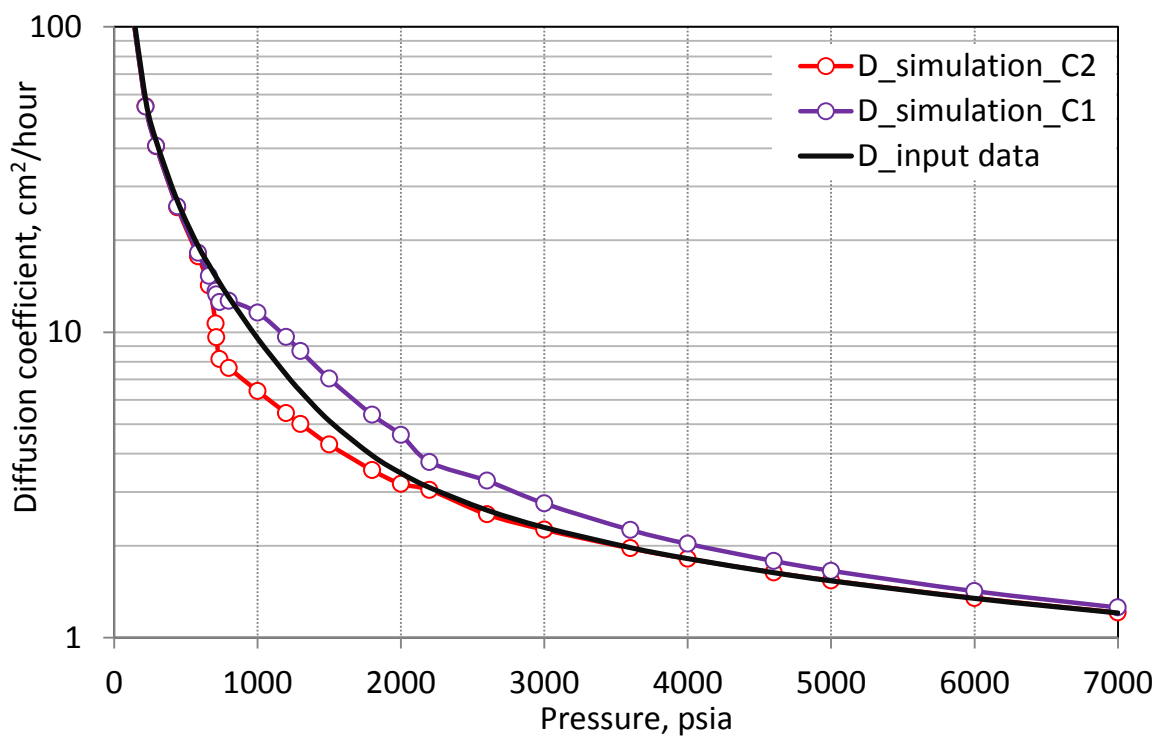


**Fig.5.1:** Diffusion coefficients obtained from simulated diffusion experiments.  
Concentration driven diffusion

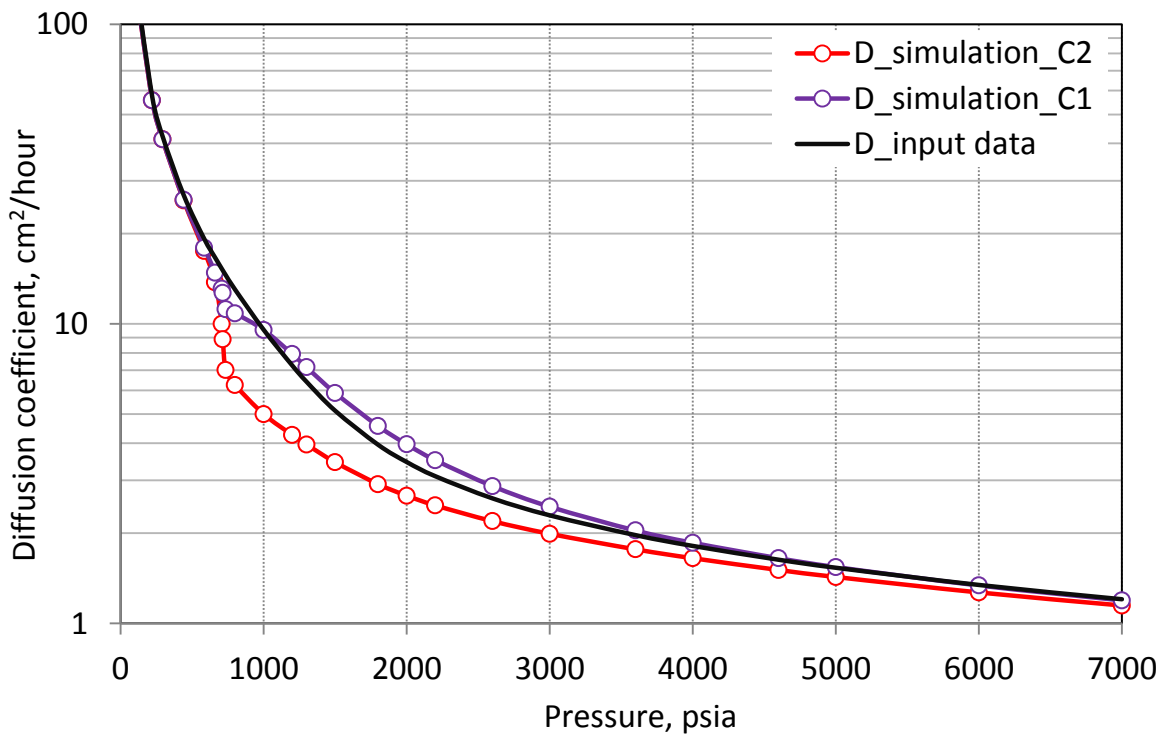


**Fig.5.2:** Diffusion coefficients obtained from simulated diffusion experiments  
Chemical potential driven diffusion

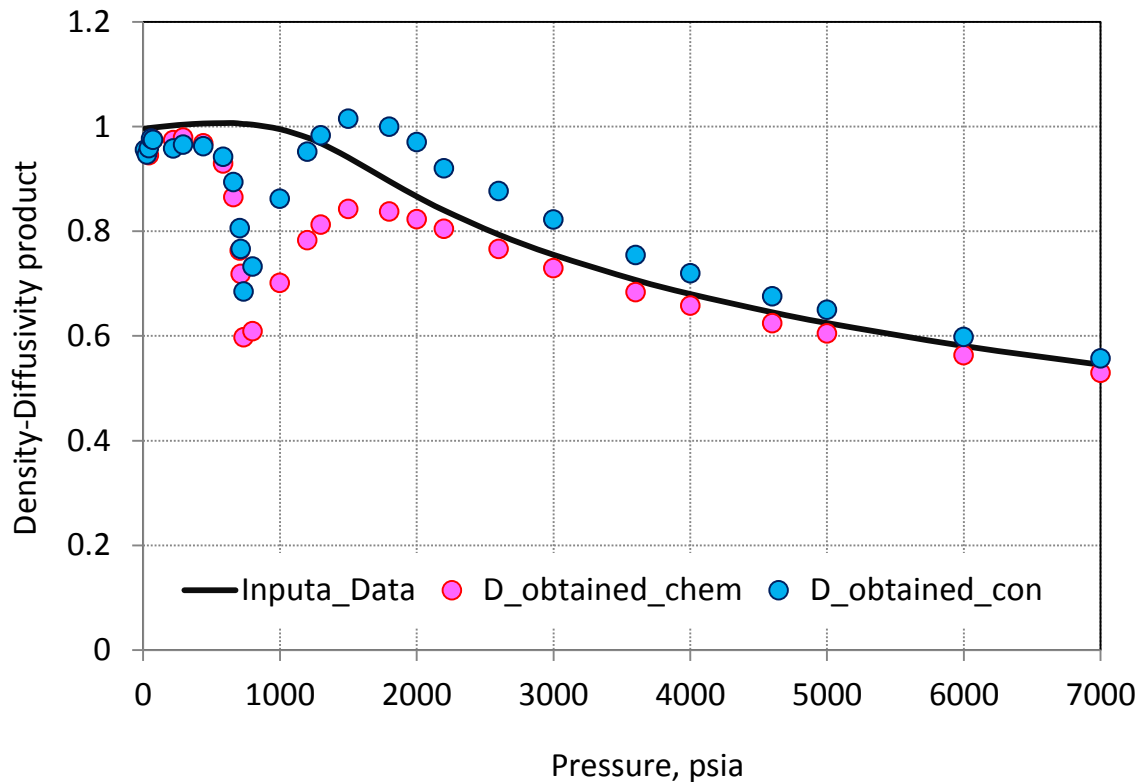


**Fig.5.3:** Density-diffusivity product as a function of pressure

The data in table 5.1 are the results from simulated diffusion experiments at number of pressure values along the isotherm  $T=90^{\circ}\text{F}$ . Referring to column 4 we can see difference in molar densities for pure component fluids (illustrated with colour intensity). Further columns give: theoretical **diffusion coefficients** calculated from Sigmund empirical correlation, **mass transfer coefficients** for  $C_1$  and  $C_2$  components for diffusivity models driven by concentration and chemical potential gradients. We are deliberately distinguishing between the terms “mass transfer coefficients” and “diffusion coefficients”.

The conception of a real mass transfer of the whole solution, expressed as a combined effect of pure diffusion transfer and compensated unequal bulk flows of  $C_1$  and  $C_2$  particles, explains why the mass transfer coefficients for two components are different and depend on mixture molar density variation.

It is following, that the total system cannot be approximated by a single pseudo-mutual mass transfer coefficient.

From the quantitative study of results from Table 5.1 we can arrive to following conclusion. At low and moderate pressure the experimental system has a variation in molar density of constituents within 20%, what results in variation of mass transfer coefficients by less than 2%. However, more significant molar density variation  $\rho=20-40\%$  have as a consequence up to 10% difference in transfer coefficients for  $C_1$  and  $C_2$ . For highly compressed system the same density ratio gives even more sensible range of diffusion coefficients - 25% at the average. Existence of phenomenological critical/near-critical region in the case of gas diffusion, introduce some additional uncertainties in predicted values and transfer coefficients for  $C_1$  can be up to 80% higher than that for  $C_2$  component (related to pressure range 708-1500psia).

We need to point it out, that conventional interpretation of simulated experiments in terms of concentration change, where diffusion is driven by chemical potential gradient, gives information with unknown errors. The component diffusive flux related to chemical potential gradient is a weak function of its concentration.

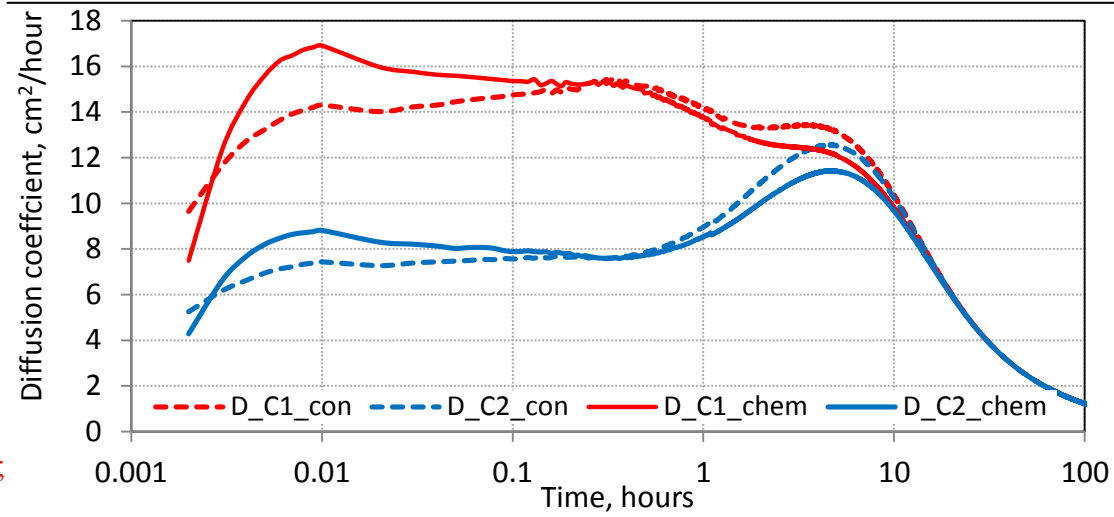


**Fig.5.4:** Diffusion coefficients from simulated experiments as a function of time (P=707psia, T=90<sup>0</sup>F)

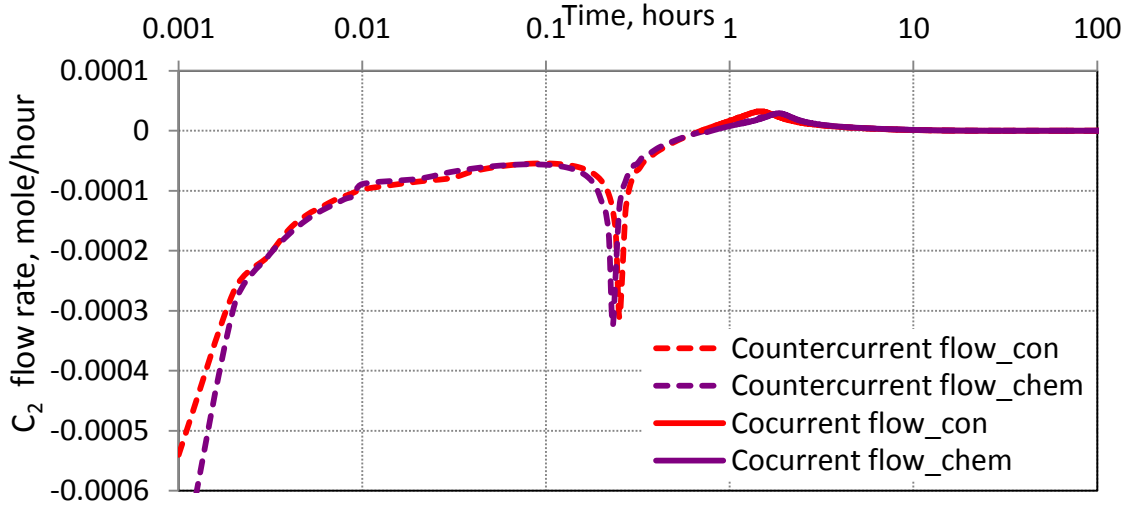


**Fig.5.5:** C<sub>2</sub> component inter-block flow rate. NY=100 ( P=707psia, T=90<sup>0</sup>F)

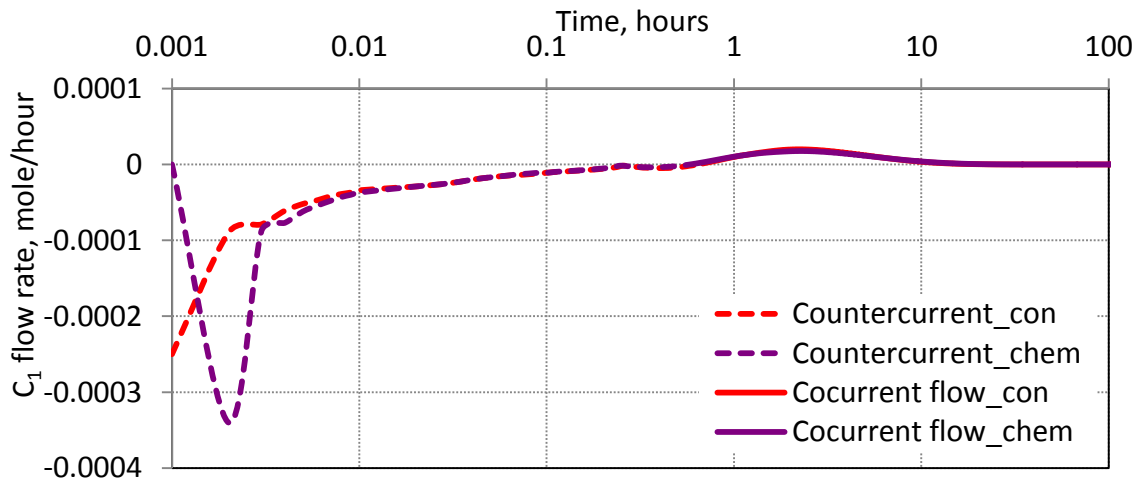


**Fig. 5.6:** C<sub>1</sub> component inter-block flow rate. NY=1 ( P=707psia, T=90<sup>0</sup>F)



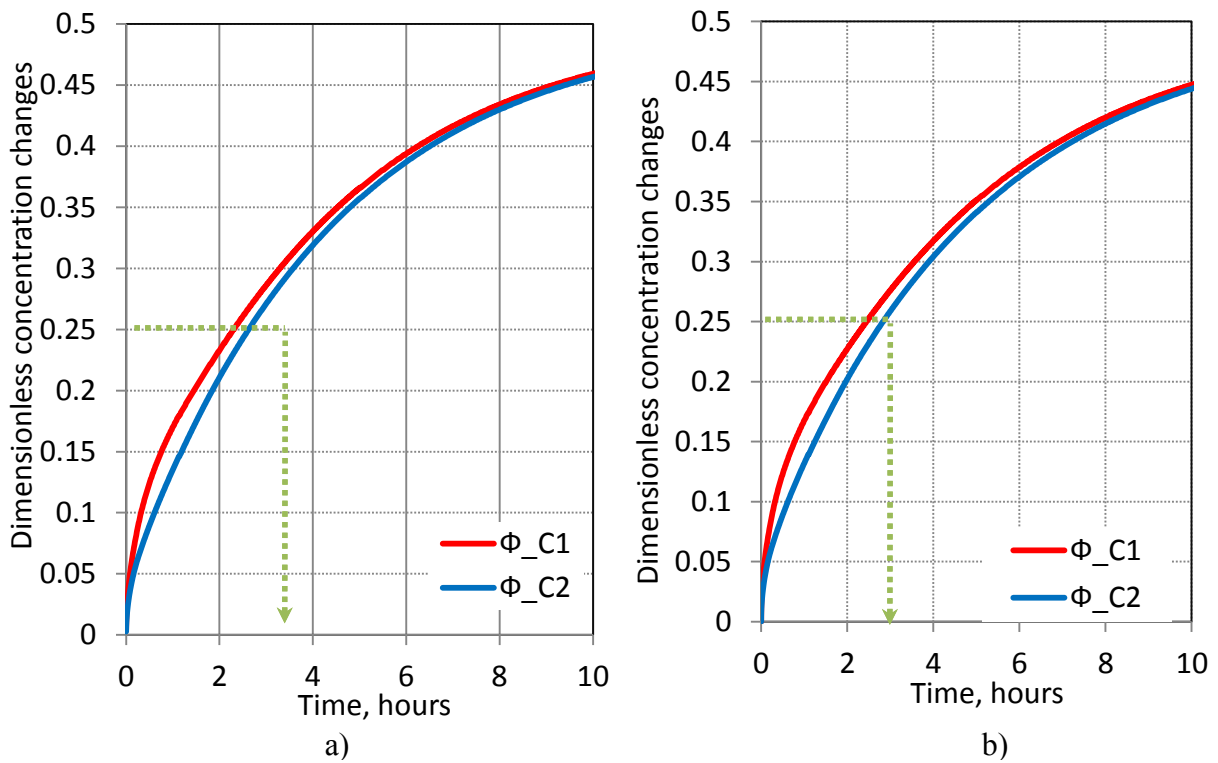


**Fig.5.7:** Dimensionless concentration changes ( $P=707\text{psia}$ ,  $T=90^{\circ}\text{F}$ ):

a) Concentration driven diffusivity model, b) Chemical potential diffusivity model

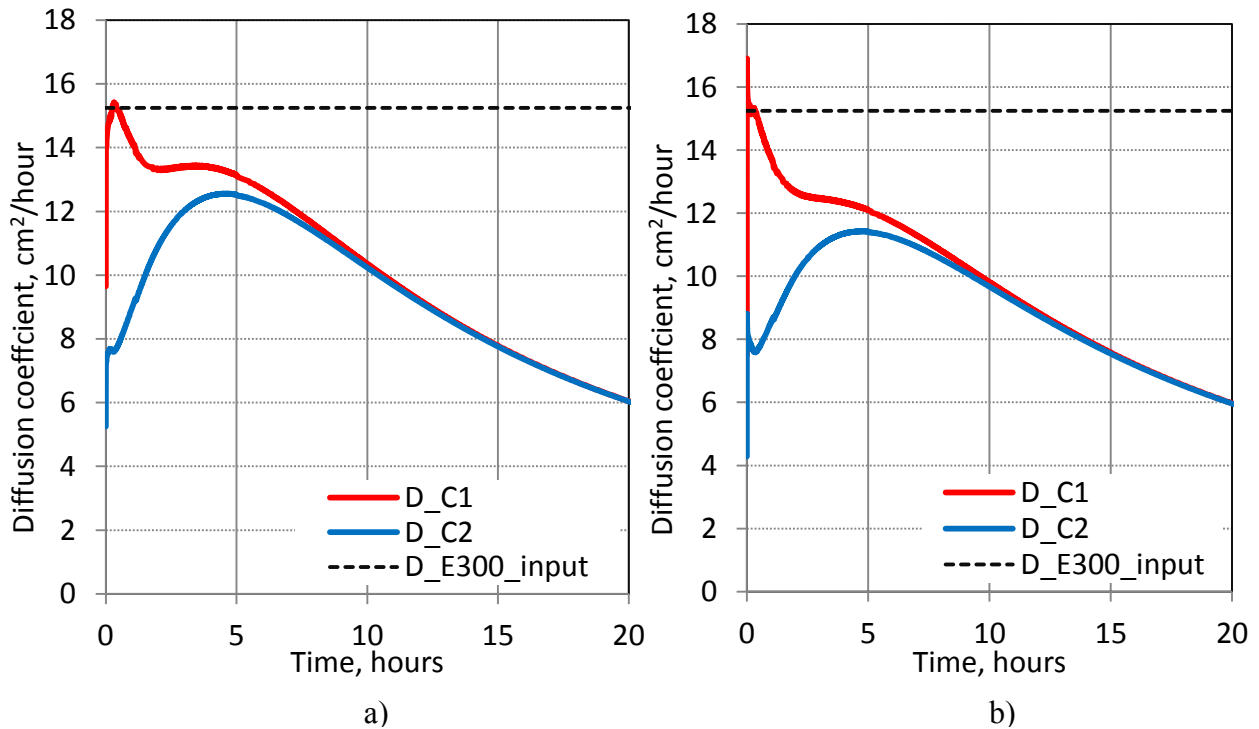


**Fig.5.8:** Diffusion coefficients obtained from simulated diffusion experiments ( $P=707\text{psia}$ ,  $T=90^{\circ}\text{F}$ ):

a) Concentration- b) Chemical potential- driven diffusivity model

TABLE 5.1 RESULTS FROM SIMULATED DIFFUSION EXPERIMENTS

| PRESSURE |      | MOLAR DENSITY                    |                                  |            | DIFFUSION COEFFICIENTS |  |                              |                              |            |                              |                              |            |
|----------|------|----------------------------------|----------------------------------|------------|------------------------|--|------------------------------|------------------------------|------------|------------------------------|------------------------------|------------|
| atm      | psia | pure C <sub>1</sub><br>mole/rcm3 | pure C <sub>2</sub><br>mole/rcm3 | Delta<br>% | Input Eclipse          | Chemical potential driven Dij                  |                              |                              |            | Concentration driven Dij     |                              |            |
|          |      |                                  |                                  |            | 300                    | D_C <sub>1</sub> =D_C <sub>2</sub><br>cm2/hour | D_C <sub>2</sub><br>cm2/hour | D_C <sub>1</sub><br>cm2/hour | Delta<br>% | D_C <sub>2</sub><br>cm2/hour | D_C <sub>1</sub><br>cm2/hour | Delta<br>% |
| 1        | 2    | 3                                | 4                                | 5          | 6                      | 7  | 8                            | 9                            | 10         | 11                           | 12                           |            |
| 1        | 15   | 0.00004                          | 0.00004                          | 0          | 906.7                  | 876.0  | 867.2                        | 1.0                          | 874.7      | 865.3                        | 1.1                          |            |
| 2        | 29   | 0.0001                           | 0.0001                           | 0          | 451.8                  | 416.7  | 407.7                        | 2.2                          | 434.1      | 425.1                        | 2.1                          |            |
| 3        | 44   | 0.0001                           | 0.0001                           | 2          | 300.0                  | 283.2  | 285.6                        | -0.9                         | 287.7      | 289.3                        | -0.6                         |            |
| 4        | 59   | 0.0002                           | 0.0002                           | 2          | 224.3                  | 218.5  | 218.5                        | 0.0                          | 219.5      | 219.7                        | -0.1                         |            |
| 5        | 73   | 0.0002                           | 0.0002                           | 3          | 178.8                  | 174.4  | 175.0                        | -0.4                         | 174.1      | 174.9                        | -0.5                         |            |
| 15       | 220  | 0.0006                           | 0.0007                           | 9          | 57.4                   | 55.8   | 55.7                         | 0.1                          | 54.9       | 54.8                         | 0.2                          |            |
| 20       | 293  | 0.0008                           | 0.0009                           | 13         | 42.3                   | 41.3   | 41.3                         | 0.0                          | 40.7       | 40.7                         | 0.0                          |            |
| 30       | 441  | 0.0013                           | 0.0016                           | 22         | 26.9                   | 25.8   | 25.9                         | -0.6                         | 25.6       | 25.8                         | -0.6                         |            |
| 40       | 585  | 0.0017                           | 0.0025                           | 34         | 19.2                   | 17.5   | 18.0                         | -2.7                         | 17.7       | 18.2                         | -2.6                         |            |
| 45       | 661  | 0.0019                           | 0.0034                           | 44         | 16.6                   | 13.8   | 14.8                         | -7.6                         | 14.2       | 15.3                         | -7.5                         |            |
| 48       | 708  | 0.0021                           | 0.0046                           | 55         | 15.2                   | 10.0   | 13.1                         | -30.9                        | 10.7       | 13.7                         | -28.1                        |            |
| 49       | 714  | 0.0021                           | 0.0050                           | 59         | 15.1                   | 8.9  | 12.7                         | -42.8                        | 9.6        | 13.3                         | -38.1                        |            |
| 50       | 735  | 0.0021                           | 0.0076                           | 72         | 14.5                   | 7.0  | 11.2                         | -59.8                        | 8.2        | 12.5                         | -53.6                        |            |
| 54       | 800  | 0.0024                           | 0.0087                           | 73         | 13.0                   | 6.2  | 10.8                         | -73.4                        | 7.6        | 12.7                         | -66.1                        |            |
| 68       | 1000 | 0.0030                           | 0.0101                           | 70         | 9.5                    | 5.0  | 9.5                          | -91.0                        | 6.4        | 11.6                         | -80.5                        |            |
| 82       | 1200 | 0.0036                           | 0.0108                           | 66         | 7.3                    | 4.3  | 7.9                          | -86.1                        | 5.4        | 9.6                          | -77.3                        |            |
| 88       | 1300 | 0.0040                           | 0.0111                           | 64         | 6.4                    | 4.0  | 7.2                          | -81.0                        | 5.0        | 8.7                          | -73.3                        |            |
| 102      | 1500 | 0.0046                           | 0.0116                           | 60         | 5.1                    | 3.5  | 5.9                          | -70.3                        | 4.3        | 7.0                          | -64.3                        |            |
| 122      | 1800 | 0.0056                           | 0.0122                           | 54         | 3.9                    | 2.9  | 4.6                          | -56.3                        | 3.5        | 5.4                          | -51.7                        |            |
| 136      | 2000 | 0.0063                           | 0.0125                           | 50         | 3.5                    | 2.7  | 4.0                          | -48.4                        | 3.2        | 4.6                          | -44.7                        |            |
| 177      | 2600 | 0.0081                           | 0.0133                           | 39         | 2.6                    | 2.2  | 2.9                          | -30.9                        | 2.5        | 3.3                          | -28.9                        |            |
| 204      | 3000 | 0.0093                           | 0.0138                           | 33         | 2.3                    | 2.0  | 2.5                          | -23.1                        | 2.3        | 2.7                          | -21.9                        |            |
| 272      | 4000 | 0.0117                           | 0.0146                           | 20         | 1.8                    | 1.7  | 1.9                          | -12.6                        | 1.8        | 2.0                          | -11.9                        |            |
| 340      | 5000 | 0.0135                           | 0.0152                           | 11         | 1.5                    | 1.4  | 1.5                          | -8.0                         | 1.5        | 1.7                          | -7.6                         |            |
| 408      | 6000 | 0.0150                           | 0.0157                           | 5          | 1.3                    | 1.3  | 1.3                          | -5.5                         | 1.3        | 1.4                          | -5.3                         |            |
| 476      | 7000 | 0.0162                           | 0.0162                           | 0          | 1.2                    | 1.1  | 1.2                          | -4.0                         | 1.2        | 1.3                          | -3.8                         |            |

The current study showed that diffusion performance is affected much by mixture molar density variation, which may be a strong function of composition. In the simple case, where molecules of component  $C_1$  and  $C_2$  have identical volumetric properties, the rates on transfer of  $C_1$  and  $C_2$  due to diffusion motion across a volume fixed media may reasonably treated to be equal and opposite.

In a solution where the diffusion coefficient does not vary with concentration, the difference in mixture molar density during diffusive flux results in pressure gradients, due to fluctuations in volumetric behaviour. This pressure is relieved by a compensating bulk flow of components together that will eventually readjust component distribution, so that to regain pressure balance. These convective mass transports may be impossible to determine in practise. However, the existence of convective bulk flow has been demonstrated in metal system (Darken, 1948) and in polymer solvent systems (Robinson, 1946) by the insertion of marker particles

The overall rate of mass transfer, say of any component, across a volume fixed section can be described making a distinction between transfer of matter due to pure diffusion and transfer by real bulk flow.

The calculation of mutual diffusion coefficient in terms of molecular motion, employing conventional concentration-based formulation (classical Fick's law), may fail when transfer of matter by bulk flow overrides substantially the pure diffusion flux.

The detailed examination should be made to determine the analytical or empirical expression that would reflect all mass transfer during diffusive mixing with significant molar density variation effects. Ideal solution should distinguish diffusive fluxes values and mass transfer coefficients due to convective bulk flow.

---

## Conclusions

---

The following major findings and conclusions have been made from the simulated diffusions experiment:

1. For low pressure experiments, when mixture follows ideal gas law, the thermodynamic factor is unity. Thus, we observed no difference in performance between the two diffusive models driven by concentration and chemical potential gradient;
2. At elevated pressure, the fugacity gradients (chemical potential) are no longer proportional to the concentration gradients, reflecting the mixture departure from ideality. While approaching to a chemical equilibrium, fugacity gradient stays almost uniform, but the concentration is not. Absence of sufficient fugacity gradients results in relatively slower diffusion driven by fugacity;
3. The simulation model has to be able to model the diffusion of components directly from the gas phase to the oil phase (cross-phase diffusion). The concentration-based diffusion is not capable to model cross-phase diffusion because of the phase discontinuity at interphase boundary. The fugacity then is correct driving force since diffusion always proceeds from high to low fugacity cross a phase boundary until chemical equilibrium is reached;
4. The pressure gradients, which depend on mixture molar density variation with composition, create convection fluxes that will eventually readjust component distribution, so that to regain pressure balance. The overall rate of mass transfer is a result of pure diffusion and transfer by real bulk flow. The

direction of the bulk flows, created by pressure gradients or exclusive critical behaviour, can either intensify or oppose diffusion fluxes.

5. The component diffusive flux related to chemical potential gradient is a weak function of concentration. That is why diffusion characteristics are in a less degree affected by the variation in mixture molar density with composition;
6. Existence of phenomenological critical region in the case of gas diffusion, stimulate some additional convective migration of components, aiming to readjust constituents distribution;
7. The total mass transfer coefficients were actually determined from simulated diffusion experiments, which are a combination of pure diffusion transfer and unequal bulk flows of  $C_1$  and  $C_2$  particles. It is proved to be difficult to obtain definitive mass transfer values from **pure diffusion**, when whole solution is contaminated with bulk flow.
8. From the point of view of interpreting diffusion coefficients from laboratory experiments one should take into account magnitude and direction of bulk flow, even its not directly observable. It is maybe important to examine the composition variation effect on fluid volumetric properties, such as compressibility factor ( $Z$ ) and molar density (inversely proportional to molar volume). To estimate diffusion coefficients accurately, it is crucial to put a value on possible uncertainties introduced by real bulk flows due to significant molar density, thus  $Z$  factor, oscillation.

## Bibliography

1. <http://petrostreamz.com/pipe-it>
2. Alavian S.A, 2011. Modeling CO<sub>2</sub> injection in fractured reservoirs using single matrix block systems. Doctoral thesis. Norwegian University of science and technology, Trondheim.
3. Berry Jr. V. J., R. C. Koeller. 1960. Diffusion in compressed binary gaseous systems. AIChE Journal Volume 6, Issue 2, 274–280.
4. Bird, R.B., Stewart, W.E. and Lightfoot, E.N., 1960. Transport Phenomena. John Wiley & Sons Inc, New York.
5. Carmichael L.T., Sage B.H., Lacey W.N., California Institute of Technology, Pasadena, California. A.I.Ch.E. Vol.1, No.3.
6. Coats, K.H. 1980. An Equation of State Compositional Model", SPE Journal, October, 1980.
7. Christoffersen, Kjell.R.: "High Pressure Experiments with Application to Naturally Fractured Chalk Reservoirs 1.Constant Volume Diffusion, 2. Gas Oil Capillary Pressure", A Dissertation for the Partial Fulfillment of Requirements for the Degree of Doktor Ingeniør, NTNU, Trondheim, 1992.
8. Crank., J. 1975. The mathematics of diffusion n. 2<sup>nd</sup> edition, Oxford.

9. da Silva, F.V and Belery, P., 1989. Molecular Diffusion in Naturally Featured Reservoirs: a Decisive Recovery Mechanism., Paper SPE 19672 presented at the 64th SPE Annual Technical Conference and Exhibition, San Antonio, Texas, U.S.A., 8-11 October.
10. Darken L.S. 1948. Diffusion, mobility and their interaction through free energy binary metallic systems.
11. Grogan, A. T., & Pinczewski, W. V. ,1987. The role of molecular diffusion processes in tertiary CO<sub>2</sub> flooding. Journal of Petroleum Technology, 39, 591–600.
12. Guerrero-Aconcha U. and Kantzas A. 2009. Diffusion of hydrocarbon gases in heavy oil and bitumen. Paper SPE 122783 presented at the Latin American and Caribbean Petroleum Engineering Conference, Cartagena de Indias, 31 May-3 June.
13. Hartley G.S., 1946. Diffusion and swelling of high polymers. Part 1.-the swelling and solution of a high polymer solid considered as a diffusion process.
14. Hoteit, H. 2011. Proper modeling of diffusion in fractured reservoirs. Paper SPE 141937 presented at the 2011 SPE Reservoir Simulation Symposium, Texas, U.S.A., 21-23 February.
15. Hoteit, H. and Firoozabadi, A. 2006. Numerical Modeling of Diffusion in Fractured Media for Gas Injection and Recycling Schemes. Paper SPE 103292 presented at the 2006 SPE Annual Technical Conference and Exhibition, San Antonio, Texas, U.S.A., 24-27 September.
16. McDougall S.R.,P.A.Salino 1997. The effect of interfacial tension upon gas oil relative permeability measurements: Interpretation using pore-scale models. Paper SPE 38920 presented at the 1997 SPE .

17. McKay W.N., 1971. Experiments concerning diffusion of multicomponent systems at reservoir conditions. Imperial Oil Limited, Calgary, Alberta.
18. McKay, A.T., 1930, Diffusion into an infinite plane sheet subject to a surface condition, with a method of application to experimental data. Proceedings of the Physical Society, Vol. 42, 547.
19. Perkins T.K., Johnston O.C., 1963. A Review of Diffusion and Dispersion in Porous Media. SPE 480, 70-84.
20. Sigmund, P.M., 1976. Prediction of Molecular Diffusion at Reservoir Condition. Part I - Measurement and Prediction of Binary Dense Gas Diffusion Coefficients. Journal of Canadian Petroleum Technology, Apr-Jun, 15(2). DOI: 10.2118/76-02-05 Annual Technical Conference and Exhibition, San Antonio, Texas, U.S.A., 5-8 October.
21. Sigmund, P.M., 1976. Prediction of Molecular Diffusion at Reservoir Condition. Part II - Estimating the effects of molecular diffusion and convective mixing in multicomponent systems. Journal of Canadian Petroleum Technology, Apr-Jun, 15(2). DOI: 10.2118/76-02-05 Annual Technical Conference and Exhibition, San Antonio, Texas, U.S.A., 5-8 October.
22. Takahashi, S., Hongo, M. 1982. Journal of Chemical Engineering of Japan, 15, 57-59
23. Reid, R.C., Prausnitz, J.M. and Poling, B.E., 1987. The Properties of Gases and Liquids. Fourth Edition, McGraw-Hill, New York.
24. Whitson, C.H. and Brule M.R., 2000. Phase Behavior. Monograph Vol. 20, Richardson, TX.



---

25. Wilke, C.R., 1950. Diffusion Properties of Multicomponent Gases. Chemical Engineering Progress, 46(2): 95-104.

26. van Brakel, J., Heertjes, P.M., 1974. Analysis of Diffusion in Macroporous Media in Terms of a Porosity, a Tortuosity and a Constrictivity Factor. International Journal of Heat and Mass Transfer 17: 1093–1103.

27. Zick Technologies: PhazeComp, [www.zicktech.com](http://www.zicktech.com).

28. Eclipse reservoir simulation software, 2011.1. Technical description. Shlumberger.

29. Eclipse reservoir simulation software, 2011.1. Reference manual. Shlumberger.

APPENDIX A

Input Data Set Used to simulate diffusion  
experiments

Eclipse 300 input data set

---

```
--RUNSPEC section-----
NOECHO
RUNSPEC
--TITLE
--IMPES
FULLIMP

DIMENS
1 100 1 /
-- Phases present
OIL
GAS
OPTIONS3
--switch 280
279* 1 /
--Enables molecular diffusion
DIFFUSE
-- Units
LAB
-- Define Component in EOS
COMPS
2 /
REGDIMS
-- Max.FIPREG FIPREG
  2  2  0  2 /
TABDIMS
--No.sat.tab No.pvt.tab max.sat.nods max.sat.nods Max.FIPREG
2    1    50    50    2 /
EQLDIMS
----Eqrgn Deptab
  2  50 /
WELLDIMS
5 10 20 20 20 20/
-- To unified output files
UNIFOUT
MULTSAVE
```

0 /

UNIFIN

--Grid section-----

GRID

--Requests output of an INIT file (Need for FloViz)

INIT

RPTGRID

DR DZ PERMR PERMZ PORO PORV TRANR TRANZ NNC /

MINPORV

0.000000001/

-- SPECIFY GRID BLOCK DIMENSIONS IN THE R DIRECTION

EQUALS

TOPS 0 1 1 1 100 1 1 / cm

PORO 0.5 1 1 1 100 1 1 / fraction

PERMX 200 1 1 1 100 1 1 / mD

-- PERMX 1000 1 1 1 100 1 1 / mD

/

DX

100\*0.5 / 1cm

DY

100\*0.25 / 2.5 mm

DZ

100\*0.25 / 1cm

COPY

'PERMX' 'PERMY' /

'PERMX' 'PERMZ' /

/

GRIDFILE

2 /

PROPS =====

EOS

SRK /

-- Reservoir temperatures Deg C

RTEMP

22.7777777777778 / C

ROCK

---

```

54.4365813826892 0 /
INCLUDE
'EOS_METRIC.inc' /
INCLUDE
'Pc_Kro_Krg.inc' /
-- Diffusion Coefficient
INCLUDE
'Diff_CHEM.inc' /
REGIONS
=====

-- Regoin 1= methane CH4
-- Regoin 2= ethane C2H6
EQUALS
FIPNUM 1 / Fluid In Place reg. no.1
FIPNUM 2 1 1 51 100 1 1 / Fluid In Place reg. no.2
SATNUM 1 / Saturation reg. no.1
SATNUM 2 1 1 51 100 1 1 / Saturation reg. no.2
EQLNUM 1 /
EQLNUM 2 1 1 51 100 1 1 /
/
SOLUTION =====
DATUMR
1.0 1.0 /
PRESSURE
100*54.4365813826892 / atma
EQUALS
SOIL 0 /
SGAS 1 1 1 1 100 1 1 /
/
NEI
1 0 / CH4
0 1 / C2H6
RPTSOL
PRESSURE SOIL SGAS ZMF PCOG PSAT DENO DENG ZMF/
RPTRST
BASIC=2 SOIL PCOG /

```

---

```

SUMMARY =====
RPTONLY
RUNSUM
NARROW
INCLUDE
'Summary.inc' /
EXCEL
SCHEDULE =====
----- THE SCHEDULE SECTION DEFINES THE OPERATIONS TO BE SIMULATED
-----

-- Creat Restart file
RPTRST
BASIC=2 SOIL STEN FMISC FMISC FPC KRO KRG XMF YMF DENO DENG STEN SOIL
SGAS BVOIL PCOG /
RTPRINT
8*/
RPTSCHED
'CPU=1' 'FIP=3' 'SOIL' 'ZMF' PRES STEN FMISC FPC KRO KRG XMF YMF DENO DENG
STEN SOIL SGAS BVOIL PCOG /
TUNING
8* /
4* /
50 1* 250 /20 1* 2*20
NSTACK
70 /
-- Uint= Hr
TSTEP
10*0.001/10 hours
TSTEP
500*0.01/10 hours
TSTEP
500*0.02 /10 hours
TSTEP
1000*0.05 /50 hours
TSTEP
1000*0.05 /50 hours
END

```

**INCLUDE FILES:****'Pc\_Kro\_Krg.inc'**

SGOF

--Sg      Krg      Krog      Pcog (PSI)

0.0000   0.0000   1.0000   0

0.05    0.05    0.9500   0

0.2013   0.2013   0.7987   0

0.4832   0.4832   0.5168   0

0.6674   0.6674   0.3326   0

0.7866   0.7866   0.2134   0

0.8447   0.8447   0.1553   0

0.8775   0.8775   0.1225   0

0.8998   0.8998   0.1002   0

0.9150   0.9150   0.0850   0

0.9262   0.9262   0.0738   0

0.9413   0.9413   0.0587   0

0.9505   0.9505   0.0495   0

0.9618   0.9618   0.0382   0

0.9705   0.9705   0.0295   0

0.9806   0.9806   0.0194   0

0.9902   0.9902   0.0098   0

1.0000   1.0000   0.0000   0

/ --table 1 (C1-region)

0.0000   0.0000   1.0000   0

0.05    0.05    0.9500   0

0.2013   0.2013   0.7987   0

0.4832   0.4832   0.5168   0

0.6674   0.6674   0.3326   0

0.7866   0.7866   0.2134   0

0.8447   0.8447   0.1553   0

0.8775   0.8775   0.1225   0

0.8998   0.8998   0.1002   0

0.9150   0.9150   0.0850   0

0.9262   0.9262   0.0738   0

0.9413   0.9413   0.0587   0

0.9505   0.9505   0.0495   0

0.9618   0.9618   0.0382   0

0.9705   0.9705   0.0295   0

0.9806   0.9806   0.0194   0

0.9902   0.9902   0.0098   0

1.0000   1.0000   0.0000   0

/ --table 2 (C2-region)

**'Diff\_CHEM.inc'**

DIFFAGAS

--C1 C2

12.0424493295986 12.0424493295986 / cm2/hour

DIFFAOIL

--C1 C2

0

---

12.0424493295986 12.0424493295986 / cm2/hour

**'Diff\_CON.inc'**

DIFFCGAS

--C1 C2

12.0424493295986 12.0424493295986 / cm2/hour

DIFFCOIL

--C1 C2

12.0424493295986 12.0424493295986 / cm2/hour

**'EOS\_METRIC.inc'**

-- Confirm number of components

NCOMPS

2

/

-- Component names

CNAMES

C1

C2

/

-- Molecular weights

MW

16.043

30.070

/

-- Critical Temperatures (K)

TCRIT

190.56

305.32

/

-- Critical Pressures (BARA)

PCRIT

45.99

48.72

/

-- Acentric factor

ACF

0.01100



---

0.09900

/

-- Equation of state shift parameters

SSHIFT

-0.00247

0.05894

/

-- Component boiling points (K)

TBOIL

111.981

184.84

/

-- Critical Z-factors

ZCRIT

0.28620

0.27924

/

-- Critical Z-factors for viscosity calculations

ZCRITVIS

0.28620

0.27924

/

-- Critical volumes (cc/gmol)

VCRIT

98.6

145.5

/

-- Component parachors

PARACHOR

71.00

111.00

/

BIC

0 0

0 0

/

